New approaches for characterizing and monitoring mammalian cell cycle and specific growth rate in production cell lines

Vom Promotionsausschuss der

Technischen Universität Hamburg-Harburg

zur Erlangung des akademischen Grades

Doktor der Naturwissenschaften (Dr. rer. nat.)

genehmigte Dissertation

von

Grischa Fuge

aus

Hamburg

2018

1. Gutachter: Prof. Dr. rer. nat. An-Ping Zeng

2. Gutachter: Prof. Dr.-Ing. Udo Reichl

Prüfungsausschussvorsitzender: Prof. Dr.-Ing. Hoc Khiem Trieu

Tag der mündlichen Prüfung 11.12.2017

I. Abstract

This study focuses on the different putative interdependencies between the cell cycle and the behaviour of mammalian production cell lines, based on a controlled physiological synchronization and cultivation method, as well as the corresponding implications for reliable process analysis and control.

In the first part, an established experimental setup for the generation of synchronized suspension cultures was adapted for the *Human Embryonic Kidney cell line 293*. This cell line could then be synchronized under near-physiological conditions. Extensive optimisation efforts were required in order to achieve and maintain high viabilities as well as aggregation free growth.

Subsequently, this method was used to examine the putative dependency of the transfection efficiency from the cell cycle state at the time of transfection. These studies are based on synchronization methods under near-physiological conditions. The following synchronized growth was confirmed by DNA based cell cycle analysis and specific growth rate determination. The results indicated that the so-called cell cycle dependencies reported by other groups, cannot be confirmed when near-physiological synchronised cultures are used. Hence it is likely that the putative cell cycle dependencies, which were reported before, are artefacts of the non-physiological synchronisation methods used in those studies.

Note that this study doesn't draw conclusions concerning potential cell cycle dependencies of production rates; they require additional studies possibly utilizing the established methods described here.

In order to facilitate the follow-up cell cycle specific research and future on-line measurements, a novel approach was chosen. Two new derivatives of the widely used Chinese Hamster Ovary (CHO-K1) production cell line were established. They indicate their cell cycle as well as growth state in an *on-line* compatible manner by fluorescence. For this purpose, three different genetic FUCCI (*Fluorescence Ubiquitination Cell Cycle Indicator*) constructs were used in two different combinations. In coherence with the original nomenclature by Miyawaki et al. [C: mKO2-hCdt1(30/120), M: mVenus-

hGeminin(1/110) and N: mVenus-hGeminin(1/60)] they were denoted *CHO-K1 FUCCI CM* und *CN*.

In order to enable quantitative and reproducible conclusions based on the fluorescence properties, two quantitative parameters were introduced. The parameter i_{red}^{n} indicates the percentage of cells with red fluorescence in relation to the total number of fluorescent cells, composed of red and green fluorescent cells. This relative parameter is generally independent from possibly altering total fluorescence intensities per single cell. Quantitative analyses revealed that i_{red}^{n} correlates well with the cell cycle state (expressed as percentage of cells in the G1 cell cycle phase) and is furthermore directly connected to the specific growth rate (μ). Hence the parameter i_{red}^{n} has a high validity but requires measuring the fluorescence of single cells in order to calculate their numerical ratio. Therefore, flow cytometry is the method of choice.

Correspondingly the parameter i_{red}^{total} is based on the total fluorescence intensity of the culture and is determined by the total red fluorescence in relation to the sum of total red and green fluorescence. This relative determination is robust with regard to variations in cell density and correspondingly changing total fluorescence intensities. Hence i_{red}^{total} is determined by the number of cells in the different cell cycle phases as well as the fluorescence intensity per cell. Consequently i_{red}^{total} is less exact compared to i_{red}^{n} but can be determined using simpler methods (fluorescence plate reader, online measurement).

It is pivotal for both approaches to detect and quantify the fluorescence intensities (red vs. green) with sufficient specificity (low cross talk) and accuracy. It was demonstrated that i_{red}^{total} can be used to indicate changes in the growth behaviour as well as limiting growth conditions, here in the form of L-glutamine limitation, early on. This was confirmed in shaking flask and bioreactor cultures alike. Significant signals, indicating emerging limitation were detected several hours earlier compared to traditional indicators (cell counts, oxygen uptake rate). Ultimately, on-line or at-line fluorescent probes are highly recommended for further analyses and process control of mammalian cell cultures.

II. Zusammenfassung

Diese Studie befasst sich mit den verschiedenen mutmaßlichen wechselseitigen Abhängigkeiten zwischen dem Zellzyklus und dem Verhalten von Säugetierzelllinien, basierend auf einer kontrollierten und physiologischen Synchronisierungs- und Kultivierungsmethode mit minimaler Artefakt-Anfälligkeit, sowie den zugehörigen Implikationen für zuverlässige Prozessanalytik und -kontrolle.

Im ersten Teil der Arbeit wurde eine bereits vorab etablierte experimentelle Anordnung zur Erzeugung synchronisierter Suspensionskulturen auf die humane Suspensionszelllinie *Human Embryonic Kidney cell line 293s* adaptiert. Diese konnte somit unter annähernd physiologischen Bedingungen synchronisiert werden. Es waren umfangreiche Optimierungen nötig, um hohe Überlebensraten sowie aggregationsfreies Wachstum zu erreichen und beizubehalten.

Im Folgenden wurde diese Technik für Studien genutzt, um die potentielle Abhängigkeit der Transfektionseffizienz vom Zeitpunkt der Transfektion relativ zum Zellzyklus zu untersuchen. Diese Studien basieren auf Synchronisationsmethoden unter annähernd physiologischen Bedingungen. Das folgende synchrone Wachstum konnte dabei durch DNA-basierte Zellzyklus-Analysen und Wachstumsraten-Analysen belegt werden. Die Resultate deuten darauf hin, dass die sogenannten Abhängigkeiten der Transfektionseffizienz von dem Zellzyklus, die von anderen Forschungsgruppen publiziert wurden, nicht bestätigt werden können, wenn annähernd-physiologisch synchronisierte Kulturen genutzt werden. Folglich ist wahrscheinlich, dass die bislang veröffentlichten mutmaßlichen Zellzyklus-Abhängigkeiten Artefakte der nicht-physiologischen Methoden sind, die in diesen Studien verwendet wurden.

Es ist anzumerken, dass diese Studie keine Aussage über potentielle Zellzyklus-Abhängigkeiten der Produktionsraten trifft; diese bedürfen weiterer zukünftiger Untersuchungen, potentiell unter Nutzung der hier etablierten Methoden.

Um daran anknüpfend weiterführende zellzyklus-spezifische Untersuchungen und darüber hinaus zukünftig Online-Messungen zu ermöglichen, wurde ein neuartiger Ansatz gewählt. Es wurden zwei neue Derivate der häufig genutzten *Chinese Hamster*

Ovary (CHO-K1) Produktionszelllinie erzeugt, die ihren Zellzyklus- sowie Wachstumszustand in einer *on-line* auslesbaren Weise mittels Fluoreszenz anzeigen. Zu diesem Zweck wurden drei genetische FUCCI (*Fluorescence Ubiquitination Cell Cycle Indicator*) Konstrukte in zwei verschiedenen Kombinationen verwendet. In Übereinstimmung mit der Originalnomenklatur von Miyawaki et al. [C: mKO2-hCdt1(30/120), M: mVenus-hGeminin(1/110) und N: mVenus-hGeminin(1/60)] werden diese bezeichnet als *CHO-K1 FUCCI CM* und *CN*.

Um quantitative und reproduzierbare Aussagen, basierend auf den Fluoreszenzeigenschaften, treffen zu können, wurden die folgenden Parameter eingeführt: Der Parameter i_{red}^{n} gibt an, welcher Anteil [%] der Zellen rot fluoresziert und steht im Verhältnis zur Gesamtanzahl fluoreszierender Zellen, zusammengesetzt aus der Anzahl von Zellen mit roter und grüner Fluoreszenz. Dieser relative Parameter ist somit weitgehend unabhängig von eventuell schwankenden Gesamt-Fluoreszenzintensitäten pro Zelle. Quantitative Analysen haben gezeigt, dass i_{red}^{n} gut mit dem Zellzyklusstatus von Kulturen korreliert (ausgedrückt als Anteil [%] der Zellen in der G1 Phase) und darüber hinaus in direktem Zusammenhang zur Wachstumsrate (μ) steht. Der Parameter i_{red}^{n} besitzt daher eine hohe Aussagekraft, setzt aber auch voraus, dass die Fluoreszenz einzelner Zellen bestimmt werden kann, um deren Anzahl in ein quantitatives Verhältnis zu setzen, weshalb Durchflusszytometrie hier die Methode der Wahl ist.

Analog dazu basiert der Parameter i_{red}^{total} auf den Gesamt-Fluoreszenz-Intensitäten der Kultur und ergibt sich aus der Gesamt-Intensität der roten Fluoreszenz zur Summe der Intensitäten von roter und grüner Fluoreszenz. Dieses relative Maß erlaubt eine große Robustheit gegenüber variablen Zelldichten bzw. Gesamt-Fluoreszenzintensitäten der Kultur. i_{red}^{total} wird somit bestimmt durch die Anzahl der Zellen in den verschiedenen Zellzyklus-Phasen sowie deren Fluoreszenz-Intensität pro Zelle. Entsprechend ist der Parameter i_{red}^{total} weniger exakt als i_{red}^{n}, kann jedoch auch mit einfacheren Methoden (Fluoreszenzphotometer, Online-Messung) bestimmt werden.

Wichtig ist für beide genannten Ansätze, dass die Fluoreszenz-Intensitäten (rot vs. grün) mit ausreichender Spezifizität (also niedrigem Übersprechen zwischen den Farbkanälen) und Genauigkeit detektiert und quantifiziert werden.

Es wurde gezeigt, dass i_{red}^{total} genutzt werden kann, um Änderungen der Wachstumsrate und wachstumslimitierende Bedingungen, hier exemplarisch in der Form von L-Glutamin-Mangel, frühzeitig zu detektieren. Dies wurde in Schüttelkolben- sowie Bioreaktor-Kulturen bestätigt. So wurden signifikante Signale für eine entstehende Limitierung mehrere Stunden früher erkannt als mit herkömmlichen Methoden (Zellzahl, Sauerstoff-Aufnahme-Rate). Daher wird die Verwendung von *on-line* oder *at-line* Fluoreszenzsonden für weitere Analysen und Prozesskontrolle von Säugetierzellkulturen empfohlen.

Content

List of Figures

List of tables

Abbreviations

A.U.	arbitrary units
AA	Amino acid
APC	Anaphase-promoting complex
APC^{Cdh1}	APC/C activator protein CDH1
ATP	Adenosine triphosphate
CHO	Chinese hamster ovary cell line
COS	fibroblast-like cell line, CV-1 (simian) in Origin, and carrying the SV40 genetic material
DAPI	4′,6-Diamidin-2-phenylindol
DCD	dead cell density
DHFR	dihydrofolate reductase
DNA	Deoxyribonucleic acid
DO	dissolved oxygen concentration
EDTA	Ethylenediamine-tetra-acetic acid
eGFP	enhanced green fluorescent protein
Em.	Emission wave length
EtOH	Ethanol
Ex.	Excitation wave length
f	Dilution factor

FDA	Food and Drug Administration
FITC	Fluorescein isothiocyanate - Fluorophore
FSC	forward scatter
FUCCI	Fluorescence Ubiquitination Cell Cycle Indicator
g	gravitational force
g	gram
G0	Quiescent state
G1	growth phase 1
G2	growth phase 2
Glu	Glucose
h	Hour
hCdt1	human chromatin licensing and DNA replication factor 1
HEK293	Human embryonic kidney cell line
HeLa	an immortal cell line, derived from cancer cells taken from Henrietta Lacks in 1951
hGeminin	human Geminin, a DNA replication inhibitor
I	Fluorescence intensity
i	Ratio of fluorescence intensities
K	Proportional constant
k	Ratio of proportional constants
kDa	kilo Dalton
L	litre
lac	lactose
ln	natural logarithm
log	common logarithm
M	molar
M	mitosis phase
mg	milligram

min	minute
Mio/ml	million per millilitre
mKO2	Monomeric Kusabira orange 2 fluorescent protein
ml	millilitre
mM	millimoles per litre
mVenus	monomeric Venus fluorescent protein
n	Cell density [Mio/ml]
NC	negative control
nm	Nanometre
OD	optical density (absorbance)
OUR	oxygen uptake rate
PAT	Process Analytical Technology initiative
PBS	phosphate buffered saline
PE	R-Phycoerythrin - Fluorophore
PerCP	Peridinin-Chlorophyll-protein - Fluorophore
PFA	Paraformaldehyde
pg	pico gram
pH	potential of hydrogen
PI	Propidium iodide
rpm	revolutions per minute
s	second
S	(DNA) synthesis phase
SCF complex	Skp, Cullin, F-box containing complex
SKP2	S-phase kinase-associated protein 2
SSC	side scatter
t	time
TCD	total cell density

tg	generation time
tPA	tissue plasminogen activator
VCD	viable cell density
µ	growth rate [1/h]
µ	specific growth rate
µg	microgram
µl	microlitre
µl	micrometre
σ	standard deviation

1. Introduction

1.1 Industrial application of mammalian cell cultures

Mammalian cell cultures are a pivotal source for various biopharmaceutical products including hormones, monoclonal antibodies and vaccines [1]. Around 60 to 70% of all recombinant protein pharmaceuticals are manufactured using mammalian cell cultures [2]. The complexity of these molecules, as well as the need for human compatible glycosylation patterns, exceed the abilities of prokaryotic organisms. Instead, the post-transcriptional machinery of mammalian cells is mandatory [3]. The production of recombinant proteins, using mammalian cells grown in bioreactors, has been developed into a powerful technology owing to intensive research and process development during the last three decades [4].

The first protein that was produced in recombinant mammalian cells and approved for the market was the tissue plasminogen activator (tPA, Genentech, San Francisco, CA, USA) back in 1986. Since then, vast improvements in process productivity could be achieved, despite the fact that the basic concepts remained the same. In the mid-1980s typical characteristics of a stirred tank process included maximum cell densities of 2 Million/ml, batch production phases of up to 7 days and a specific productivity just under 10 pg/cell/day. In total product titres of 50 mg/l were common [2].

Less than two decades later, in 2004, a process applied in the industry was reported to yield cell densities well over 10 Mio/ml, high viabilities for slightly below 3 weeks, specific productivities of up to 90 pg/cell/day and total, accumulated concentrations of 4.7 g/L [2].

Today's high performance processes can reach around 10 g/L, while reducing the bulk cost from previously $ 2000/g to approx. $100/g [5].

These achievements are the result of multiple incremental developments. They include novel vector systems, engineered host cells as well as optimised media, feeding strategies and processes. They became available through years of intense research targeting gene expression, the delay of apoptosis and different aspects of the metabolism [2, 5].

1.1.1 The Chinese Hamster Ovary (CHO) cell line

With about 70% of all recombinant protein therapeutics produced [2, 4, 6, 7] the Chinese Hamster Ovary (CHO) cell line and its derivatives are the most popular mammalian production cell line. They have become extensively used, since they combine several advantageous properties: they can be cultured in suspension at high cell densities, in chemically defined, protein-free media, yield good titres of product [6, 8] and have been regularly approved for pharmaceutical protein production [2]. Although their glycosylation patterns are not human, they are human compatible [8].

The original CHO cell line was first described in 1956 [9, 10], followed by a plethora of different variants. The first was CHO-K1, a single clone of the original CHO cell line [6]. Subsequently, CHO-K1 was mutated in order to obtain a novel sub-clone deficient for dihydrofolate reductase (DHFR) activity, called CHO-DXB11. Since the DHFR activity could be regained as a result of reverse mutation, applicability was limited [11]. Consequently, CHO cells were exposed to gamma radiation to generate a new cell line, CHO-DG44, with both alleles of the *dhfr* gene eliminated. Their lack of DHFR activity causes the cells to depend on glycine, hypoxanthine and thymidine for proliferation [12].

The dependency on thymidine is commonly employed as selective marker, when generating clones for protein production. The gene of interest is inserted into the DHFR deficient CHO cell line in combination with a functional copy of the *dhfr* gene. Subsequently, the cells are grown in thymidine free medium, hence under selective conditions. Surviving cells have the exogenous *dhfr* gene, as well as the gene of interest integrated into their genome. From this set of clones, the most productive ones can be screened [13].

Of these cell lines mentioned above, numerous additional recombinant protein-producing CHO cell lines were generated by further mutagenesis, gene transfer and clone selection [13]. Lately, extensive sequencing studies were employed to bring a systematic order to the variety of CHO cell lines [6].

The large variety of CHO derived cell lines mentioned above illustrates their general importance. In order to yield results with the broadest applicability, the latest common ancestor still in use, CHO-K1, was chosen for the experiments in this study.

1.1.2 The Human Embryonic Kidney (HEK293) cell line

Much like the CHO cell lines, the Human Embryonic Kidney (HEK293) cell line is amongst those with frequent regulatory approval for recombinant pharmaceutical protein production [2].

Its main advantages are high transfection efficiencies, compared to CHOs, as well as good protein production capabilities [8]. Furthermore the glycosylation patterns are more human like, since the HEK cell line is of human origin [14], while CHO cell lines lack several glycosylation enzymes present in human cells [8].

On the downside, HEK293 cells are not commonly used as suspension cultures in production processes. However there are derivatives adapted to growth in suspension like HEK293s [15] and the sub-clone 293SF-3F6 [16].

1.2 The Process Analytical Technology (PAT) initiative

In 2004, a novel program, the Process Analytical Technology initiative (PAT), was introduced by the U.S. Food and Drug Administration (FDA). The acclaimed goal of the PAT initiative is to develop thorough understanding and control of manufacturing processes, in accordance with the present drug quality system - *“quality cannot be tested into products; it should be built-in or should be by design”* [17].

The following areas were defined as “*PAT tools:*

- *Multivariate tools for design, data acquisition and analysis*
- *Process analysers*
- *Process control tools*
- *Continuous improvement and knowledge management tools* [17]“

In the context of this thesis, it is worthwhile to consider the types of subdivision of the "*Process analysers:*

- *At-line: measurement where the sample is removed, isolated from, and analysed in close proximity to the process stream.*
- *On-line: measurement where the sample is diverted from the manufacturing process and may be returned to the process stream.*
- *In-line: measurement where the sample is not removed from the process stream and can be invasive or non-invasive"* [17]

The program specifically states that on-line, as well as in-line process analysers are suitable to enhance the knowledge of processes in the sense of the acclaimed goals. Furthermore, it defines that a process can only be considered as well understood if, among others, the following two criteria are fulfilled:

- *"all critical sources of variability are identified and explained*
- *variability is managed by the process"* [17]

Industrial production processes based on mammalian cell cultures are subject to a broad range of possible variations. In order to detect these, a variety of sensors can be used.

1.3 Sensors for bioprocess monitoring

At the present day, there is an increasing range of sensor techniques available to probe various physical, chemical and biological variables with little or no time delay. However only a fraction of these is commonly used in industrial production. Most are excluded due to their complexity, unsatisfying sensitivity or specificity, cost and incompatibility with standard bioreactor sterilisation techniques. From this point of view, optical and spectroscopic methods have several advantages. They can be used without direct contact to the sample, which excludes problems connected to cleaning and sterility. Furthermore, depending on the method, different variables can be detected

simultaneously. However correct data interpretation and extraction can be challenging [18].

In general, three classes of variables can be discerned:

- Physical variables

  Most physical parameters, like temperature, viscosity and pressure, can be measured directly. Furthermore foam formation can be detected by electric resistance measurements in the reactors headspace [18].

- Chemical variables

  Rapid and accurate measurement of the dissolved oxygen concentration (DO) is essential to avoid oxygen limitations. Additionally, it allows, in conjunction with defined aeration parameters, the calculation of the oxygen uptake rate (OUR), the most important variable to estimate the total rate of aerobic metabolism. Other parameters include the pH, concentrations of substrates, products, volatile gasses and carbon dioxide [18].

- Biological variables

  Despite the fact that relevant properties determining the product quality (e.g., glycosylation) can be a direct consequence of the production cell line's biological state [19], comparably few biological variables are measured in-line / on-line. These are mainly limited to biomass, cell morphology and certain aspects of the metabolism [18]. More advanced on-line capable technologies, based on, e.g., Raman spectroscopy, dielectric properties and mass-spectrometry are possible to some extend but are not frequently used in production environments as reviewed in [20–24]. After all, one key variable, the mammalian cell cycle state, is rarely monitored (see Sections 1.5 & 1.6).

1.4 Population heterogeneity as a challenge in production processes

One of the main aims in bioreactor design and operation is to ensure optimal growth and production conditions for the organism of interest in a bioprocess. Despite decades of development and progress, the latter one can pose a significant challenge.

It is pivotal for the cell physiology as well as the product yield and quality to maintain the environmental conditions within well-defined and reproducible ranges. This requirement is demanding because commonly, different regions in bioreactors exhibit significant variations of conditions. Possible causes are plentiful. They can be related to suboptimal mixing behaviour and local introduction of feed, acid, base or air / oxygen, leading to, e.g., sedimentation or local concentration variations. On the other hand, control of conditions is achieved using a limited number of probes. Conventionally, these are installed in predefined positions, deemed as representative.

Minimization of these bioreactor inhomogeneities is performed by active mixing. Also, mixing type and intensity are subjected to limitations, mainly imposed by the resilience of the organism of interest. In stirred tank reactors, the most commonly used type in recombinant protein production, maximum tip speeds are restrained by the acceptable level of shear stress. As a consequence, certain levels of inhomogeneity remain.

When suspended cells are moved through these gradients in bioreactors, they are subjected to alternating conditions. This in turn will most likely impact the culture performance [25]. Furthermore, and additional to variations in genetic background, it can induce additional inhomogeneities, as individual cells respond to the level of available nutrients. This includes remaining in the G1 cell cycle phase due to limitation of amino acids, like L-glutamine [26].

It is generally understood that the overall behaviour and productivity of cell cultures can be influenced by the different state, behaviour and mutual interaction of its sub-populations. However, population inhomogeneity, especially in perspective of process scale up has received comparably little attention so far.

One major factor contribution to population inhomogeneity, which is interconnected to the physiological and potentially also the metabolic behaviour is the cell cycle [27]. Nevertheless, its implications for the behaviour of cultures was rarely studied in detail. Only few studies have targeted the question of sub-populations differing in their cell cycle states [28, 29].

This is unsatisfying since, on the other hand, the cell cycle has been repeatedly reported to alter the metabolic behaviour of cells, including the susceptibility to transfection [30–32]. Furthermore, it is inevitably connected to proliferation and hence, the specific growth rate (μ).

1.5 The mammalian cell cycle and specific growth rate (μ)

The mammalian cell cycle consists of a series of distinct phases; cells go through them in order to create two identical daughter cells [33]. They are conventionally divided into G1, S, G2 and M phases [34].

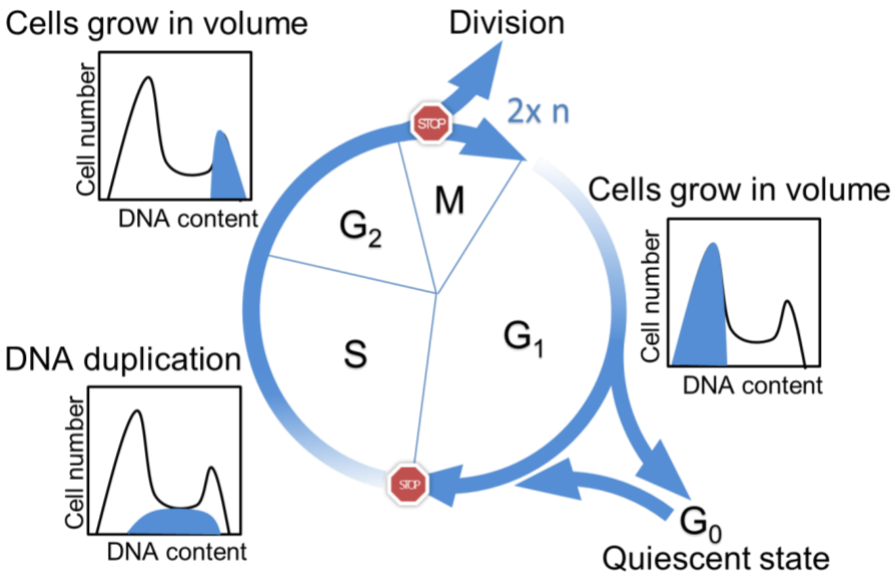

Figure 1: The mammalian cell cycle and its phases.
Cells pass through the G1, S and G2/M phases between each duplication. In the G1 phase cells mainly grow in volume and contain one relatively constant amount of DNA. Cells can also reversibly enter the non-proliferating G0 phase, which is characterised by the same size and DNA content as in G0. During the S phase cells duplicate their DNA. In G2 they grow before they divide by mitosis.

The G1 Phase (*gap phase* or *post mitotic phase*) is characterised by volumetric growth and synthesis of cellular components like cytoplasm and cellular organelles. In preparation for the following S phase, all required enzymes (e.g. DNA polymerase) and other proteins are synthesised. The increased energy demand is met by higher GTP and ATP synthesis. As in every step of the mitosis the genome is diploid, but chromosomes exist in their one-chromatid form. The DNA is checked for damage and repairs are conducted if necessary. From the G1 phase cells can reversibly enter the G0 Phase if problems are detected or the nutrient supply is insufficient. This is controlled by a checkpoint, also called the restriction point, which is explained below.

The G0 Phase is frequently regarded a special case of the G1 Phase. It is technically not part of the cell cycle but a quiescent state outside it. Even the existence of such a defined state has been argued [35]. Cells are conventionally considered to reversibly enter this state for a variety of reasons e.g. because their biological function in an organism does not require them to proliferate, or due to limitations in culture. However, they can re-enter the cell cycle.

The S Phase (*synthesis phase*) takes place if the cell has passed the first *check point*. During its course, DNA synthesis takes place and all one-chromatid chromosomes are replicated to yield two-chromatid chromosomes.

The G2 Phase (also called *post-synthetic* or *pre-mitotic phase*) is used by the cell to prepare for mitosis. Proteins, synthesised in G1, are maturated to make them functional. Cells growing in tissues or on surfaces reduce or omit their adhesion. Importantly, there is a second *check point*, which can only be passed if the cell is large enough and the DNA replication is complete and successful.

The M Phase (*Mitosis*) is the phase in which the cell, the nucleus and the cytoplasm including all organelles divide into two identical daughter cells. In this process all 46 two-chromatid chromosomes are divided as well, causing the daughter cells to enter the G1 phase with a diploid set of 46 one-chromatid chromosomes each. At the end of the M Phase, yet another *check point* controls the proper procedure of the division [36].

Ultimately, the result of mitotic cell division is two, identical daughter cells. The rate, at which this happens can be described using the generation time t_g [h] or the specific growth rate μ [1/h] (also referred to as "growth rate" for simplicity) [37].

If a closed system is assumed and cell death is neglected, the increase of the cell number at a given time point depends only on the cell number (n) and the specific growth rate μ (Eq.1); the cell proliferation follows an exponential growth [37].

$$\frac{dn}{dt} = \mu n \qquad \textbf{Equation 1}$$

Furthermore, if a constant μ is presumed, the cell number (n_2) after a given time can be calculated from the following form (Eq. 2) after integrating Equation 1 over the time (t_1, t_2) [37]:

$$n_2 = n_1 e^{\mu (t_2 - t_1)} \qquad \textbf{Equation 2}$$

Consequently, the specific growth rate (μ) and the generation time (t_g) can be calculated (Eq. 3 and 4). However, it needs to be kept in mind that the calculated specific growth rate may differ from the actual specific growth rate μ (t) since some cells can enter the quiescent state or die (see above).

$$\mu = \frac{\ln \frac{n_2}{n_1}}{\Delta t} \qquad \textbf{Equation 3}$$

$$t_g = \frac{\ln 2}{\mu} \qquad \textbf{Equation 4}$$

1.6 The mammalian cell cycle in production processes and research of cell cycle dependent behaviour

As described above, the biological functions of each cell cycle phase differ largely [36]. This is why previous studies used a multi-staged population balance model, based on cell volume and DNA content, to describe myeloma cell cultures in terms of cell cycle dynamics. Comparisons of simulated results and experimental data from flow cytometry showed that this model is capable of describing the cell population dynamics qualitatively [38].

Nonetheless, process control strategies conventionally neglect these effects. Instead, a common, averaged cell behaviour is mostly assumed [29]. This can describe the macroscopic behaviour of cultures in a sufficiently accurate manner for many purposes, as proven by successful applications [4]. However, this approach is intrinsically biased, since culture inhomogeneity can arise from a variety of causes with the progress of the cell cycle being one of the main contributors (see Section 1.4).

In order to better understand the quantitative impact of such population heterogeneities, it is necessary to obtain highly time and cell cycle resolved metabolic data.

There are studies aiming to implement flow cytometry in an automated, on-line compatible manner to obtain such data. They are basically approaches to re-implement manual off-line protocols with the means of automation. Accordingly, hardware and financial requirements are high [39–41].

By its very definition, research on cell cycle dependent behaviour requires knowledge of the behaviour as well the cell cycle phases of the cells. There are two general approaches to obtain such data. For both of them, the cell cycle status needs to be assessed:

a. Single cell analysis:
   By design, the measured data can be assigned to a single cell and therefore to a single cell cycle phase. However, this approach is very challenging and not

feasible for most quantitative questions due to limited sample amounts and low analytical sensitivity.

b. Synchronised cell culture:
   The basic principle is to generate cultures, in which the number of individual cells undergoing a specific cell cycle phase is larger than that in non-synchronised cultures. Thereby, macroscopic measurements of metabolic behaviour can be assigned to distinct cell cycle phases. Ideally, all cells should be in a specific cell cycle phase at the same time. However, this is not mandatory.

For the purposes of this study, synchronised cell cultures are the more suitable option.

1.6.1 Synchronisation techniques: Overview

Synchronised cell culture is a powerful method to examine possible interdependencies between the mammalian cell cycle and cellular behaviour. In order to yield biologically meaningful and applicable data, studies have to be conducted under near-physiological conditions.

There is a variety of proclaimed synchronisation methods available. They differ in their approaches or modes of action and only a subset is suitable for cell cycle specific studies. Optimally, cells should form a homogeneous culture with regard to all major biologic characteristics and - most importantly - maintain physiological conditions [29, 35]. Those criteria have previously been summarised as follows:

1) *“In synchronized culture, every cell parameter should have similar value as cells in the corresponding cell cycle phase in an unsynchronized culture.*

2) *Further unaffected cell growth after synchronization. Average kinetics should behave similarly in both non-synchronized and synchronized cultivations after integration over integer multiples of the cell cycle duration.*

3) *Minimal increase in cell number during the interdivision time. This corresponds to a short fraction of time for division, compared to the duration of the cell cycle.*

4) *Narrower DNA distribution and narrower size distribution compared to non-synchronized culture. The progress of both distributions must be coherent with the cell growth and the doubling times."* [29]

The first two criteria are important to distinguish actual synchronization from arbitrary perturbations of the metabolism. The third and fourth ones can be measured and used to assess the synchronicity of cultures.

Over time, different methods have been developed and used in quest of suitable and ideally simple ways to obtain synchronized cultures. They can be subcategorized into two schools of thought [29]: whole culture and selective synchronization methods, as described in the following.

1.6.2 Whole culture synchronisation methods

The axiom of all whole culture synchronisation methods is that the treatment of whole cell cultures in order to force them into synchronised behaviour is a permissible method to generate synchronised cultures.

This category is largely synonymous with chemical methods (with the exception of the physical method of temperature reduction). The most popular protocols are serum starvation and thymidine block. In case of serum starvation, cells are pointedly deprived of serum. As a consequence, they cease to proliferate. When serum is added, cells resume to proliferate and start to divide at approximately the same time [42, 43]. In case of thymidine block, the medium is supplemented with excessive amounts of thymidine. Due to negative feedback regulation, the high thymidine concentrations interrupt the deoxynucleotide metabolism. As a result, cells become arrested at some point in the S phase, when they lack the remaining three nucleotides for proper DNA replication [44, 45].

These methods, among others, have been shown to align cells in respect to a certain property, e.g. DNA content. In case of thymidine block, cells were reported to be arrested with an S Phase like DNA amount [46]. In case of serum starvation, it is a G1 Phase like DNA amount [42, 43].

However, the size distributions do not decrease [46]. This is a common flaw of whole culture methods – partial alignment of certain properties, while others e.g. cell size indicate that the progression through the cell cycle has been perturbed, rather than synchronised [35, 42–47] (see criteria above).

Notably, it is not generally agreed that selective methods are superior to whole cell culture methods. There are groups arguing in favour of their applicability. Nevertheless even they acknowledge that whole cell cultures can't be employed without inevitably changing the size-to-cell-cycle-relationship to arbitrary states [47].

1.6.3 Selective synchronisation methods

The approach of selective synchronisation methods is considerably more stringent. In order to yield synchronised cultures, cells in the cell cycle phase of interest must be selected and separated to form a new culture. Accordingly, these methods mostly fall into the category of physical methods. Also, they are substantially more laborious. Nevertheless, the resulting cultures fulfil the synchronisation criteria (see Section 1.6.1) and the cells have - ideally - not undergone any interference.

Of course, in practical application different methods come with certain limitations. These include synchronisation rates below 100%, the cultures are regarded as partially synchronised.

Typical selective synchronisation methods are gradient centrifugation [48], live cell sorting [49] as well as microfluidic sorting, both according to size [50, 51]. These Methods share the approach to select cells based on their size, which is closely linked to their cell cycle state (see Section 1.6.3.1). However, they also share their major disadvantage: only a relatively low number of cells can be selected, putting them closer

to single cell analysis than to synchronised cultures at scales in which common process control is applicable.

The “eukaryotic baby machine” (membrane elution) as well as the “mitotic shake-off” methods are based on the fact that adherent cell lines are less firmly attached to surfaces during mitosis. Accordingly, cells in early G1 Phase can be obtained by flushing to form highly synchronous and unperturbed cultures [52, 53]. Nonetheless, up-scaling is equally challenging. Furthermore, the methods are only applicable to adherent cell lines.

An additional method, combining better scalability with sufficiently accurate selection, is the centrifugal counter flow elutriation [54].

1.6.3.1 Counter flow elutriation

Counter flow elutriation and its application to synchronise mammalian cell cultures have been described previously [54, 56, 57], especially in regard to the physical conditions [28, 29, 58, 59]. Hence, only a short summary will be given here.

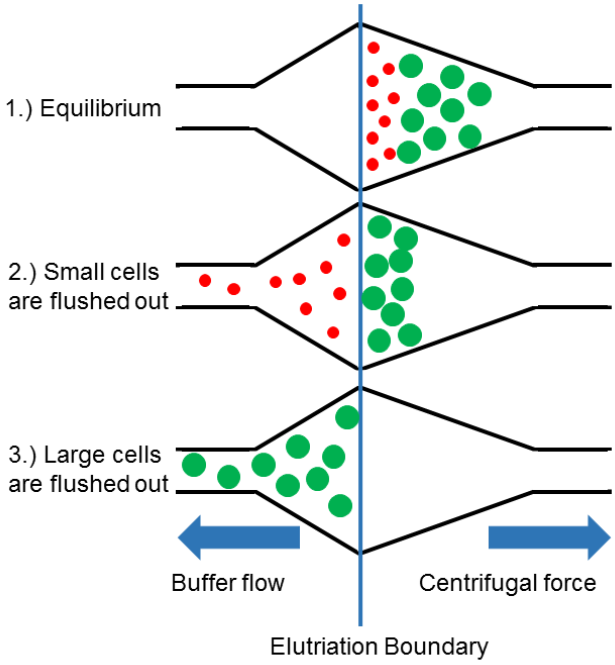

Figure 2: Counter flow elutriation.
During initial conditions (1.) all cells reach an equilibrium, smaller cells closer the elutriation boundary, larger cells further away from it. When the buffer flow is increased gradually, small cells are flushed out at lower flow rates, hence earlier (2.) than larger cells (3.) [55].

Elutriation is a physical, selective method to separate mammalian cells according to their size. Since mammalian cells grow in size, as they progress through G1-, S- and G2 Phase until they divide in mitosis (M) to yield two identical daughter cells, each cell cycle phase is characterised by a unique size. Therefore, different cell sizes are synonymous with different cell cycle

phases, especially in the context of monocultures of homogeneous mammalian cell lines. This is why mammalian cells sorted by size can yield (partially) synchronised cultures, in which an increased number of cells undergo the same cell cycle phase at the same time.

An elutriation setup consists of a centrifuge with a special rotor. In this rotor, a flow chamber and a counter weight are mounted. The flow chamber is characterised by a double funnel shape, yielding different cross-sectional areas at different points in the chamber.

In operation, the rotor is spinning at a defined speed, creating a constant centrifugal force (g force) away from the axis of rotation. Meanwhile a constant flow of aqueous buffer is applied through the elutriation chamber, towards the axis of rotation, yielding a counter flow velocity. These two forces can be adjusted in order to create an equilibrium for the particle properties of interest: size and density. This is possible as long as the density of the particle is higher than the density of the aqueous buffer, which is the case for mammalian cell lines.

Cellular densities remain nearly constant throughout the cell cycle and their change can be omitted in this context. Hence, cells are separated depending on their size. Although flexible, the shape of mammalian cells can be approximated by a sphere. Since the surface of a sphere increases with the radius to the power of 2, while the volume increases with the radius to the power of 3, small spheres have a higher surface/volume ratio. Hence, small cells have a higher surface/weight ratio and are predominantly affected by the buffer flow, rather than the centrifugal force. As a result, they enter the state of equilibrium at a point in the flow chamber with larger cross-sectional area and lower flow/area ratio, closer to the axis of rotation.

Correspondingly, larger cells are mainly affected by the centrifugal force and enter their state of equilibrium further away from the axis of rotation at a point with lower cross-sectional area and higher flow/area ratio.

Starting from this equilibrium, cells can be separated by increasing the buffer flow rate and/or decreasing the rotor speed. As the buffer flow increases in comparison to the centrifugal force, all cells shift towards the axis of rotation to find a new equilibrium. If

cells cross the elutriation boundary, from which the flow/area ratio increases, those cells are flushed out of the chamber and are collected as a fraction. By further increasing the buffer flow in comparison to the centrifugal force, larger cells can be elutriated from the chamber, yielding fractions of different cell sizes and hence, cell cycle phases.

1.7 Fluorescence ubiquitination cell cycle indicator (FUCCI)

Apart from bioprocess control, there are other fields of research with a keen interest in the mammalian cell cycle. In order to better understand the embryonic development on a cellular level, a novel tool of intracellular fluorescent probes was generated - the Fluorescence Ubiquitination Cell Cycle Indicator (FUCCI) [60, 61]. It is a remarkable tool, precisely based on the mammalian ubiquitination system and well suited for applications beyond its initial use.

1.7.1 Ubiquitination

Ubiquitination is a form of post translational modification with different functions in eukaryotic cells. The term denotes the covalent linking of the small regulatory protein ubiquitin (8.5 kDa) [62] to a target protein. While it can be associated with different functions, poly-ubiquitination, the addition of several ubiquitin molecules in a chain, leads to proteasomal degradation. This ubiquitin-proteasome system is responsible for most of the protein degradation and, in combination with transcriptional and post-transcriptional regulation, essential for the control of the cell cycle [63, 64].

1.7.2 Design of the FUCCI system

The Fluorescence Ubiquitination Cell Cycle Indicator (FUCCI) system is designed in a way, which allows the expression of fluorescent proteins of different colours under the control of the cell cycle without affecting it. This was achieved by designing corresponding genes for a variety of fusion proteins. Each consists of the desired fluorescent protein, linked to domains of proteins which are part of the cell cycle regulation.

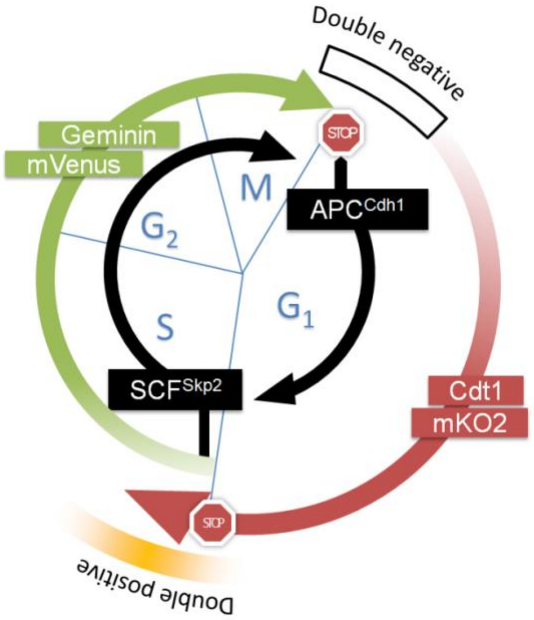

Figure 3: Cell cycle regulation and FUCCI
Graph was published previously [98].

The elegance of the system lies in the fact that only those protein domains were included, which allow the constructs to be passively expressed and degraded under control of the cell cycle. Meanwhile, the constructs have no active impact on the cell cycle. This was developed and validated in extensive deletion studies [60, 61]. The two essential proteins in this context are Cdt1 and Geminin, which accumulate in the G1 and S/G2/M phase, respectively [65]. These proteins are under control of the protein complexes APC^{Cdh1} and SCF^{Skp2} , respectively and involved in the accurate regulation of "licensing" origins of replication [66], which is meant to happen only once per cell cycle.

This is realised by the fact that the SCF^{SKP2} complex is a substrate of the APC^{Cdh1} complex but also an inhibitor for it. Hence they are active in different phases of the cell cycle: APC^{Cdh1} in the late M and G1 phases, SCF^{SKP2} in the S and G2 phases [67–69].

The FUCCI constructs used in this work harness this regulatory process by fusing the amino acids 30-120 of the human Cdt1 (hCdt1) to the fluorescent protein mKO2. Likewise, different domains of the human Geminin, hGeminin(1/60) and hGeminin(1/110), were combined with mVenus, a fluorescent protein of a different colour. While the florescent properties of mKO2 (Excitation: 551 nm, Emission: 565 nm) and mVenus (Excitation: 515 nm, Emission: 528 nm) differ from one another,

both are monomeric proteins that can be expressed, maturated and degraded rapidly enough to indicate the cell cycle phase. This is a pivotal requirement, only specialised fluorophores are capable of it [61, 70, 71].

To date, the FUCCI system was implemented in different organisms [72] comprising various adherent cell lines and animal models including mice [73, 74], zebra fish [75], drosophila [76] and even *ciona intestinales*, a sea squirt [77]. They were used for various developmental studies, stem cell research [78] as well as drug screening [79, 80].

1.8 Applicability of the FUCCI system in bioprocess monitoring

So far, the FUCCI system has not been implemented in any industrially relevant production cell line (like CHO-K1), as all established FUCCI cell lines stem from HeLa, NMuMG or COS [72].

To the best of our knowledge, no work of using the FUCCI system as a potential fluorescence read out of the cell cycle distributions in bioreactors has been done yet. Due to the inevitable interconnection of cell cycle distribution and specific growth rate (μ) such a method would not only be helpful in the determination of cell cycle dependent behaviour but also most useful in process monitoring and control. Therefore, such a method was developed and evaluated in this thesis.

2. Elutriation and near physiological synchronisation of HEK293s cells

The following Chapter[1] focuses on a near-physiological method for cell cycle synchronisation and synchronized cultivation, as well as their implications on growth and basic metabolic behaviour. This kind of validated synchronization using widely undisturbed cells of known cell cycle status is pivotal for further analysis in order to understand the cell cycle dependent behaviour of mammalian cells. Here this was achieved by partial synchronization using centrifugal counter flow elutriation.

2.1 Technical and theoretical background

2.1.1 Validation of near-physiological conditions

The core requirement of studies targeting the cell cycle is basic, yet essential: correlations and effects identified in these need to be transferrable to unaltered, e.g. not artificially synchronized cultures under physiological conditions. As discussed above, several methods of synchronisation – including all whole culture and therefore all chemical methods - fail with regard to this requirement. Technologies based on influencing the cell cycle, by definition, can never be utilised to monitor an undisturbed cell cycle progression.

[1]The content of this Chapter, including Figure 4, Figure 7 and Figure 9, was published previously [59, 103] and adapted for the this thesis.

Various experiments were performed with the involvement of student Alan Eduardo Castillo Salvador during his diploma project [104].

Nonetheless, even methods based on principles, which are *a priori* compatible with an undisturbed cell cycle progression, in this case counter-flow elutriation, need to be monitored for their physiological conditions, in order to validate that observed effects do not arise from other types of limitation (e.g. insufficient oxygen supply).

As the hardware setup and work flow do not permit to guarantee and monitor physiological conditions at all times during handling, the assessment of overall near-physiological conditions has to be achieved indirectly, by assessing the cellular behaviour after elutriation.

2.2 Material and methods

2.2.1 Mammalian cell line and culture

The Human Embryonic Kidney cell line 293s (HEK293s) used for these experiments is a derivative of HEK293 (ATCC no. CRL 1573), adapted to growth in suspension [15, 16]. They were kindly provided by Dr. Manfred Wirth, Dept. of Gene Regulation and Differentiation, Helmholtz Centre for Infection Research (HZI), Braunschweig, Germany.

Two different chemically defined, serum free media were used in different cultivations steps throughout the experiment.

- 293 SFM II (Gibco, No. 11686-029, Thermo Fisher Scientific, Waltham, MA, USA) supplemented with 4 mM L-Glutamine.
- FreeStyle 293 Expression Medium (Gibco, No. 12338-018, Thermo Fisher Scientific, Waltham, MA, USA)

FreeStyle 293 was used for the initial expansion cultures, which consisted of several subsequent expansion steps. Each culture was inoculated at a density calculated based on the average specific growth rates for the used media type (FreeStyle $\mu = 0.029$ [1/h], generation time: 24 h; SFMII: $\mu = 0.023$ [1/h], generation time: 30 h) and Equation 2. All cultures were kept in the range of 0.3 – 2.5 Mio/ml at all times.

Depending on the required volumes, cells were cultured in Erlenmeyer baffled cell culture flasks (125 ml: type 431405, 250 ml: type 431407; Corning, New York, USA) with filling volumes of 40 ml and 80 ml respectively.

Exactly 64 h prior to elutriation the medium was replaced with 293 SFM II to minimize cell aggregation. The inoculation cell density was calculated to yield about 2 Mio/ml at the time of elutriation.

A constant humidified atmosphere of 37°C and 8% CO_2, as well as a continuous shaking (200 rpm) were kept throughout the culture. All cultures were maintained free of any antibiotics and were tested negative for mycoplasma (PCR Mycoplasma Test Kit I/C, PromoCell, Heidelberg, Germany).

2.2.2 PBS

Phosphate-buffered saline was prepared according to the Cold Spring Harbour Protocols without Ca^{2+} and Mg^{2+}, pH adjusted to 7.4 [81].

Table 1: PBS composition

Reagent	Amount to add (for 1× solution)	Final concentration (1×)	Amount to add (for 10× stock)	Final concentration (10×)
NaCl	8 g	137 mM	80 g	1.37 M
KCl	0.2 g	2.7 mM	2 g	27 mM
Na_2HPO_4	1.44 g	10 mM	14.4 g	100 mM
KH_2PO_4	0.24 g	1.8 mM	2.4 g	18 mM

2.2.3 Elutriation

Centrifugal elutriation was performed using a JE-5.0 Elutriation System [55]. In part at the UKE in the group of Prof. Dr. Ansgar Lohse and PD Dr. Johannes Herkel.

Later experiments were conducted using a new Elutriation setup consisting of an Avanti J-26S XP Centrifuge and a JE-5.0 Elutriation System (Beckman Coulter, Brea, CA, USA).

The process was adapted from earlier publications [54] and experience in our group [28, 58]. As described in the latter publications, minor changes were applied to the tubing system. The unsynchronised cells were injected into the system after the bubble trap, to avoid sedimentation of cells in it.

Prior to each run, the elutriation setup was sterilised using 100 ml 5% sodium hypochlorite solution. Subsequently the system was thoroughly flushed with at least 1 L sterile, ultrapure water (Millipore, Billerica, MA, USA) and a constant flow of 10 ml/min Ca^{2+} and Mg^{2+} free PBS, including 2 mM EDTA, was established at a rotor speed of 1500 rpm. During loading with the unsynchronised HEK293s culture (545 Mio. Cells), the PBS flow rate was decreased to 5 ml/min and the elutriation boundary was monitored optically using the stroboscope lamp.

After formation of this initial equilibrium state, cells with gradually increasing sizes were elutriated out of the chamber by incremental increase of the buffer flow rate. For each fraction 100 – 150 ml were collected to ensure proper formation of each equilibrium stage. Collected fraction were centrifuged for 5 min at 300 g, the PBS supernatants were discarded, the cell pellets resuspended in pre-warmed 293 SFM II medium (Gibco, No. 11686-029, Thermo Fisher Scientific, Waltham, MA, USA) supplemented with 4 mM L-Glutamine and pooled. VCD, DCD, TCD and viability were quantified to assess the elutriation efficiency.

Three fractions were collected, based on prior optimisation experiments.

Table 2: Elutriation flow rates HEK293s

Fraction	Lower flow rate [ml/min]	Upper flow rate [ml/min]
X0	5 + Loading	10
X1	>10	17
X2	>17	34

In parallel a negative control culture (NC) was generated. These cells underwent the thermal conditions of the elutriation process and, where applicable in the earlier experiments, the transport stress. However, they were not elutriated.

2.2.4 Cultivation of synchronised cell cultures

The synchronised cultures from elutriation and the negative control were cultured under the conditions explained earlier. The first 15 h of culture were conducted in SFMII medium in order to let the cells recover without the need to adapt to changed medium conditions. Subsequently the medium was exchanged for pre-warmed FreeStyle medium.

Every 6 h 1.2 ml samples were taken for subsequent analysis of the viable cell density, the cell viability, the total cell count and size distribution, the glucose and lactate concentrations and the cell cycle state using flow cytometry (FACS Canto II). Each sample volume was replaced with pre-warmed FreeStyle medium. 72 h after elutriation 50% volume of all cultures were replaced with fresh, pre-warmed medium as well, to avoid growth inhibition by high cell densities.

2.2.5 Viable cell density and cell viability

Viable and dead cells were differentiated and quantified using an *Improved Neubauer*-Chamber (BRAND, Wertheim, Germany). Cell suspensions were diluted in a 0.2% Trypan-Blue/PBS solution (Lonza, Basel, Switzerland). Trypan blue cannot enter living

cells due to their membrane potential. Dead cells however are stained by it and appear blue under the optical microscope. Hence, living and dead cells can be distinguished. The viable cell density (*n*), the dead cell density (n_D), total cell density (n_T) and viability [%] are calculated as follows (Eq. 5-8):

$$n = \frac{\bar{n}_L \, d}{V_{sq}} \qquad \textbf{Equation 5}$$

$$n_D = \frac{\bar{n}_D \, d}{V_{sq}} \qquad \textbf{Equation 6}$$

$$n_T = n + n_D \qquad \textbf{Equation 7}$$

$$viability\ [\%] = \frac{\bar{n}_L \times 100}{\bar{n}_L + \bar{n}_D} \qquad \textbf{Equation 8}$$

n: Viable cell density [cells / ml]

n_D: Dead cell density [cells / ml]

n_T: Total cell density [cells / ml]

$viability\ [\%]$: Percentage of all cells negative for Trypan blue = alive

$\bar{n}_L$: average number of viable cells per large square (*Improved Neubauer chamber*)

$\bar{n}_D$: average number of dead cells per large square (*Improved Neubauer chamber*)

$V_{sq} = 10^{-4}$ ml: Volume per large square of *Improved Neubauer chamber* (length x width x height):

1mm x 1mm x 0,1mm = 0,1 mm^3 = 10^{-4} ml

d: Dilution factor (Trypan blue solution)

2.2.6 Cell counter

Total cell count and cell size distributions were quantified using a Z2 Particle Counter (Beckman Coulter, Brea, CA, USA). For each measurement, 100 µl cell suspension were diluted in 9.9 ml PBS without Ca^{2+} and Mg^{2+}. The size data, expressed as a histogram composed of 256 bins were exported and evaluated using Microsoft Excel (Microsoft, Redmond, CA, USA). Analysis was limited to the size range of the cells (10.76 – 21 µm), debris was omitted. Prior to analysis, data was averaged using a sliding window covering seven bins. The typical data showed a Gaussian curve with tailing. The total cell count was calculated by addition of all cells under this curve. Since the counting principle does not distinguish between living and dead cells, this value corresponds to the living plus dead cells. Furthermore, the most common cells size was detected (modal value), it is referred to as the characteristic cell diameter (CCD).

2.2.7 Calculation of the specific growth rate (µ)

The specific growth rate (µ) was calculated from the Z2 Particle Counter data based on Equation 3, considering all exchanges of sample and medium. The data obtained from the Z2 Particle Counter has proven to vary less than that from the *Neubauer* chamber used in parallel.

The average standard error of the Z2 was about 2% (n = 3, technical replicates). Due to limited volume of the synchronised cultures, biological samples could not be taken in triplicates.

Calculating the time-dependent specific growth rate from this data needs to compensate for (a) dilution during the cultivation time caused by sampling loss and adding fresh medium and (b) noise (uncertainty) of each sample count.

The first was accomplished by introducing a theoretical cell density [59] which would theoretically be reached if dilution would not occur. Note that it does not consider any biological density related effects. From this, the oscillating specific growth rates were computed by fitting sub-sets of sampling points to a logarithmic oscillation function in a sliding window manner (method by U. Jandt, [59]; Fig. 4A), thereby directly allowing

to reconstruct the most probable specific growth rate for each time point by computing the first derivative of the oscillation function (Fig. 4B).

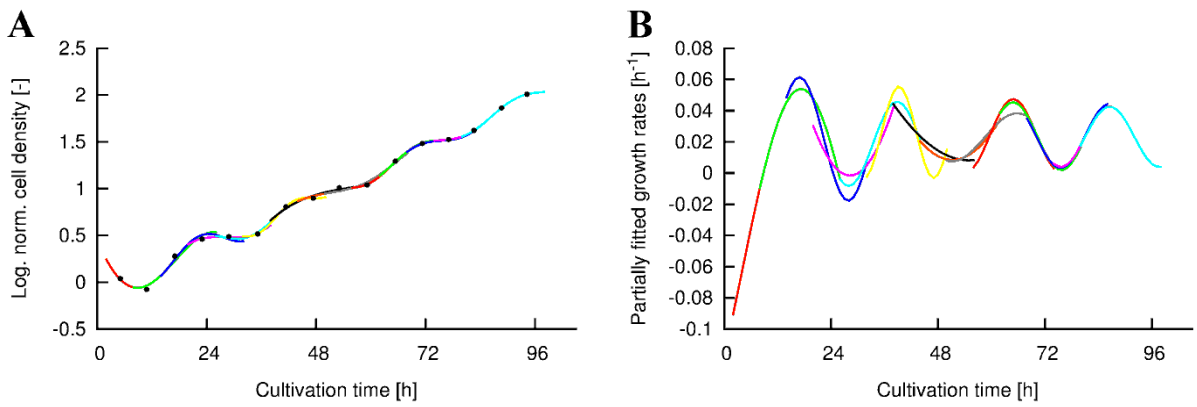

Figure 4: Example of the overlaying sliding window fits
for the data points of fraction X2, by U. Jandt [59]. A: Logarithm of the theoretical cell density. B: Corresponding estimated growth rates. The different colours represent the partially defined independent fitting functions, hence the calculated oscillating growth rates. Model and illustration by U. Jandt [59].

2.2.8 Cell cycle analysis using flow cytometry – FACS Canto II

HEK293s cells were fixated with PFA and stored in 70% EtOH at -20°C for later analysis at the Flow Cytometry Core Facility, Universitätsklinikum Eppendorf. The protocol was adapted from [82, 83].

2.2.8.1 Fixation of cells with formaldehyde

1 ml culture containing up to 2 Mio HEK293s cells/ml was transferred into a 1.5 ml Eppendorf tube and centrifuged for 2 min at 2000 rpm corresponding to 381 g at 4°C on a Bio Fresco Table top centrifuge (Thermo Fisher Scientific Inc., Waltham, MA, USA).

The supernatant was removed, frozen and stored at -20°C for later analysis. Subsequently the cells were washed once with PBS by additional centrifugation for 2 min at 2000 rpm at 4°C.

Again, the supernatant was removed by aspiration and 500 µl of cold PBS were added to the cell pellet. After gentle mixing, 500 µl ice cold, buffered 2% formaldehyde solution was added and mixed again. Incubation was conducted exactly 30 min at 4°C.

2.2.8.2 Permeabilisation and storage of cells using ethanol

The cells were spun down by centrifugation for 3 min at 2000 rpm corresponding to 381 g at 4°C Bio Fresco Table top centrifuge (Thermo Fisher Scientific Inc., Waltham, MA, USA) or 1800 rpm corresponding to 300 g at room temperature on a Fresco 21 Table top centrifuge (Thermo Fisher Scientific Inc., Waltham, MA, USA).

The supernatant was removed by aspiration. The cell pellet was subsequently washed once with cold 1x PBS and 1 ml of 70% ethanol at -20°C added drop-wise with the tube sitting on a vortex. The resulting cell suspension was stored at –20°C for at least 30 min for later flow cytometry analysis.

2.2.8.3 Staining with Propidium iodide

Propidium Iodide staining, and RNase digestion were conducted directly prior to flow cytometry measurement.

Cells were spun down by centrifugation for 5 min at 300 g and 4°C using a 5702R Refrigerated Centrifuge (Eppendorf, Hamburg, Germany), supernatant removed by aspiration and 500 µl of a solution containing 40 µg/ml of PI and 100 µg/ml of RNAse were added. Incubation of the cell suspension took place for 30 min at 650 rpm and 37°C in the dark on a Thermomixer R (Eppendorf, Hamburg, Germany).

After incubation, the tubes were transferred into a fridge at 4°C until analysis. If needed, samples were filtered through a cell trainer (Falcon 35-2235) to remove clumps before acquisition on the flow cytometer.

2.2.8.4 Flow cytometry - FACS Canto II

A FACS Canto II (Becton Dickinson, Franklin Lakes, NJ, USA) at the Flow Cytometry Core Facility, Universitätsklinikum Eppendorf, was used to analyse the cells in regard to their individual properties. Those include size and granularity (approximately represented by forward scatter = FSC and side scatter = SSC, respectively) as well the fluorescent markers. In this case fluorescence of DNA bound Propidium Iodide (detected in the PE-A or PerCP-A channel) was used to assess the total DNA content of the cells. Expression of the reporter gene d2eGFP was monitored in the FITC-A channel.

2.2.8.5 Flow cytometry data analysis

For reasons of simplicity and readability, this Section also includes the analysis of d2eGFP expression which is discussed in the 3rd Chapter.

Flow cytometry data was analysed using Flowing Software, version 2.5.1 [84]. SSC-A vs. FSC-A was gated less stringent and only small debris was excluded. Doublets were removed by gating using FSC-H vs. FSC-W and SSC-H vs. SSC-W. All gates and the region were combined using the AND operator for the histogram, analysis was conducted consistent for all data.

Where applicable, expression of the reporter plasmid d2eGFP was detected in the FITC-A channel. The same threshold value was used for all samples of each experiment to define d2eGFP positive cells.

In non-transfected cells, Propidium iodide stained DNA was detected in the PE-A channel. For transfected, d2eGFP expressing cells, PerCP-A was used to detect Propidium iodide stained DNA to minimise crosstalk from d2eGFP (FITC-A channel).

Independent of the detection channel DNA histogram data was exported and quantified using a Microsoft Excel script (Microsoft, Redmond, CA, USA). The numeric analysis of the cell cycle was conducted by setting determined limits, relative to the first maximum of the DNA distribution. The 1st maximum corresponds to the G1 phase, when all chromosomes exist in their one-chromatid form.

These strict limits represent the criteria to distinguish the cell cycle phases from another. The G1 Phase was defined 0.7-1.3x the DNA-amount of the first maximum, the S Phase 1.3-1.8x and the G2/M Phase 1.8-2.3x. The integration within these ranges, divided by the total number of cells in the histogram, multiplied by 100 yields the percentage of cells in this specific cell cycle phase. This approach using pre-defined borders can limit the accuracy if samples show large shifts of total PI fluorescence (PE-A / PerCP-A channel) despite comparable histogram pattern. This is a possible artefact arising from fixation, storage and/or staining procedures. However, it allows reliable, fully automated relative comparison between different experiments and reduces subjectivity.

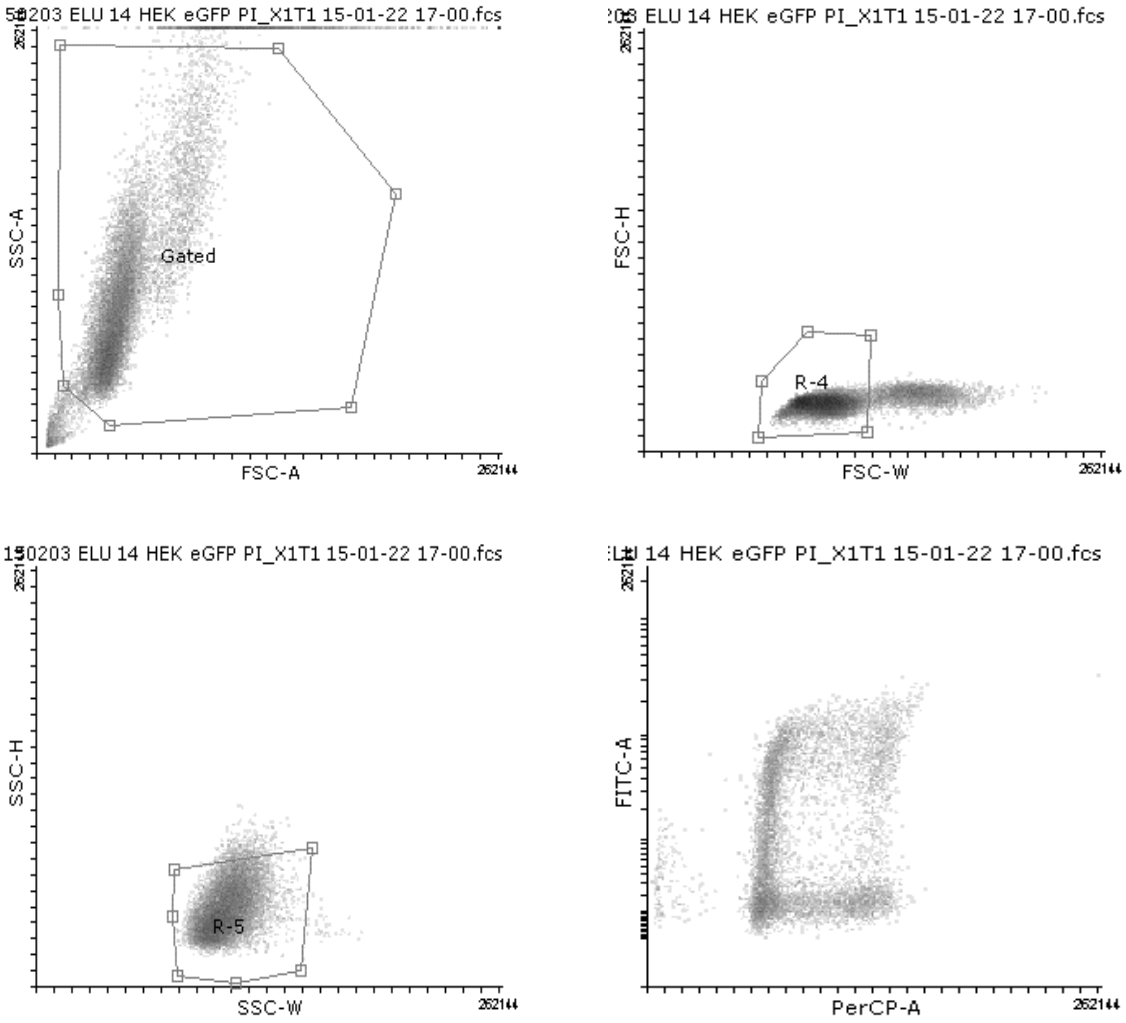

Figure 5: Gating strategy HEK293s cells
A: Removing debris. B and C: Gating for single cells. D: PerCP vs. FITC-A - crosstalk is moderate.

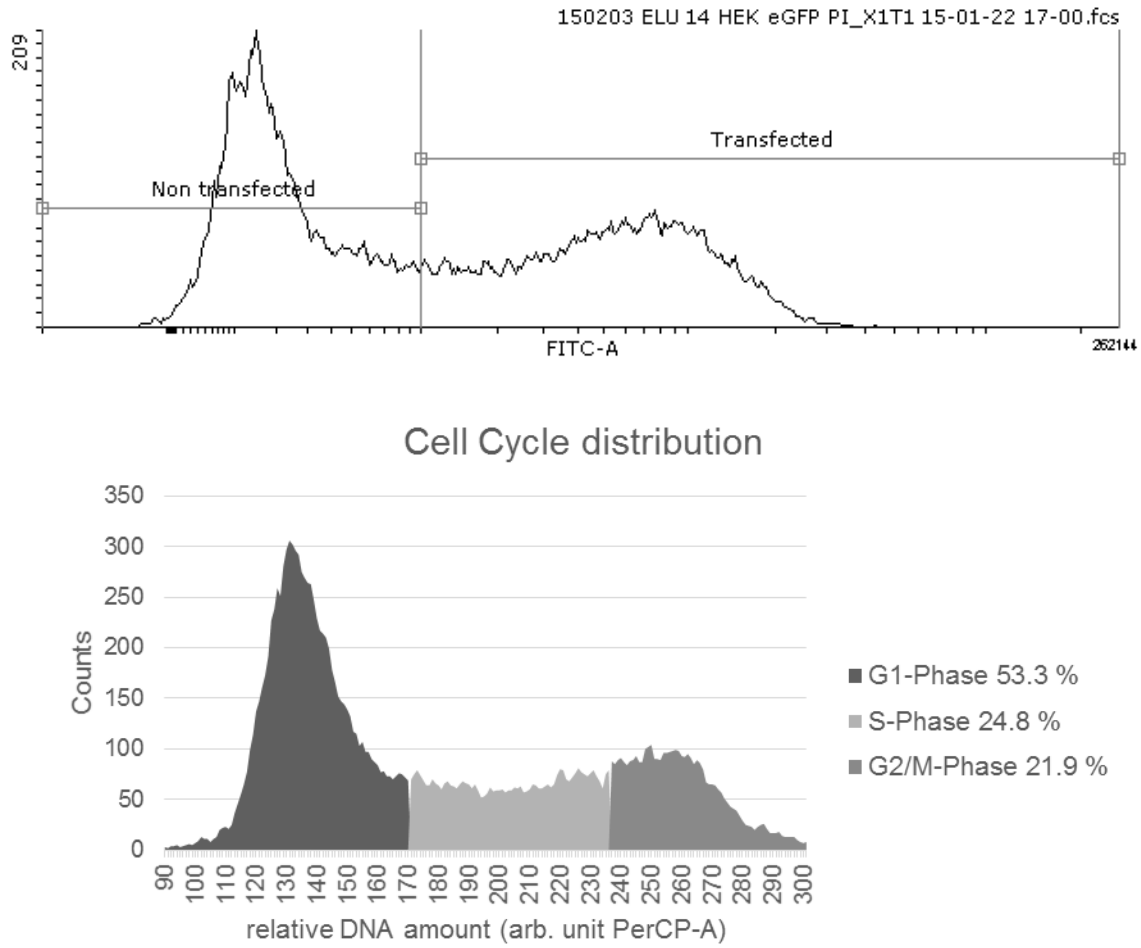

Figure 6: Quantification of eGFP and DNA
Upper Section: d2eGFP expression (detected in the FITC-A channel), determination of positive transfection based on threshold. Lower: Example of DNA content-based determination of cell cycle distribution (PE-A / PerCP-A channel) with fixed thresholds and variable peak detection.

2.2.9 Calculation of normalised cell cycle position

The results of the flow cytometry analysis, expressed in percentages of G1, S and G2/M were used to calculate the normalised cell cycle position as described by U. Jandt in a previous publication [59].

It is a polar coordinate description with two characteristics:

1. t_{CC}: The normalised cell cycle position – a one-dimensional value in the range [0,1]

2. I_{CC}: The amplitude of the “excitation”

In short, the t_{CC} represents the cell cycle position of the culture. In other words, which cell cycle phases (G1, S or G2/M) are most abundant at a given point in time. The I_{CC} is a measure about the quantitative relation of the most abundant cell cycle phase to the less abundant ones.

In synchronised cultures all or most cells are in the same cell cycle phase. They progress through the cell cycle in a synchronised manner, hence from one cell cycle phase to the next. Likewise, the t_{CC} value of the culture changes. Since a synchronised culture can perform several iterations of synchronous proliferation, it can reach the same t_{CC} values multiple times.

Meanwhile, the degree of synchronicity (represented by the I_{CC}) is likely to decrease over time, as the duration of a cell cycle is not necessarily identical for all cells in the culture.

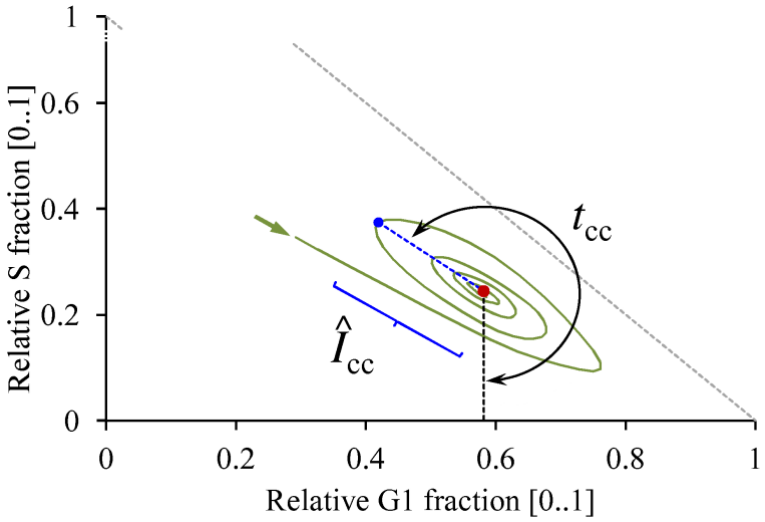

Figure 7: Calculation of t_{CC} and I_{CC} based on G1 and S
The relative S fraction [0..1] is plotted against the relative G1 fraction [0..1]. Synchronised cultures follow a spiral, heading towards the steady, unsynchronised state (the centre of gravity). The normalised cell cycle position (t_{CC}) is represented by the angle, relative to the starting position. The amplitude (I_{CC}) by the distance to the centre of gravity. Model and illustration by U. Jandt [59].

2.3 Results and discussion

The stated procedures for pre-culture and Elutriation are the result of extensive optimization efforts concerning the cell culture medium, elutriation conditions and transport procedures.

The used cell line HEK293s was previously adapted to growth in suspension [15, 16]. Nevertheless, it has a certain tendency to grow in doublets or larger aggregates, especially at higher cell densities. Self-explanatory, this is obstructive for the use of counter flow elutriation. The approach of separating cells by size and therefore cell cycle phase obviously can only be applied to single cells. Doublets of smaller cells (G1) could be enriched in the fraction of larger (G2/M) single cells. Furthermore, aggregates of more than two cells are too large for the targeted equilibrium conditions. They form dense pellets in the elutriation chamber.

These pellets are unable to resuspend properly throughout the course of elutriation. If they get disrupted towards the end of the elutriation run, the resulting aggregates consist of cells in different cell cycle phases, yielding inhomogeneous fractions. In order to minimize this obstacle, the cell culture conditions were optimised in a successive manner.

According to the manufacturer [85], the FreeStyle medium is suitable for transient transfection and protein production, the main criteria for this application. Unfortunately, it is not optimised for suspension cultures and therefore increases the stated tendency to form aggregates. The SFMII medium on the other hand, is not suitable for transfection but optimised for suspension cultures. Consequently, the described regime of different culture steps was developed.

The elutriation process was modified in the following manner. Compared to previous studies, using CHO-K1 and AGE1.hn cells [29, 58], the number of revolutions per minute (RPM) had to be decreased to 1500 to yield best separation efficiencies in combination with the available, linear, pulsation free range of flow rate (5 – 45 ml/min).

One major challenge was the geographic distance between the different pieces of equipment, as elutriation and subsequent culture were initially performed in different

laboratories. Negative controls simulating the transport conditions indicated substantial stress for the cultures. With which the used HEK293s cultures were less capable of coping with compared to the CHO-K1 and AGE1.hn cells in previous studies [29, 58]. This is in line with multiple incidents with total loss of viability (data not shown). In order to minimize stress, all cultures were diluted to a maximum cell density of 1 Mio/ml in fresh, pre-warmed media, prior to each transport.

Data from biological experiments was only used for analysis if the growth behaviour subsequent to the elutriation procedures and all transport processes validated at least near-physiological conditions.

For further experiments (3rd - 6th Chapter), a new Avanti J-26S XP based elutriator setup (Beckman Coulter, Brea, CA, USA) could be installed locally, cancelling out any transport related obstacles (see acknowledgements and funding).

2.3.1 Separation of mammalian cells based on their size

In Table 3: Distribution of cell characteristics after elutriation the cell properties of the fractions after elutriation (X0 - X2) as well as a negative control (NC) are listed. They include the characteristic cell cycle diameter (CCD [µm]), the yield [%], and the percentages of the cell cycle phases (G1, S and G1/M) as well as the resulting normalised cell cycle position (t_{CC}) and amplitude (I_{CC}) values.

Fraction X0 represents the flow through, collected during loading of the elutriation chamber. It displays the smallest characteristic cell diameter, compared the other fractions.

As intended, a difference in size (here 1.1 µm) between fractions X1 and X2 could be detected. It illustrates that the method was capable to separate the culture into two subcultures enriched in different sizes. More importantly, this difference in size is associated with different cell cycle distributions. While fraction X1 is rich in G1 (74.4%) and very low in G2/M (5.1%), fraction X2 shows strongly differing relations (36% G1, 30% G2/M).

This is even more obvious from the one dimensional cell cycle position (t_{CC}) values of X1 and X2, which are 0.21 and 0.61, respectively.

Furthermore, Fractions X1 and X2 exhibit relatively high amplitudes (I_{CC}) of 0.16 and 0.24, indicating strong oscillation. In line with expectations, the negative control (NC) displays a very low I_{CC} value of 0.04. A t_{CC} value is not provided for NC, since it is poorly defined and hence arbitrary.

Due to the fact that the flow through of Fraction X0 is slightly enriched for smaller cells an I_{CC} of 0.10 was detected.

Table 3: Distribution of cell characteristics after elutriation
Modification of [59]**.**

Fraction	CCD (µm)	Yield (%)	G_1 (%)	S (%)	G_2/M (%)	t_{CC}	I_{CC}
NC	15	–	55.9	28	16.1	–	0.04
Fraction 0	14.3	34	68.1	23	8.9	0.23	0.10
Fraction 1	14.4	16	74.4	20.5	5.1	0.21	0.16
Fraction 2	15.5	22	36	34	30	0.69	0.24

2.3.2 Synchronised cultivation

The different fractions, as well as the negative control were used to inoculate cultures. Those fractions enriched for cells in different cell cycle phases (fraction X1: G1, fraction X2: G2/M) were expected to display synchronised growth.

One pivotal factor is an appropriate initial cell density. The used HEK293s cell line can react sensitive to insufficiently low inoculation densities. If a certain density is undershot, cultures are prone to long lag phases or may die of entirely. On the other hand, high densities (>3 Mio/ml) inhibit growth and contribute to the formation of aggregates as discussed above. Hence, an optimised initial density of 0.5 Mio/ml was chosen to allow an undisturbed growth for as long as possible. Subsequently a 1:1 dilution was applied to prolong the exponential growth.

The resulting growth data is shown in Figure 9. A represents the negative control (NC), B fraction X0, C fraction X1 and D fraction X2. The first graph in each panel depicts the characteristic cell diameter (CCD), the second (white rhombus) illustrates the specific growth rate (µ), calculated from the theoretical cell densities. The third graph visualizes the percentages of cell cycle phases. For the fraction X1 and X2 the relative cell cycle position (t_{CC}) and the intensity of synchronization (I_{CC}) are shown in an additional plot.

The negative control (NC) and fraction X0 displayed a certain amount of variation for different parameters but not in a synchronization implying manner. None of the curves follow any clear periodic pattern. The CCD curve of fraction X0 displays 3 maxima, separated by about 24 h which is in line with the slight enrichment for smaller cells. Nevertheless, growth rate (µ) and cell cycle data don't confirm synchronization.

The growth rates (µ) and CCDs of the fractions X1 and X2 follow periodical oscillations with a phase length of 24 h. This value is to be expected for the cell line HEK293s as it has a generation time of approximately 24 h. Both curves display a saw tooth pattern. While the growth rates oscillate relatively smoothly, the characteristic cell diameter decrease rather rapidly from values from around 16 µm to 14 µm. This reflects the synchronised mitosis. By definition, the difference in the mass and hence the volume of cells throughout the mitosis, supposed equal distribution of cell mass to the daughter cells, should change by a factor of 2. This is not directly represented by the characteristic cell diameter values of 16 µm and 14 µm.

The volume of mammalian cells can be approximated as a sphere:

$$V = \frac{4}{3}\,\pi\, r^3 \qquad \textbf{Equation 9}$$

Using 8 µm and 7 µm as radius (Eq. 10), corresponding to the characteristic cell cycle diameters, the ratio is < 2.

$$\frac{r_{X2}^3}{r_{X1}^3} = \left(\frac{8}{7}\right)^3 = 1.49 \qquad \textbf{Equation 10}$$

This is to be expected, as the characteristic cell diameter does not represent the largest and the smallest cell size in the sample but the most common (modal value).

Considering the typical diameter distribution, between approx. 13 µm – 16.5 µm (see Figure 8), the G2/M: G1 volume relation of 2 can be calculated as expected (Eq. 11):

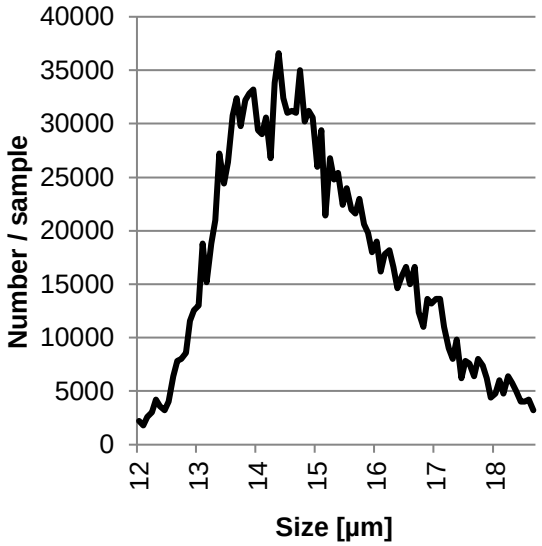

Figure 8: Size distribution HEK293s cell
Unsynchronised, exponentially growing pre-culture. Sizes range from 12-18 µm with approx. 13-16.5 µm being the most common ones.

$$\left(\frac{8.25}{6.5}\right)^3 = 2.04 \qquad \textbf{Equation 11}$$

The percentages of the cell cycle phases (G1, S, and G2/M) and therefore the t_{CC} follow a similar but shifted pattern.

In summary, all data is in line with the expectations for synchronised growth. In every cycle of mitotic cell division, the cells increase in size while the pass from G1 to S to the G2/M phase. At the end of the mitosis, two smaller, identical daughter cells are present.

In regard to the discussed parameters the following is to be expected in a synchronized cultivation:

While the CCD is decreasing (meaning that an increasing fraction of cells just underwent mitosis), μ should increase. Simultaneously, t_{CC} as well as the cell cycle phases (G1, S, G2/M [%]) should indicate a transition from M to G1.

With regard to the methods accuracies, this is the dynamics the data displays. In line with the expectations, fractions X1 and X2 show a similar yet shifted behaviour of about 12 h. This corresponds to half a generation time and hence the intended separation of cells in G1 and G2/M.

Over time the following effects are visible: the intensity of synchronization (I_{CC}) decreases over time. The plotted values are averaged over full cell cycles to circumvent the intrinsic oscillation, as the G1/S trajectory is non-linear (see Section 2.2.9).

Furthermore, all other parameters (CCD, μ, cell cycle phases and t_{CC}) cease to oscillate and approach a constant, intermediate value.

The driving force behind this effect is the variability in cell cycle durations. While all cells in the culture have a generation time of approx. 24 h, minor differences lead to a more statistical distribution of all cell cycle phases over time.

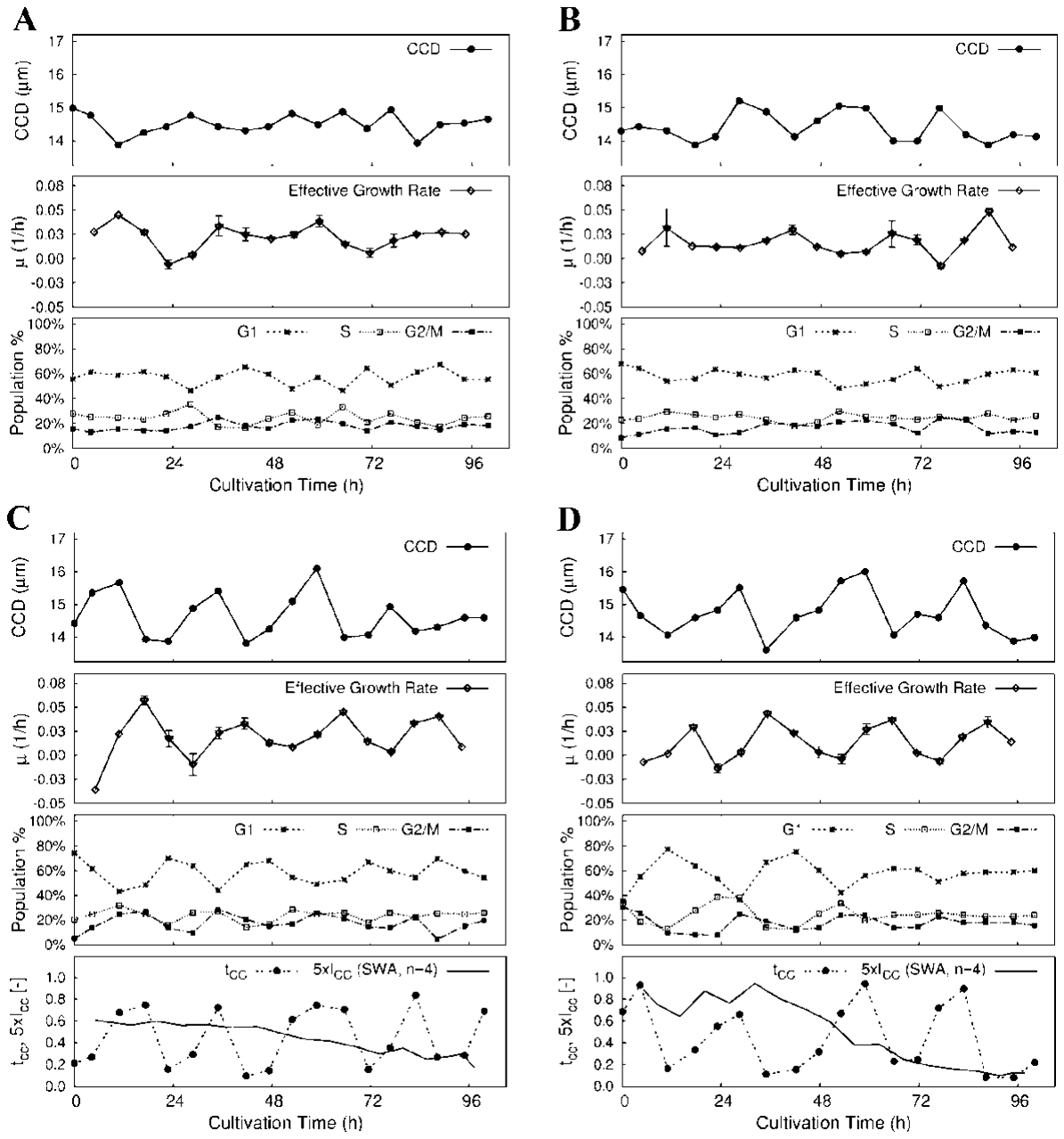

Figure 9: Synchronised growth of elutriation fractions
Progression of the cultures [A: negative control (NC); B: Fraction X0; C and D: Synchronised cultures from fractions X1 and X2, respectively] over 100 h of cultivation. Depicted are the characteristic cell diameter (CCD), the specific growth rate (µ) with estimation error of the underplayed growth curve fits, and the cell cycle distributions as percentages (G1, S, G2/M) as well as calculated relative cell cycle position (t_{CC}) and corresponding amplitude (I_{CC}, averaged over a full cell cycle). Model and illustration by U. Jandt [59].

2.3.3 Assessment of physiological conditions

As stated above, near physiological conditions had to be concluded from the cellular behaviour following the synchronization process.

The cell cycle is controlled by several mechanisms, aimed to ensure that only healthy cells with sufficient nutrient supply proliferate. Hence, distortive effects on the cellular metabolism should be indicated by decreased proliferation, equalling increased generation times.

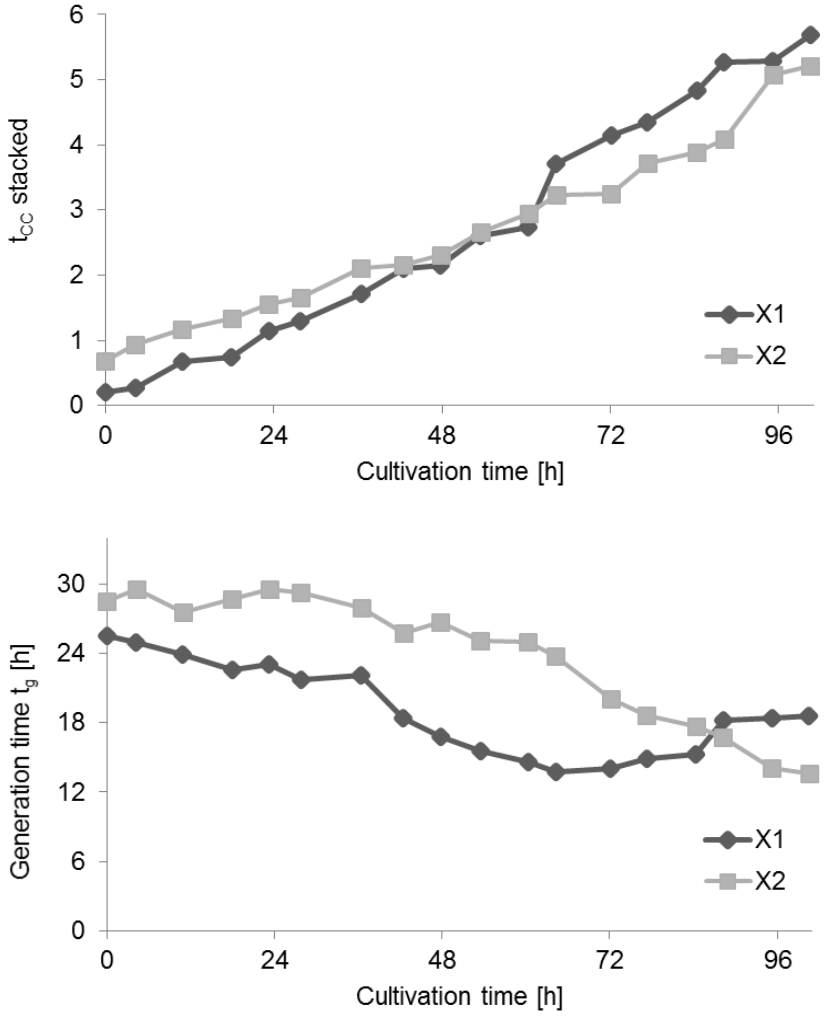

Figure 10: Stacked t_{CC} values and generation times
The calculated t_{CC} values were stacked for both synchronised cultures (upper graph). The slope of these curves correspondent to the generation time (t_g), based on the cell cycle progression at each point in time. Model by U. Jandt [59]. Data for both fractions display a certain amount of variation but decrease throughout the cultivation.

In fact, both synchronised cultures display a change in generation time (t_g). Directly after elutriation, both fractions display prolonged generation times of 25.5 h (X1) and 28.5 h (X2), indicating cellular stress. However, the generation time gradually decreases, demonstrating that the cells return to physiological conditions.

2.4 Conclusion

The physical, selective synchronization method of counter flow centrifugal elutriation was adapted and optimised for the human producer cell line HEK293s. This includes a pivotal regime of different cell culture media and strictly controlled cell densities to avoid the formation of cell aggregates as well as states of limitation.

Proper separation of subcultures, enriched for different cell cycle phases, and subsequent synchronised growth were validated by time resolved assessment of the growth rate (μ), the characteristic cell cycle diameter (*CCD*) and the cell cycle distribution (G1, S, G2/M [%]; t_{CC}) as well as the intensity of synchronization (I_{CC}).

In conclusion, it was shown that synchronised cultures of HEK293s cells, can be generated by counter flow elutriation under near-physiological conditions and maintain their freely oscillating state for 72 - 96 h, while their intensity of synchronization decreases over time.

It was further important to observe that reliable cultivation conditions could be reached 18-24h post elutriation, allowing for 3-4 freely oscillating cycles of synchronized cultivation under near-physiological conditions. This shows that any subsequent characterization of synchronized cultures should be started not earlier than these 18-24 h after elutriation to minimize synchronization artefacts.

3. Examination of putative cell cycle dependent transfection efficiencies of HEK293s cells

In the 2nd Chapter it was shown that centrifugal counter flow elutriation is a suitable method to generate near-physiologically synchronised cultures of the human producer cell line *HEK293s*.

Transfection efficiency has been suggested to be a suitable parameter for cell cycle dependent behaviour. Transfection with reporter plasmids, e.g. including fluorescent proteins can easily be detected. Furthermore, results showing increased transfection efficiencies could directly be used to improve existing procedures.

In fact, previous studies have used cultures described as synchronised and reported differences in transfection efficiencies by orders of magnitude [30–32]. However, none of these studies were conducted using (near-) physiological methods of synchronisation. Instead chemical and/or physical methods including thymidine block and serum starvation were used or temperature reduction steps included - despite their systematic flaws [35, 43, 46].

Accordingly, this Chapter[2] focuses on using the validated synchronised culture setup in order to examine potential interdependencies of the cell cycle and transfection efficiencies.

[2]Some content of this Chapter was published previously [59, 89].

3.1 Technical and theoretical background

In order to easily assess the transfection and protein production efficiency, the fluorescent protein d2eGFP was chosen as reporter plasmid. This is a derivate of the enhanced green fluorescent protein, fused to the destabilising PEST sequence, which is rich in Proline (P), Glutamate (E), Serine (S) und Threonine (T) and causes a shortened biological half-life of the protein. Due to the PEST sequence the intracellular fluorescent protein concentration, and hence its fluorescence signal, are reduced faster - about 60% every 24 h [86]. Therefore, the detected fluorescent signal intensities represent the expression levels more accurately than stable fluorescent proteins whose concentrations accumulate over time.

3.2 Materials and methods

Unless indicated otherwise, materials and methods are as described in the 2nd Chapter and published [59].

3.2.1 Mammalian cell line and culture

Cell culture conditions were further optimised. Instead of 64 h, 44 h prior to elutriation the FreeStyle 293 medium was replaced with 293 SFM II to minimize cell aggregation.

Directly after elutriation, cell fractions were resuspended in pre-warmed, pH adjusted FreeStyle 293 instead of 293 SFM II medium (both Thermo Fisher Scientific, Waltham, MA, USA) and diluted to an initial density of 0.5 Mio/ml. The intermediate culture step in 293 SFMII medium was omitted. In parallel, a negative control culture of the same density was prepared.

After 18 h of incubation at 37°C, 200 rpm and 8% CO_2 in a constantly humidified atmosphere transient transfection was conducted.

3.2.2 Transient transfection with a d2eGFP reporter plasmid

Each transfection was performed with 40 ml of the synchronised cultures from fractions X1 and X2 at different points in time, representing different t_{CC} values (see

Figure 11). At every point in time 40 ml of the negative control culture were transfected in parallel.

Transfection was conducted using Lipofectamine 2000 [87], following an protocol adapted for CHO-K1 suspension cultures [88]. In short, 40 ml of each suspension culture were transfected with 72 µl Lipofectamine and 24 µg reporter plasmid (pcDNA3.3_d2eGFP, Addgene plasmid #26821, a kind gift from Derrick Rossi).

In order to ensure maximal reproducibility between different transfections, all shaking steps were performed on a *Vortex Genie 2* (Bender and Hobein AG, Zürich, Switzerland) at the speed "Vortex 1".

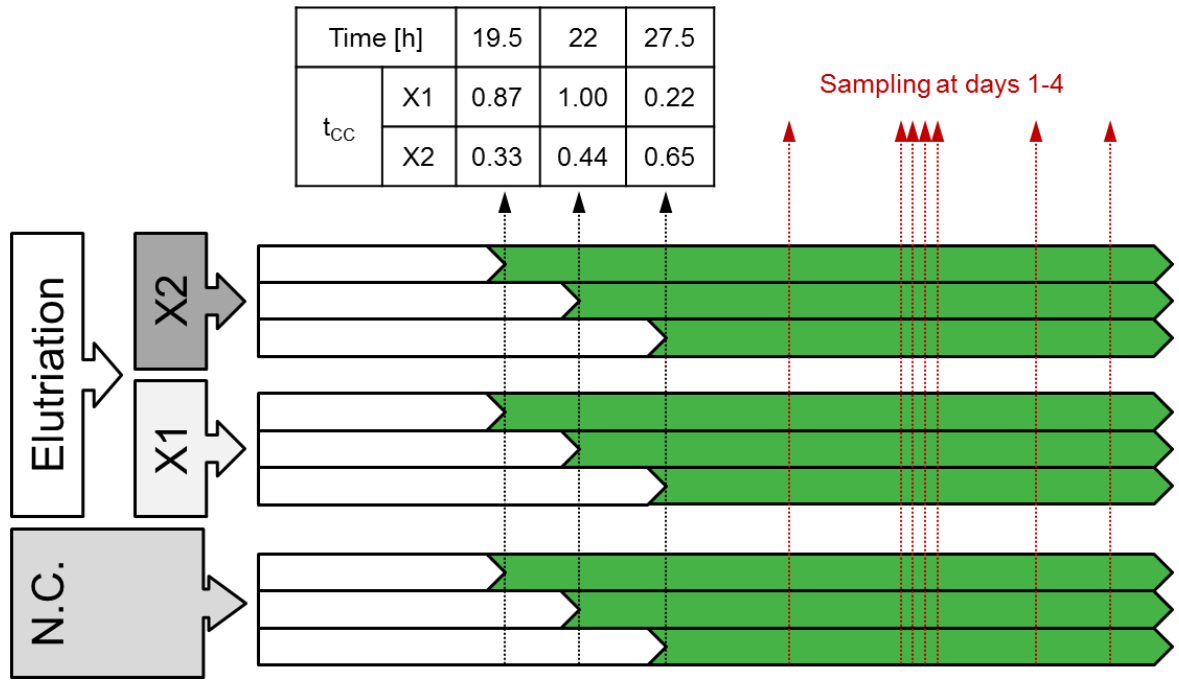

Figure 11: Cell cycle dependent transfection scheme
Schematic representation of the synchronous cultures being transfected at different points in time. The resulting t_{CC} values are represented in the box. The synchronised cultures X1 (high in G1 = high t_{CC} value) and X2 (high in S and G2/M phase = low t_{CC} value) were generated using elutriation. A culture of unaltered cell cycle distribution was cultured in parallel as a negative control (N.C.). 19.5 h, 22 h and 27.5 h after elutriation, transient transfection with the reporter plasmid (pcDNA3.3_d2eGFP) was conducted. Samples for quantification of the reporter protein (d2eGFP) were taken exactly 48 h after transfection. Model and illustration by U. Jandt [89].

3.2.3 Transfection control experiments: Time dependent transfection efficiencies and vesicle functionality

In order to elucidate the interdependency of incubation time and transfection efficiency as well as vesicle stability, the following two control experiments were conducted. For each set of experiments, the same unsynchronised pre-culture was used and adjusted to 0.5 Mio/ml with fresh pre-warmed medium. Furthermore, one batch of Lipofectamine 2000 DNA complexes was prepared and split accordingly.

1. Incubation time

One cultures of HEK293s cells, 40 ml at 0.5 Mio/ml in FreeStyle medium, was transfected and divided into 4 cultures of 10 ml (t_0). After 3 h, 6 h, 9 h and 24 h, respectively the potentially remaining DNA-Lipofectamine complexes were removed by medium exchange.

2. Vesicle stability

Four 10 ml cultures of HEK293s cells at 0.5 Mio/ml in Free Style medium were prepared and cultivated in parallel to the experiment mentioned above. They were transfected with Lipofectamine 2000 DNA complexes from the same batch, kept under cultivation conditions (37°C, 200 rpm, 8% CO_2 and humidified atmosphere), at different points in time: 3 h, 6 h, 9 h and 24 h, respectively after the DNA-Lipofectamine complexes were prepared.

48h after the transfection, cell density and viability were determined using a *Neubauer* chamber. All remaining cells were fixated in 1% PFA at 4°C for 30 min and stored in 70% EtOH at -20°C until flow cytometry analysis.

3.2.4 Flow cytometry - FACS Canto II

Flow Cytometry was performed as described in Section 2.2.8. For reasons of simplicity and readability, the measurement of d2eGFP expression discussed this Section is also explained in Section 2.2.8.

As depicted in Figure 5, minor crosstalk between the FITC-A channel (d2eGFP expression) and the PerCP-A channel (Propidium Iodide bound DNA) is detectable but acceptable in the context of the standardised analysis and its accuracy.

3.2.5 Calculation of the normalised cell cycle position

The method for calculation of the normalised cell cycle distribution (see Section 2.2.9), was used to convert the cell cycle distribution information from the flow cytometry data into an one-dimensional value (t_{CC}).

The aim was to transfect the cultures at representative cell cycle distributions, indicated by evenly distributed t_{CC} values between 0 and 1. Based on knowledge from previous studies, the given points in time were chosen to yield these t_{CC} values with sufficiently strong excitations (I_{CC}) from two different synchronised cultures. Additionally, the t_{CC} and I_{CC} values were determined after transfection in order to monitor the effect of lipofection on the cell cycle distribution and excitation.

3.2.6 Cell cycle dependent transfection model

The experimental data obtained in this study, were subjected to a model-based analysis by U. Jandt. The results are part of a mutual publication [89].

In brief, the model consists of a simplified population balance model, previously described in [28] in combination with a population based transfection model [90]. It is aimed at quantifying the expected impact of the presumed cell cycle dependent plasmid uptake rates on overall measured data.

3.3 Results & discussion

3.3.1 Flow cytometry - FACS Canto II

The reporter protein d2eGFP was successfully detected using the FITC-A channel. As indicated in Figure 6, upper Section, only highly positive cells were gated as transfected. In accordance with the manufacturers protocol [87], the peak expression level was reached 48 h after transfection. The following analyses and graphs focus on these peak values at 48 h post transfection.

In parallel, the described automated analysis (Figure 6, lower Section) was used to calculate the percentages of the different cell cycle phases.

In this context it is important to evaluate the crosstalk of the PerCP-A and FITC-A channel. In Figure 5 a certain amount of crosstalk is visible, hence high *d2eGFP* expression shifts the PI stained DNA pattern to higher values, while a strong PI/DNA signal increases the *d2eGFP* signal.

Nonetheless, these effects are minimal and neglectable in comparison to the standard sample-to-sample variation. The main reason is the working principle of the automated cell cycle quantification:

The G1 peak is simply determined by automatically finding the first maximum in the plot. The S phase region and G2/M peak are subsequently defined by their relative distance.

A common source for sample-to-sample variation are inevitable variations in the DNA staining process. Even comparable DNA patterns shift in regard to their total intensity (the x-axis in the histogram). When cell cycle phase analysis is based on fixed values, arbitrary shifts can occur. On the other hand: manual adaptations of the regions for each sample includes the experimenter’s subjectivity.

This is avoided by the automated, peak based method (see Section 2.2.8.5). Meanwhile the cross-talk of *d2eGFP*, detected in the PI/DNA channel (PerCP-A) is compensated in the process.

The PI/DNA signal, detected in the d2eGFP channel (FITC-A) is relative stable due to the standardised procedures and cause no systematic variation.

3.3.2 Incubation time and Lipofectamine 2000 DNA complex stability

In this study, two factors are of pivotal importance: the stability of Lipofectamine 2000 DNA complexes over time as well as the rate at which they fuse with the HEK293s cells.

At the time of this study, no well-defined data about the complexes stability was available from the manufacturer. Neither on the product page, nor on request through the customer service.

In a previous version of the manufacturers protocol [91], it is stated that the cell culture medium including the Lipofectamine 2000 DNA complexes and can be exchanged after 4 to 6 h without diminishing the transfection efficiency. Additionally, the complex is described to be stable for 6 h. Therefore, transfection was expected to occur within the first 4 to 6 h.

This is in line with the results displayed in Figure 12. Neither the *transfection efficiency* nor the *mean brightness* correlate with the incubation time. Maximum values for both parameters are reached within 3 h or less.

However, Lipofectamine 2000 DNA complexes, stored under suspension culture conditions were able to successfully transfect HEK293s cells after 6 h, and with a much lower percentage even after 24 h.

Note that the analytical setup including the “highly positive” region was chosen to yield values around 40 – 50% in order to display variations more accurately (Figure 6). Setting the “highly positive” threshold to a value, defining higher percentages as “highly positive” could underestimate the change in intensity.

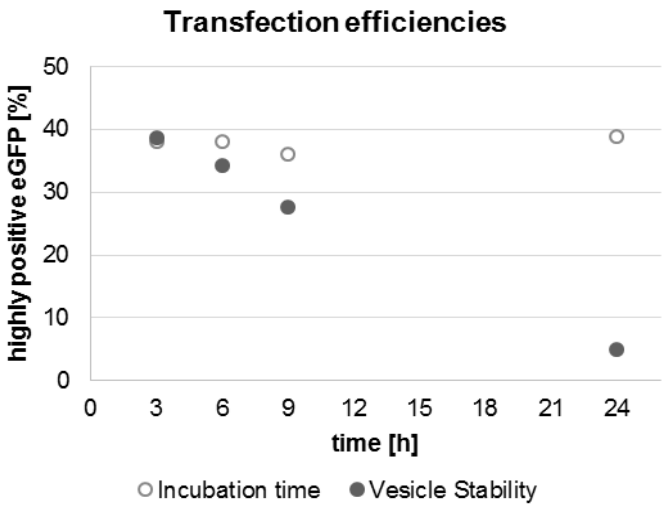

Figure 12: Incubation time and Lipofectamine 2000 DNA complex stability
Transfections efficiencies (highly positive *eGFP* expressing HEK293s cells [%]). Incubation time: Cells were incubated with Lipofectamine 2000 DNA complexes for 3/6/9/24 h before the medium was replaced. Vesicle stability: The same complexes were stored under suspension culture conditions before added to the cells. Modification of [89].

3.3.1 Distortive effects of lipofection on the cell cycle

The method of counter flow elutriation was used to generate synchronised cultures of *HEK293s* cells, like described in 2nd Chapter.

Here, these synchronised cultures were used for transfection studies. Cell cycle data prior to transfection confirmed proper synchronization. However, directly after transfection, synchronicity of the cultures decreased abruptly (Figure 13).

This is in line with previous data, obtained in the experiments of the 2nd Chapter (Figure 14). It shows a direct effect of the lipofection event, leading to a flattening of the curves, representing the cell cycle percentages.

In the direct comparison between the graphs, representing the G1 percentage of the non-transfected culture [G1 (NT)] and transfected culture [G1], this effect is clearly recognizable. Both graphs display an oscillation, with decreasing amplitude over time but their courses differ. The non-transfected culture [G1 (NT)] follows a damped oscillation, as expected. In contrast, the transfected culture [G1] shows a strong

response to the transfection, including reduced G1 percentage and very low remaining oscillation.

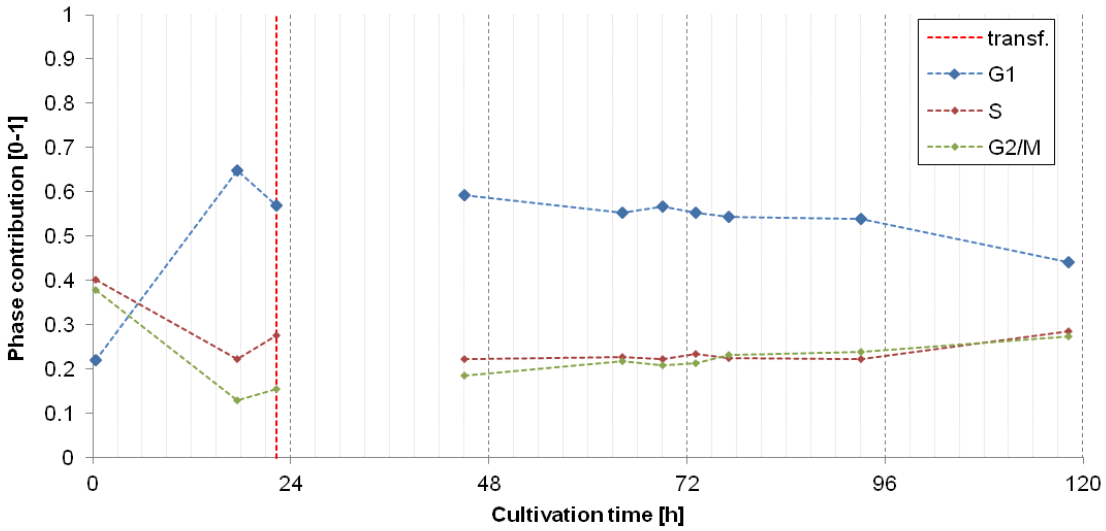

Figure 13: Synchronised cell cycle progression after transient transfection
Synchronised cell cycle progression after transient transfection with Lipofectamine 2000 - All cell cycle phases (G1, S, and G2/M) display decreased oscillation, after transfection (red line). Model and illustration by U. Jandt [89].

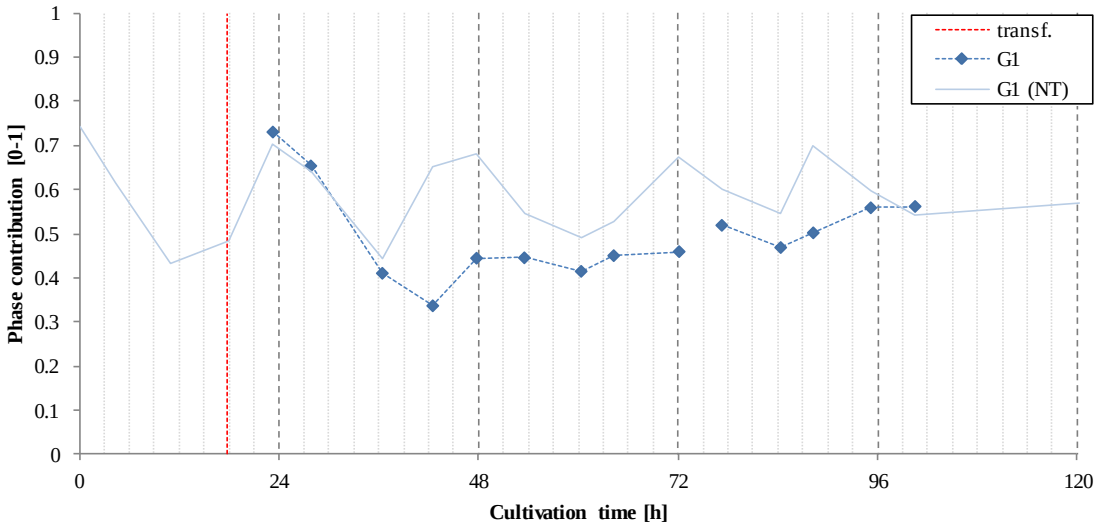

Figure 14: Comparison of transfected to non-transfected synchronised cultures
Comparison of transfected to non-transfected synchronised cultures using G1 for illustration. The non-transfected culture [G1 (NT)] displays unaffected oscillation (data of fraction X1 from the 2nd Chapter). In contrast to this, the transfected culture [G1] - an otherwise unaltered branch of the non-transfected culture [G1 (NT)] shows a strongly diminished oscillation, directly after the event of transfection (red line). A faint oscillation remains for about 24 h before it diminishes entirely. Model and illustration by U. Jandt [89].

3.3.2 Cell cycle dependent transfection

The experiments concerning the cell cycle dependent transfection efficiencies were based on different branches of the same synchronised cultures. Meaning that one preculture was subjected to counter flow elutriation to yield two synchronised cultures X1 and X2. Out of these cultures, different subcultures were created at three points in time (see

Figure 11). These points in time were pre-calculated to cover well distributed t_{CC} values. Note that the different t_{CC} values were obtained from both synchronised cultures.

In theory, it would be possible to obtain all t_{CC} values from a single, synchronised culture. However, since the synchronicity decreases over time (see Figure 14), a combination of two fractions was used in a shorter time frame.

The time course of all transfection experiments is depicted in Figure 15. All expression values are plotted relative to the time of transfection. As expected, the peak expression is detected 48 h after transfection. Before the peak, data varies slightly depending on the source culture (X1, X2) but not on the transfection time point (T1 to T3). Likewise, the decay of fluorescence scatters to some extent.

Nonetheless, all peak vales, detected around 48 h, are very similar and do not correlate systematically with source culture (X1, X1, NC) or any of the points in time (T1 to T3).

The same conclusion can be drawn from Figure 16 and Figure 17: Mean brightness [A.U.].

Interestingly, all transfection efficiencies are relatively similar with 48.1±1.5%. There is no correlation between the t_{CC}, hence the cell cycle distribution, at the time of transfection and the transfection efficiency. There is also no correlation between the transfection efficiency and the fractions X1, X2 or the negative control.

The same holds true for the mean brightness. The values are in the range of 8750±750 arbitrary units (A.U.) and show no pattern of correlation.

These results strongly disagree with the studies published earlier [30–32].

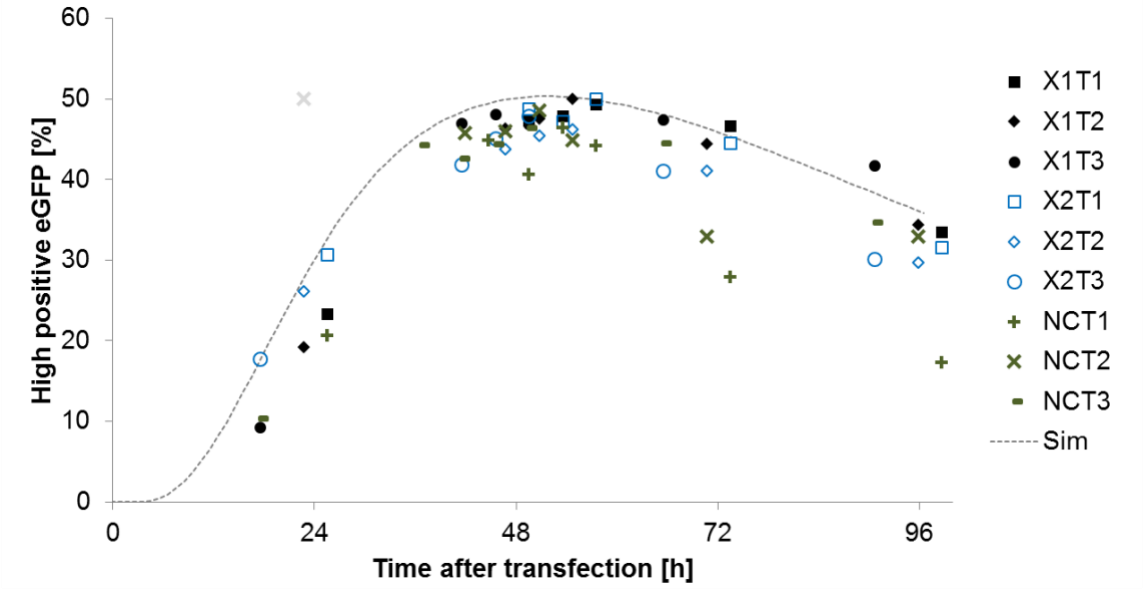

Figure 15: eGFP expression over time
9 transfection experiments (3 points in time of each: X1, X1 and the negative control). Data points are overlaid with an example of a simulated transfection course (see Section 3.3.3). One single outlier sample at t≈23 h was excluded from analysis due to flawed staining and subsequent inaccurate gating. Model and illustration by U. Jandt [89].

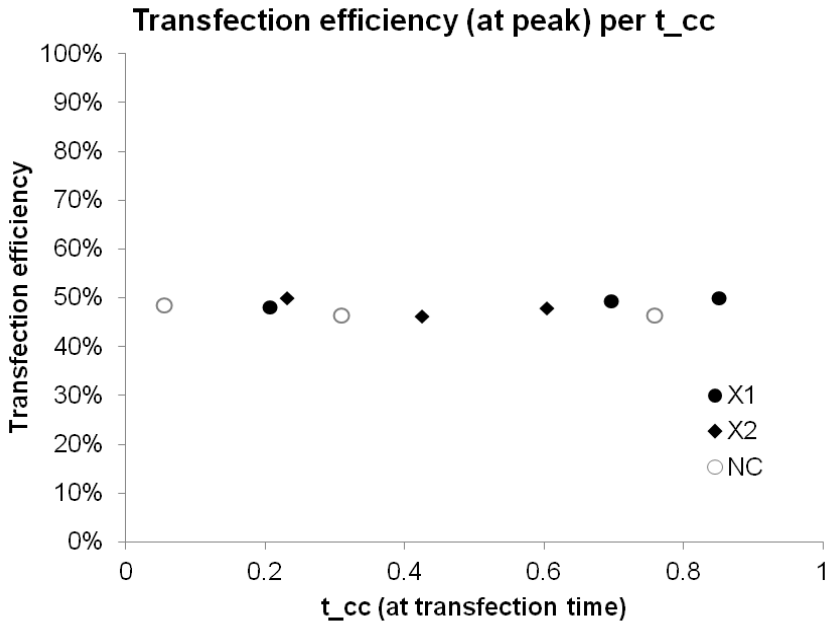

Figure 16: Transfection efficiencies [%]
plotted against the cell cycle distribution (t_{CC}). The graph depicts the transfection efficiency as a result of the cycle distribution (t_{CC}) at the time of transfection. The fluorescence signal (d2eGFP) was measured at the time of peak expression (48 h after transfection). The values vary only minimally (48.1±1.5%) and show no correlation, neither with the t_{CC}, nor with the fraction (X1, X2 or negative control). Model and illustration by U. Jandt [89].

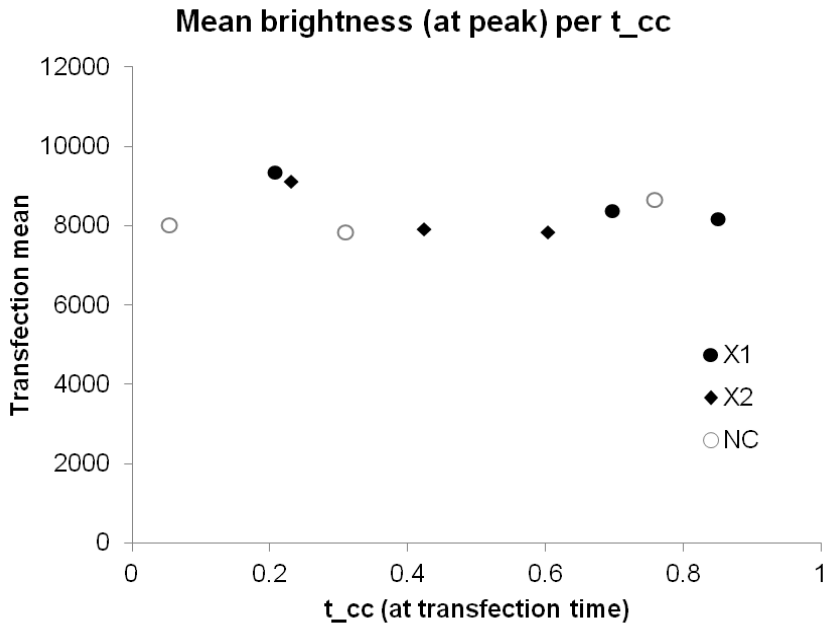

Figure 17: Mean brightness [A.U.]
plotted against the cell cycle distribution (t_{CC}). The graph displays the mean brightness [A.U.] as a result of the cycle distribution (t_{CC}) at the time of transfection. The fluorescence signal (d2eGFP) was measured at the time of peak expression (48 h after transfection). Like transfection efficiencies, values vary only minimally (8750±750 A.U.) and do not correlate with t_{CC} or the fraction. Model and illustration by U. Jandt [89].

3.3.3 Comparison to the model-based estimation of the cell cycle dependency

The results stated above show no apparent cell cycle dependency. Nevertheless, these results should be discussed in regard to two systematically limitations.

First of all, the used cultures are enriched for cells in a specific cell cycle phase but never perfectly synchronised.

Secondly, the Lipofectamine 2000 DNA complexes appear to cause the transfection effect within the first 3 h after addition (Figure 12). Nonetheless, there is a theoretical option of active Lipofectamine 2000 DNA complexes remaining in the cell culture and conducting transfection at a later point in time, when cells are in different, potentially more susceptible cell cycle phases.

Both effects are subject to a more in-depth modelling approach by U. Jandt. The results in line with the conclusions drawn here and part of a mutual publication [89]. They can

be summarised as follows: the variations of transfection efficiencies assigned to single cell cycle phases are considerably lower than assumed. According to the results of this study, it is likely that the relative efficiency at the end of the cell cycle (S and/or G2/M) is smaller than 10-fold the efficiency at the beginning (G1). Hence, the factor is notably smaller than previously reported factors of 15-500 [30]. If the rate of inactivation for the Lipofectamine 2000 DNA complexes is as high as stated by the manufacturer (causing inactivation after 6 h under cultivation conditions), which could not be validated in comparison experiments, the results of this study could be considered to be more precise. Hence, the corresponding upper limits of the derived relative efficiency factors would be even lower.

3.3.4 Conclusion

This study does not support the notion that transfection efficiency is strongly dependent on the time point of transfection with respect to the cell cycle position, as it was reported previously [30–32].

If this was true, the samples of different cell cycle states should display strong variations in transfection efficiency, which they did not.

Note that from this study, no conclusions can be drawn whether or not the production rate after transfection is cell cycle dependent.

Also, it needs to be pointed out that the results, obtained in this combination of cell line, transfection reagent, protocol and reporter plasmid have to be considered in the context of these specific conditions. Comparison to results from other experimental setups have to be made with caution.

Nevertheless, this study was the first to use freely oscillating, synchronized cultures under near-physiological conditions to examine this putative dependency. This is a noteworthy difference to the mentioned studies where cells have been elutriated using lower temperatures (15°C), were stored at 4°C until re-cultivation and transfection [30] or chemical synchronization methods were used [31, 32].

As stated earlier, these approaches are intrinsically flawed [42, 46]. For all whole culture synchronisation methods, the basic principle is identical: the cultures are meant to be synchronized by adding an external stimulus to the whole culture for a defined period of time. The different cell cycle distributions (t_{CC} values) occur one after another, following the stimulus.

Hence, the effect of the cell cycle (t_{CC}) cannot be investigated independently from possible additional effects from the synchronisation method itself. It is reasonable to ask if the reported strong differences in transfection efficiency may have been influenced by the whole culture synchronisation method rather than the cell cycle state.

Additionally, the use of recombinant protein expression by lipofection should be reconsidered. As evident from Figure 14, the method coincides with substantial cell growth influencing effects. These effects might be reduced by further optimised protocols but can't be avoided entirely.

The first causative agent is the lipofection reagent, in this case Lipofectamine 2000. The second influence is the expression of the fluorescence protein. Forcing cells to produce a reporter protein is inevitably associated with a higher metabolic load, which was reported to influence the overall metabolic state [92] and is plausible to influence the progression of the cell cycle, cell growth and further metabolic behaviour [27].

4. Generation of two novel CHO-K1 cell line derivatives with intrinsic cell cycle indicators

In the previous Chapters (2 & 3) a near physiological synchronization method was established and validated for HEK293s cells and applied for cell cycle resolved transfection experiments. Using validated synchronised cultivation, no significant cell cycle dependent variation of transfection efficiency could be observed, which is in stark contrast to previous publications.

In order to obtain higher resolved, statistically significant and reproducible cell cycle dependent results, a novel, more robust system is required to elucidate interdependencies of cell cycle and cellular behaviour. For this Chapter[3], genetic FUCCI constructs (see Section 1.7.2) were used to design two new derivatives of the widely used *CHO-K1* production cell line, with the ability to indicate their cell cycle state in an on-line feasible manner through fluorescence.

This Section describes the generation of new production cell line derivatives that are able to indicate their cell cycle status by fluorescence: *CHO-K1 FUCCI CM* and *CHO-K1 FUCCI CN*. They can be measured directly with any fluorescence compatible method of sufficient accuracy e.g. flow cytometers, plate readers and fluorescence probes.

[3]Some content of this Chapter was published previously [98].

4.1 Technical and theoretical background

Flow cytometry in combination with DNA staining is a well-established and widely used method to determine the cell cycle state of mammalian cell cultures. However, it requires staining prior to measurements [82, 83]. There have been different approaches to establish on-line flow cytometry methods in process control e.g. in the fermentation process of brewing beer [93]. Also there were studies aiming at integrating automated flow cytometry and cell cycle monitoring in CHO cell culture [94]. These extensive protocols however re-implement classic staining approaches including some of their limitations regarding reproducibility and effort.

In order to assess the cell cycle state in cell cultures more directly, with less effort and minimal perturbations for the cells, intracellular cell cycle probes - ideally based on fluorescence - would be beneficial.

Therefore, two new CHO-K1 cell line derivatives were generated in cooperation with Dr. Kristoffer Riecken (Forschungsabteilung Zell- und Gentherapie, Interdisziplinäre Klinik und Poliklinik für Stammzelltransplantation, Universitätsklinikum Hamburg-Eppendorf, Martinistrasse 52, 20246 Hamburg, Germany).

4.1.1 Designing CHO-K1 FUCCI CM & CN

Out of the variety of available FUCCI plasmids, the following combinations were chosen:

- C+M: mKO2-hCdt1(30/120) and mVenus-hGeminin(1/110)
- C+N: mKO2-hCdt1(30/120) and mVenus-hGeminin(1/60)

The nomenclature is consistent with the system of Miyawaki et al. [72] and will be used for the cell line derivatives CHO-K1 FUCCI CM and CHO-K1 FUCCI CN alike. The main priority was to choose fluorescent proteins that could be detected separately in terms of the wave length but also in comparable intensities. While other fluorescent proteins e.g. AmCyan and mCherry offer a larger spectral diversity and minimise the

cross-talk, only mVenus and mKO2 are sufficiently similar in terms of *quantum yield* and *relative brightness of eGFP* (see Table 4).

For the sake of simplicity, the fluorescence properties of mKO2 and mVenus will henceforth be referred to as "red" and "green", respectively, despite the fact that their emission wave length would more accurately be termed "orange" and "yellow-green".

Table 4: FUCCI fluorescent protein properties
Modification of [70]**.**

Fluorescent protein	Excitation maximum [nm]	Emission maximum [nm]	Quantum yield	Relative brightness [% of eGFP]
mVenus	515	528 (“green”)	0.57	156
mKO2	551	565 (“red”)	0.62	118

The different sizes of the hGeminin domain influence the subcellular localisation. While mVenus-hGeminin(1/110) and mKO2-hCdt1(30/120) are only located in the nucleus, mVenus-hGeminin(1/60) can also be found in the cytosol. The different localisations of the fluorophores are likely to influence the detectable fluorescence intensity. Additionally, the cytosolic localisation of mVenus-hGeminin(1/60) allows to assess the shape of the cell in fluorescence microscopy. Hence, both combinations were generated to use the more suitable combination for each application.

4.1.2 Application of lentiviral transduction and life cell sorting

Lentiviral transduction is a method to stably integrate genes of interest in genomes using replication deficient virus particles [95].

As a first step, the genes of interest, here mKO2-hCdt1(30/120), mVenus-hGeminin(1/110) and mVenus-hGeminin(1/60) were cloned into a lentiviral transfer plasmid (in this case pCSII-EF). To generate the viral particles, each of the transfer plasmids can be transfected into a culture of cells with good virus particle production properties (e.g. HEK293T cells, ATCC, Middlesex, UK) in combination with suitable

envelope and *packaging plasmids*. Together these plasmids contain all genes to produce one generation of viral particles, which are secreted into the cell culture medium.

After production the viral particles can be removed from virus producing cells with the medium. These resulting viral particles are replication deficient since they only contain the genes of interest (e.g. mKO2-hCdt1). Hence, the lentiviral particles can infect cells only once to deliver the genes of interest. Before use, viral particle suspensions need to be titrated to assess functional virus particle concentrations and use the required amounts.

Subsequently, the virus particles can be used to stably integrate the genes of interest into the genome of mammalian cells. This is also possible with combinations of virus particles, containing different genes of interest. After the virus particles have been added to the cells, cells in which the lentiviral transduction (integration of the genes of interest into the genome) was successful have to be separated from the non-transduced ones. This can be achieved by delivering genes for different types of chemical resistance alongside with the genes of interest while adding of those toxic chemicals to the cell culture media. Alternatively, Life Cell Sorting can be utilised for selection.

Here, this technology was applied to generate the cell line derivatives CHO-K1 FUCCI CM and CHO-K1 FUCCI CN. After each double transfection, only cells that exhibited a high red (mKO2) fluorescence were selected and expanded in culture. In a second round, only cells with a high green (mVenus) and no red (mKO2) fluorescence were selected from these cultures. Therefore, only cells which are able to alternate between red and green fluorescence (mKO2 / mVenus expression) were selected. Single positive, negative as well as potentially non-alternating double positive cells were discarded. Nonetheless, these cell line variants are still polyclonal.

4.2 Materials and methods

4.2.1 Mammalian cell line & medium

Cultures of CHO-K1, kindly provided by Prof. Dr. Thomas Noll (Cell Culture Technology Group, University Bielefeld, Germany) were maintained in suspension in complete chemically-defined, animal-component-free, protein-free CHOMACS CD Medium (Miltenyi Biotec GmbH, Bergisch Gladbach, Germany) supplemented with 4 mM glutamine, without antibiotics. A constant humidified atmosphere of 37°C and 5% CO_2, as well as a continuous shaking (200 rpm) were kept throughout the culture.

4.2.2 FUCCI plasmids

The complete FUCCI transfer plasmids are a generous gift from the Group of Dr. A. Miyawaki (Laboratory for Cell Function Dynamics, RIKEN Brain Science Institute, Saitama, Japan).

They consist of a third generation lentiviral SIN vector and express different cell cycle specific fluorescent proteins. The nomenclature has been adopted unchanged:

C: mKO2-hCdt1(30/120)

M: mVenus-hGeminin(1/110)

N: mVenus-hGeminin(1/60)

4.2.3 Lentiviral transduction

Lentiviral transduction and Life Cell Sorting were conducted by Dr. Kristoffer Riecken (Forschungsabteilung Zell- und Gentherapie, Interdisziplinäre Klinik und Poliklinik für Stammzelltransplantation, Universitätsklinikum Hamburg-Eppendorf, Hamburg, Germany) as described earlier [96]. The protocols are available online [97].

Transductions were performed in 24 well plates using 50000 CHO-K1 cells in 500 µl CHOMACS CD Medium (Miltenyi Biotec GmbH, Bergisch Gladbach, Germany) per well. Double transductions were conducted using 30 µl of viral particle containing supernatants in the following combinations:

CM: mKO2-hCdt1(30/120) and mVenus-hGeminin(1/110)

CN: mKO2-hCdt1(30/120) and mVenus-hGeminin(1/60)

Four days after transduction, labelled cells were determined by flow cytometry, yielding 14% and 22% respectively. Since each fluorescent protein is only expressed in a certain cell cycle state, the transduction rate is systematically underestimated by flow cytometry. In accordance with the legal regulations cells were classified as S1 one week post transduction.

4.2.4 Life cell sorting and flow cytometry

Life Cell Sorting was performed using a FACSAria IIIu (Becton Dickinson, Franklin Lakes, NJ, USA). Highly positive red cells (detected in the channel *PE-Texas Red-A* - Laser 561 nm, Filter 610/20 nm) were selected and expanded for about two weeks. Subsequently, from those cultures highly positive green cells (detected in the channel *Alexa Fluor 488-A* - Laser 488 nm, Filter 543/22 nm) were selected and expanded again. Verification measurements were performed using a LSR-Fortessa flow cytometer: *PE-Texas Red-A* - Laser 561 nm, Filter 610/20 nm; *Alexa Fluor 488-A* - Laser 488 nm, Filter 530/30 nm.

4.3 Results and discussion

The goal of this Section was to create two stable derivatives of the *CHO-K1* suspension cell line. The first variant, *CHO-K1 CM*, carrying the genes for mKO2-hCdt1(30/120) and mVenus-hGeminin(1/110); the second *CHO-K1 CN* including *mKO2-hCdt1(30/120)* and *mVenus-hGeminin(1/60)*.

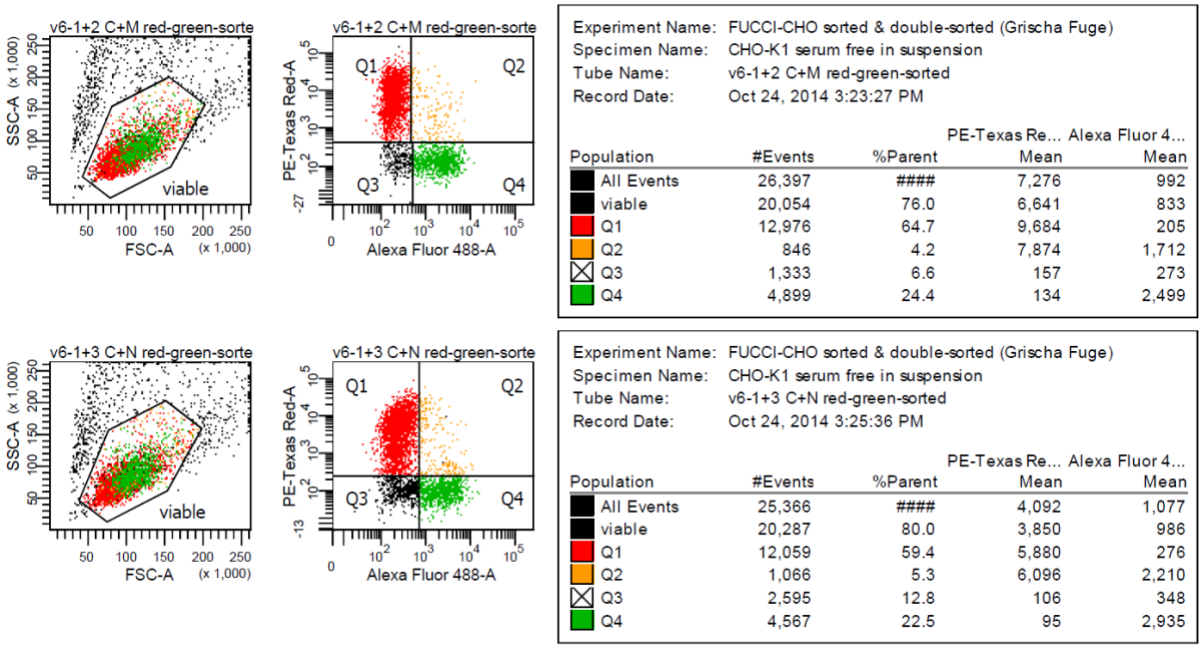

Figure 18: CHO-K1 FUCCI CM and CN after life cell sorting
Left: Dot plots - gating for living cells; middle: Dot plots - FUCCI fluorescence pattern; right: Statistics panel. Selected polyclonal cell lines CHO-K1 FUCCI CM and CN are able to exhibit all fluorescent states. Data and graph were published previously [98].

As a result, those cells should either show red (*mKO2*) or green (*mVenus*) fluorescence, depending on their cell cycle state. Therefore, cells were first sorted for highly positive red cells, excluding all cells that were either non-transduced by the corresponding plasmid and/or not in the G1 phase and/or showed low *mKO2-hCdt1* expression at the time of sorting. After cell expansion, cells were sorted for highly green cells, generating the same effect in regard to mVenus-hGeminin expression.

Hence, every cell in the resulting polyclonal culture was able alternate between red and green (*mKO2* / *mVenus*) fluorescence, distribution of the fluorescence is in line with the durations of the cell cycle phases (see Figure 18 and Figure 3). The most likely

case is the functional integration of both plasmids. Double positive cells were excluded in both sorting stages, alongside with double negative ones, therefore no selected cell could constantly express both or none of the fluorescence proteins. Furthermore, only highly positive clones were selected to ensure good signal intensities for the following experiments.

4.4 Conclusion

The procedures, described in this Section, do not exclude the theoretical option of cells alternating their fluorescence in a pattern different from the intended one. Major differences, like inverted expression, however are unlikely since the *Geminin* / *Cdt1* system is essential for proper cellular proliferation [60, 61]. Minor differences may be possible since the cultures were maintained polyclonal. The number and *loci* of gene integration are plausible to differ. These variations might include total fluorescence intensity as well as build up and degradation kinetics.

In order to guarantee a more homogeneous behaviour, monoclonal subcultures may be generated. At this point however, the cultures were maintained polyclonal to ensure genetic diversity for later clone selection. After all, properties deemed beneficial at this point may cause limitations in the future, e.g. extremely high fluorescence signal could be detrimental in the context of recombinant protein production as the fluorescence protein expression comes with higher protein synthesis demand (metabolic burden).

5. Cell cycle dependent expression of the FUCCI fluorescence proteins by the novel cell lines derivative CHO-K1 FUCCI CN

In the previous Chapter, the design and generation of two novel cell line derivatives *CHO-K1 FUCCI CM* and *CHO FUCCI CN* were described. Life cell sorting confirmed their ability to alter between red and green fluorescence, most likely depending on their cell cycle state (Figure 18).

This Chapter[4] investigates if and to which extent the expression of the FUCCI fluorescence proteins can be confirmed to be cell cycle dependent. Vice versa, it is investigated if the cell cycle state of cultures can be reliably determined by fluorescence measurements.

5.1 Technical and theoretical background

The central question of this Chapter is if the FUCCI expression of the novel cell line derivatives *CHO FUCCI CN* is strictly cell cycle dependent. If so, measurements of the fluorescence could replace DNA based cell cycle analysis – a significant simplification since laborious staining procedures could be omitted. The following analyses were conducted targeting the single cell level using a simple threshold-based model. The matter of cultures total fluorescence is addressed in a later Section (see 6th Chapter).

Experimentally, two different approaches were chosen. The first, is a rather simple one: cells from an exponentially growing culture were measured, using the described

[4]Some content of this Chapter was published previously [98].

protocols. Subsequently, gating was applied to determine if FUCCI fluorescence and DNA based cell cycle determination display the expected relationship.

In order to support the results, the same relationship should be apparent in samples which are actually different in their cell cycle distribution. For this the second approach, counter flow elutriation was the method of choice to generate samples of varying G1 [%]. Evaluation of different measurement protocols and combinations thereof were needed to assess the most suitable method.

Finally, the correlation between cell cycle distribution (G1 [%]) and FUCCI fluorescence was quantified.

5.2 Materials and methods

5.2.1 Mammalian cell line derivatives, medium & flasks

The novel cell line derivatives *CHO-K1 CM* and *CHO-K1 CN* were maintained in suspension in complete chemically-defined, animal-component-free, protein-free CHOMACS CD Medium (Miltenyi Biotec GmbH, Bergisch Gladbach, Germany) supplemented with 4 mM glutamine. A constant humidified atmosphere of 37°C and 5% CO_2, as well as a continuous shaking (200 rpm) were kept throughout the culture. Erlenmeyer baffled cell culture flasks (125 ml: type 431405, 250 ml: type 431407; Corning, New York, USA) were used with culture volumes of 40 ml and 80 ml respectively. No antibiotics were used at any time.

5.2.1 Elutriation

Elutriation was performed as described in the 2nd Chapter, with optimised conditions for the two cell line derivatives *CHO-K1 FUCCI CM* and *CHO FUCCI CN*. In concordance with earlier studies, conducted with CHO-K1 cells, 1800 rpm and flow rates of 10 - 50 ml/min were used [28, 58].

5.2.2 Fixing and storage of mammalian cells

In order to store cells for longer periods of time and/or for permeabilisation prior to DAPI staining, the protocol from Section 2.2.8.2 was used.

5.2.3 Sample preparation for flow cytometry - CytoFlex

Different sample preparation protocols were applied, depending on the property of interest.

5.2.3.1 Unstained

0.5 ml culture of CHO-K1 CM or CN cells was transferred into a 1.5 ml Eppendorf tube and centrifuged for 3 min at 1800 rpm corresponding to 300 g at room temperature on a Fresco 21 Table top centrifuge (Thermo Fisher Scientific Inc., Waltham, MA, USA).

The supernatant was removed, the cells resuspended in 500 µl PBS and directly subjected to analysis by flow cytometry.

5.2.3.2 Life staining with Hoechst33342

0.5 ml culture of CHO-K1 CM or CN cells was transferred into a 1.5 ml Eppendorf tube, 1 µl of Hoechst33342 stock solution (5 mg/ml) were added directly into the medium, yielding a total concentration of 10 µg/ml.

Incubation was conducted for 1 h at 37°C and 650 rpm in the dark on a Thermomixer R (Eppendorf, Hamburg, Germany).

After centrifugation for 3 min at 1800 rpm (300 g) at room temperature on a Fresco 21 Table top centrifuge (Thermo Fisher Scientific Inc., Waltham, MA, USA) the supernatant was removed.

Subsequently, the cells were washed another time and cells were resuspended in 500 µl PBS and directly subjected to analysis by flow cytometry.

5.2.3.3 Staining of permeabilised cells with DAPI or Hoechst33342

Subsequent to permeabilisation, described in Section 2.2.8.2, cells were stained with DAPI [99] or Hoechst33342. For this purpose, 1 ml of PBS was added to 500 µl cells, suspended in 70% EtOH.

The tubes were subjected to centrifugation for 3 min at 1800 rpm (300 g) at room temperature on a Fresco 21 Table top centrifuge (Thermo Fisher Scientific Inc., Waltham, MA, USA), the supernatants were removed by aspiration.

The resulting pellets were resuspended in a solution composed of PBS [81], 0.1% Triton X-100 and 1 µg/ml DAPI (VWR International, Darmstadt, Germany). Alternatively, Hoechst33342 (VWR International, Darmstadt, Germany) with a final concentration of 10 µg/ml in PBS was used.

After 30 min incubation at room temperature, cells were analysed by flow cytometry.

5.2.4 Flow cytometry – *CytoFlex*

A CytoFlex flow cytometer (Beckman Coulter, Brea, CA, USA) was used for analysis. Quality control was conducted at least once a week, as well as prior to each series of measurements that extended over several days, using the QC-Beads, recommended by the manufacturer.

The 488 nm laser was used for FSC and SSC as well as mKO2 (PE = 585/42 nm filter) and mVenus (FITC = 525/40 nm filter) detection. DAPI and Hoechst33342 were detected using the 405 nm laser (PB450 = 450/45 nm filter).

The acquisition settings were optimised to be suitable for all sample preparation protocols. Furthermore, gain values for the mVenus detection as well as mKO2 detection were manually set to identical values, for better comparability of the fluorescent signal intensities (see Figure 19).

The compensation matrix was set up to compensate for the cross talk between the channels and proteins, stated above (see Figure 20). For the detection of the DNA stains DAPI or Hoechst33342, no compensation was required.

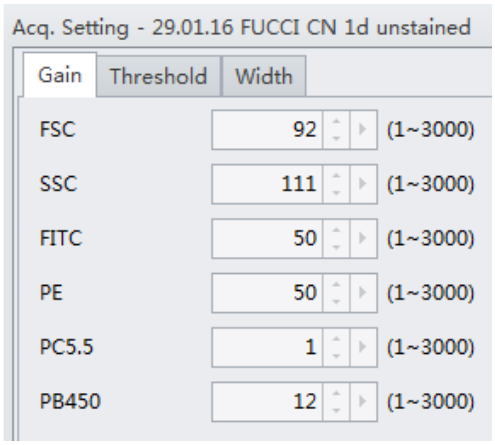

Figure 19: Acquisition settings – CytoFlex
Equal gain values were used for the detection of mVenus (FITC channel) and mKO2 (PE channel) in order to obtain comparable data.

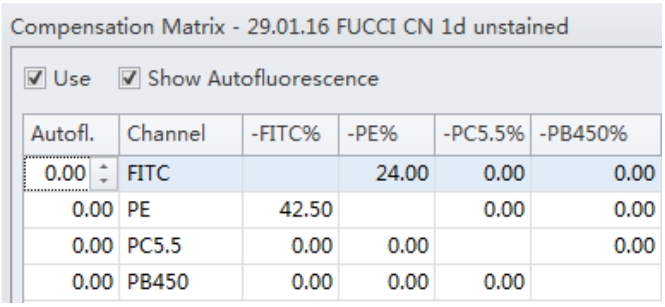

Autofl.	Channel	-FITC%	-PE%	-PC5.5%	-PB450%
0.00	FITC		24.00	0.00	0.00
0.00	PE	42.50		0.00	0.00
0.00	PC5.5	0.00	0.00		0.00
0.00	PB450	0.00	0.00	0.00	

Figure 20: Compensation matrix - CytoFlex
Crosstalk due to similar fluorescence properties of mVenus and mKO2 was compensated using the compensation matrix values stated above.

5.2.5 Quantification of FUCCI fluorescence distribution (i_{red}^{n}) of viable cells using a flow cytometer - *CytoFlex*

FUCCI fluorescence distribution was quantified (Eq. 12) from the data sets of viable cells (see Section 5.2.3.1), detected on the *CytoFlex* flow cytometer. Note that this approach is based on cell counts rather than total fluorescence. For the data analysis, thresholds were defined for mKO2 as well as mVenus. These were consistent for all samples. They were set, based on the direct comparison of *CHO-K1 FUCCI CN* (positive control) and *CHO-K1* cells (negative control). Hence, for mVenus all cells within channel numbers above $2*10^4$ were defined as positive. For mKO2 the corresponding value was 10^4. The total number of cells in these gates as well as the mean value of the gates were exported to .csv files in order to calculate the different i_{red} values.

$$i_{red}^{n}[\%] = \frac{mKO2^{n}}{mKO2^{n} + mVenus^{n}}$$

Equation 12

5.2.6 Quantification of cell cycle distribution – G1 [%]

This method of data processing was applied to yield quantitative cell cycle distributions, while circumventing experimenters' bias. It is an improved version of the method used in the 2nd and 3rd Chapter, based on the new equipment and staining procedures described above (see Section 5.2.3.3). The KALUZA Analysis 1.3 Software (Beckman Coulter, Brea, CA, USA) was used due to its superior data export function. The gating strategy was a direct re-implementation of the one described in the qualitative analysis (see Section 5.3.2.2). It was designed to include dead cells, since all cells were expected to be dead as a result of the EtOH sample preparation but exclude doublets. Finally, DNA histogram data was exported as .csv files and subjected to analysis by a Microsoft Excel (Microsoft, Redmond, CA, USA) script. Its function can be summarised as follows: (1) find the first Peak, corresponding to G1 (2) find the second peak (3) calculate the G1 [%] based on fixed ranges around the found peaks. All distances were

calculated in “channel numbers” of the histogram. The ranges for the G1 and G2 peak were determined manually to avoid artefacts in fractions with only one dominant peak (e.g. the first fractions, high in G1).

5.2.7 Correlation of i_{red}^{n} and G1 [%]

The i_{red}^{n} values of two elutriation experiments (biological replicates) were plotted against their corresponding G1 [%] values. The data was fitted using linear regression.

5.3 Results and discussion

5.3.1 Qualitative relationship between FUCCI fluorescence and the conventional cell cycle determination

In this Section it is investigated whether the information obtained based on the *FUCCI* system is qualitatively related to the cell cycle information based on the established DNA staining protocols.

The different sample preparation protocols were used to represent different properties most accurately. The "unstained" protocol was used to measure the expression of the fluorescent *FUCCI* proteins *mKO2* and *mVenus* without additional staining. The cells remain vital (cell membrane intact). The same information obtainable by this measurement is also available to on-line capable methods like fluorescence probes. However, no DNA based quantification of the cell cycle state is available.

In contrast to this, permeabilisation of the cells with EtOH and subsequent staining with DAPI yields accurate DNA patterns, but the intrinsic fluorescence signals of the FUCCI proteins lose their characteristic pattern on the dot plots (see Figure 21). Hence, a single cell can’t be subjected to both methods to yield its accurate cell cycle state and *FUCCI* fluorescence.

As a work around, samples of different cell cycle distributions were generated using counter flow elutriation. Subsets of these samples were subjected to both methods in

parallel, in order to yield accurate FUCCI fluorescence as well as DNA amount-based cell cycle data. Thereby, the information of these measurements can be linked.

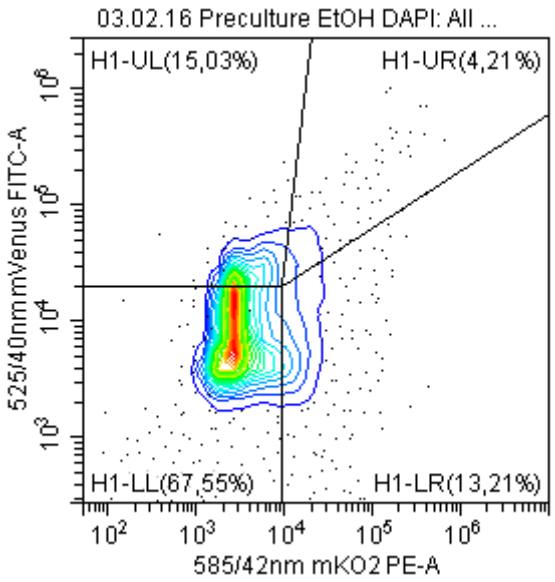

Figure 21: EtOH DAPI stained pre-culture FUCCI fluorescence

An alternative approach is the staining of viable cells with Hoechst33342. It yields both, FUCCI fluorescence as well as DNA data of each individual cell. Unfortunately, it comes with the limitation of lower accuracy. In the following Section, the differences of these protocols are explained using data from exponentially growing cultures with typical characteristics.

5.3.1.1 Gating and staining: Hoechst33342

The gating strategies were applied, depended on the type of sample preparation. Here the strategy for living cells, unstained or stained with Hoechst33342 is explained.

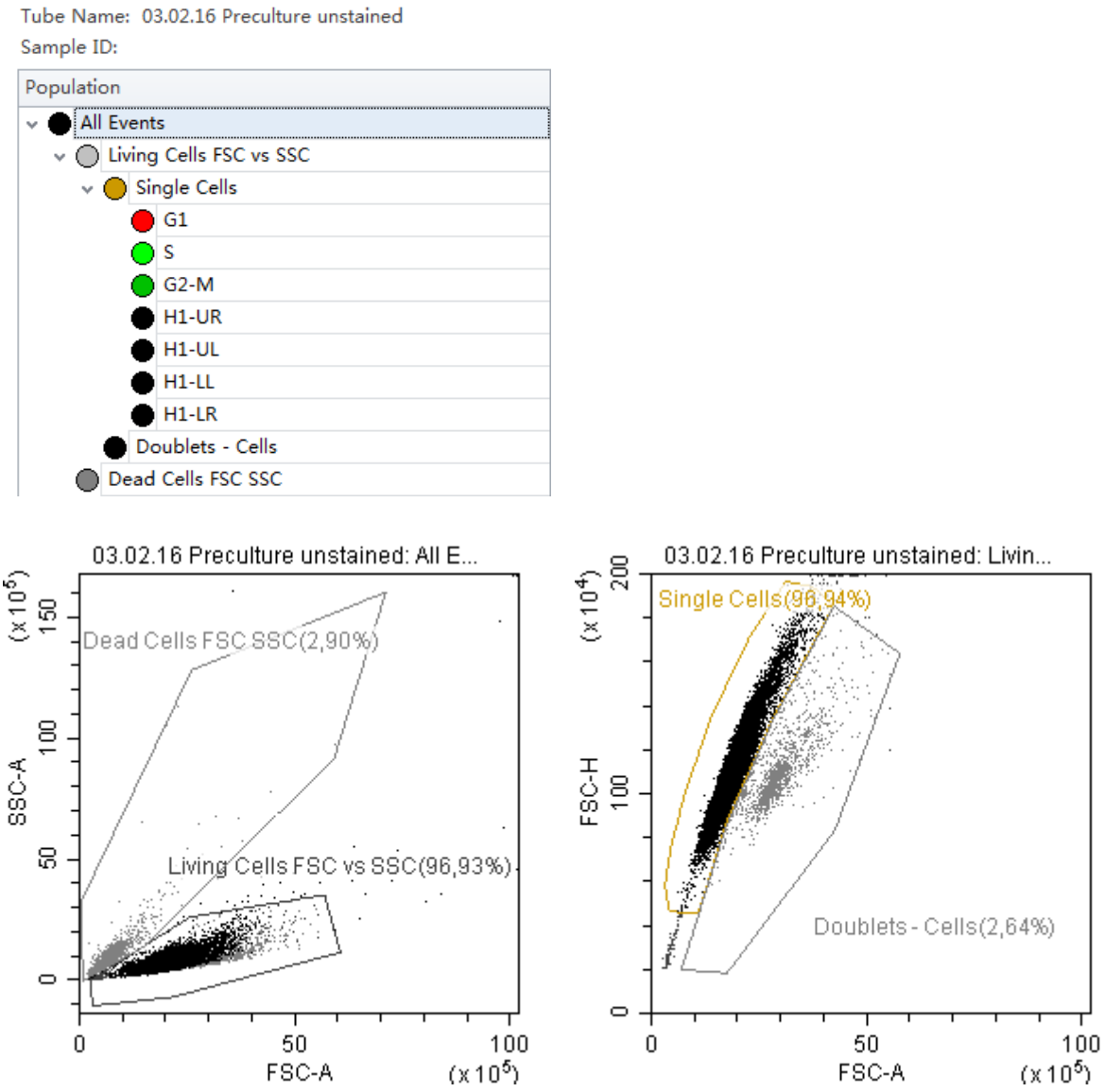

Figure 22: Gating living cells
Upper graph: Gating hirachy for living cells; lower left: Gating for living cells; lower right: gating for single cells.

First, cells were gated by morphology as dead or alive, using forward scatter (FSC-A) and side scatter (SSC-A). Here the living cells are plotted in a consecutive plot, to remove doublets (see Figure 22). This is important since doublets of cells in G1 can yield false positives for G2/M single cells (see Section 2.2.8).

Subsequently, the "Single Cells" gate was used to plot the DNA as well as FUCCI fluorescence patterns.

As expected, Figure 23, upper left Section, doesn't display any stained DNA specific fluorescence. The upper right displays the typical FUCCI fluorescence pattern. In the lower left Section, typical DNA pattern is visible. Note that the FUCCI fluorescence pattern in the lower right Section (Hoechst33342 stained) resembles the upper right Section (unstained) to a rather large extent. However, minor changes in the percentages of the hinged regions occur.

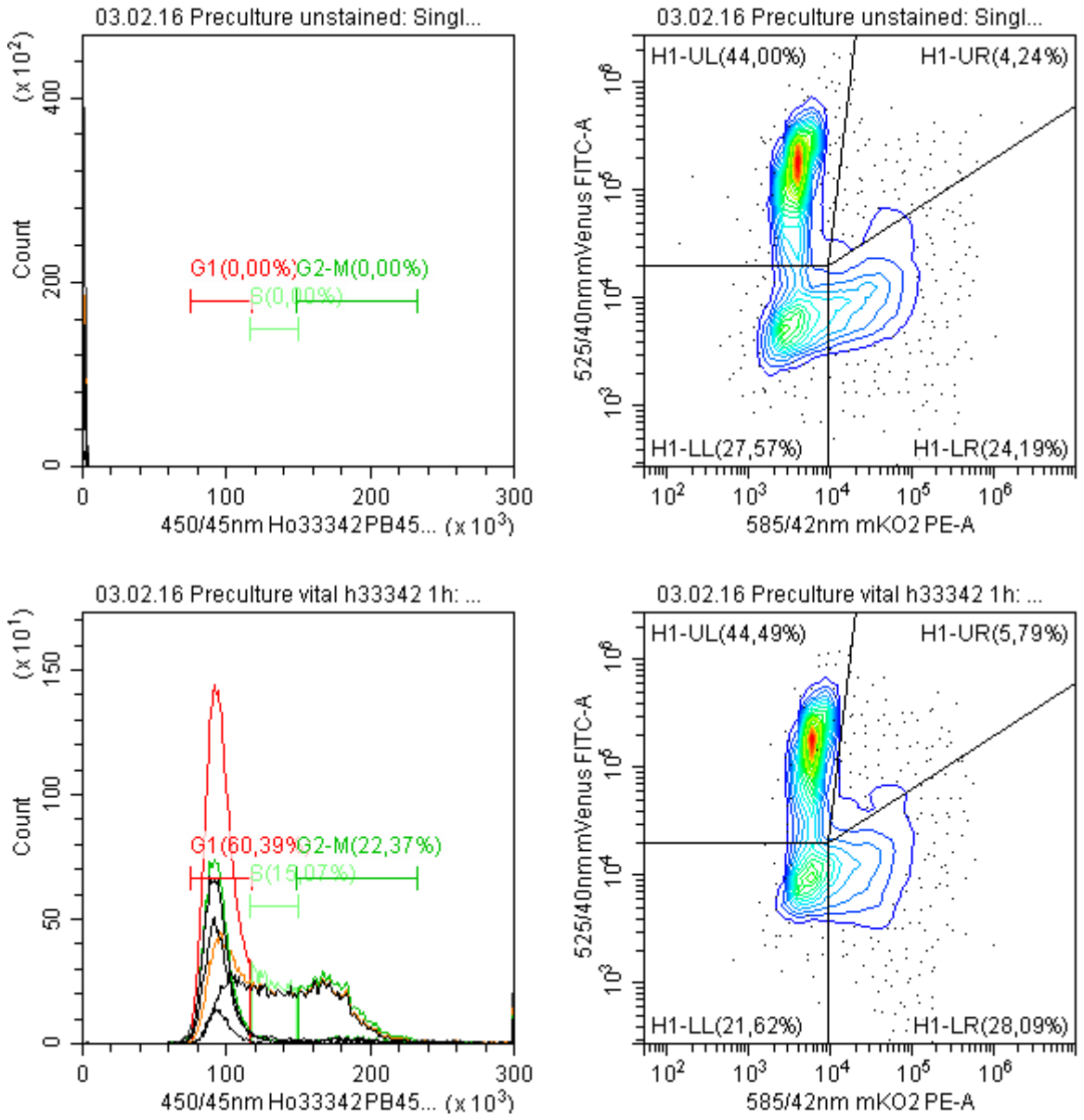

Figure 23: Gating unstained and Hoechst33342 stained pre-culture
Left side: DNA histogramms; right side: FUCCI fluorescence pattern; upper Section: Unstained; lower Section: Stained using Hoechst33342. While Hoechst33342 enables the detection of DNA it slightly alters the FUCCI fluorescence pattern.

5.3.1.2 Relationship between FUCCI fluorescence and the cell cycle - based on Hoechst33342

In order to elucidate if the FUCCI fluorescence represents the cell cycle phases, obtained from the Hoechst33342 DNA histogram, the gating strategy was used in the following manner.

As depicted in Figure 3, the G1 phase is associated with expression of the mKO2, leading to red fluorescence. Towards the end of the G1 phase and the beginning of the S phase, *mKO2* is being degraded while *mVenus* is expressed, leading to double positive cells.

The later S, entire G2 and early M phase are positive for *mVenus* and therefore green fluorescent. At the end of the M phase, mVenus is degraded and the cells are non-fluorescent until *mKO2* is expressed in the G1 phase.

When applying the cell cycle phase specific gates, defined in Figure 23, lower left Section, to the FUCCI fluorescence dot plots, it can be tested if cell cycle and FUCCI fluorescence display the expected relationship (see Figure 24).

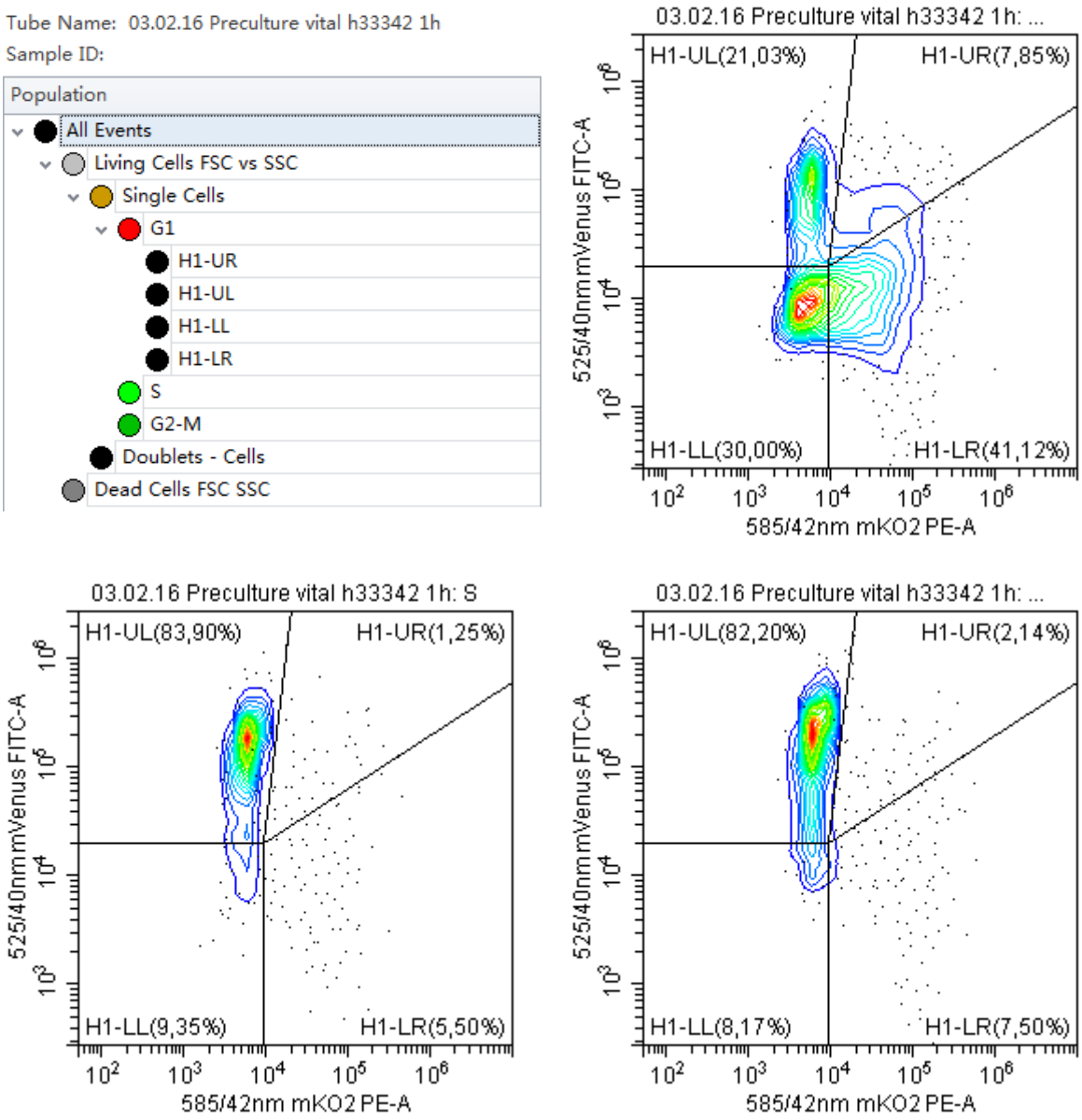

Figure 24: Cell cycle phase specific FUCCI fluorescence using gating
Upper left: Gating hirachy; upper right: G1 phase specific FUCCI fluorescence; lower left: S phase specific FUCCI fluorescence; lower right: G2/M phase specific FUCCI fluorescence

G1 phase specific fluorescence

See: Figure 24, upper right Section

The largest percentage of cells is found in the lower right region (LR) of the hinged gating on the dot plot, representing mKO2 expression. Furthermore, a certain number

of cells are in the upper right region (UR) indicating to be double positive for mKO2 and mVenus. This is in line with the hypothesis (see above).

Interestingly, more cells are found in the upper left (UL) region than in the upper right (UR). This indicates that they are only positive for mVenus. Therefore, mKO2 degradation and mVenus expression may be faster than initially expected.

The second largest percentage is found in the lower left (LL) region. These cells just completed mitosis and didn't express detectable levels of mKO2, at the time of measurement.

S phase specific fluorescence

See: Figure 24, lower left Section

In line with the hypothesis, by far the largest percentage of cells is found in the UL region. Also, relatively few cells are double positive or still single positive for mKO2. Interestingly, the second largest percentage of cells is double negative (LL).

G2/M phase specific fluorescence

See: Figure 24, lower right Section

The percentages are very similar to those of the S phase-specific fluorescence, which is also to be expected. Also, a certain number of cells is double negative.

In summary, these results, obtained from an exponentially growing culture, are in line with the hypothesis. Cell cycle and FUCCI fluorescence display the expected relationship. Not only in terms of association between fluorescence colour and cell cycle, but also concerning their chronological progression.

The relatively high values of double negative cells (LL region) can be accounted to the rather stringent gating conditions. This is a compromise, as the same gating strategy has to be applicable for all sample preparation protocols.

Additionally, the life staining with Hoechst33342 is another compromise. Since living cells take up the dye slower, the method is less accurate. This is also visible from the G2/M: G1 ratio in Figure 23, lower left Section. Under ideal conditions, the fluorescence signal, represented by the channel number of the G1 and G2/M peaks should differ by a factor of 2. Here this factor is <1.9.

In order to validate these findings, the same relationship between cell cycle and FUCCI fluorescence should be detectable when samples of differing cell cycle distributions are analysed. They can be generated by counter flow elutriations.

5.3.2 Qualitative relationship between FUCCI fluorescence and the cell cycle - subsequent to elutriation

For this Section a culture of exponentially growing CHO-K1 FUCCI CN cells was separated by size, using counter flow elutriation.

It was demonstrated in the 2nd Chapter that mammalian cells can be separated by size and hence, by cell cycle phase. If the working hypothesis is right and *FUCCI* fluorescence behaves in a strictly cell cycle dependent manner, samples of different cell cycle distributions should yield correlating FUCCI fluorescent patterns.

5.3.2.1 Size distribution after elutriation

In this Section, the results of the elutriation process are considered in detail. Figure 25, upper Section, includes the normalised size distributions of the untreated preculture. It shows the characteristic, broad size distribution, containing cells of all growth phases.

Furthermore, the three fractions obtained at 20, 30 and 40 [ml/min] are displayed. Their characteristic cell size differs, spanning 11.86 to 14.39 µm, as represented in Table 5: Characteristic cell sizes [µm] after elutriation.

Table 5: Characteristic cell sizes [µm] after elutriation
Preculture (13.16µm) was separated into three fractions between 11.86 and 14.39 µm.

Fraction	Characteristic cell size [µm]
Preculture	13.16
20 ml/ml	11.86
30 ml/ml	12.99
40 ml/ml	14.39
50 ml/ml	12.99
50 ml/ml rotor stop	13.16

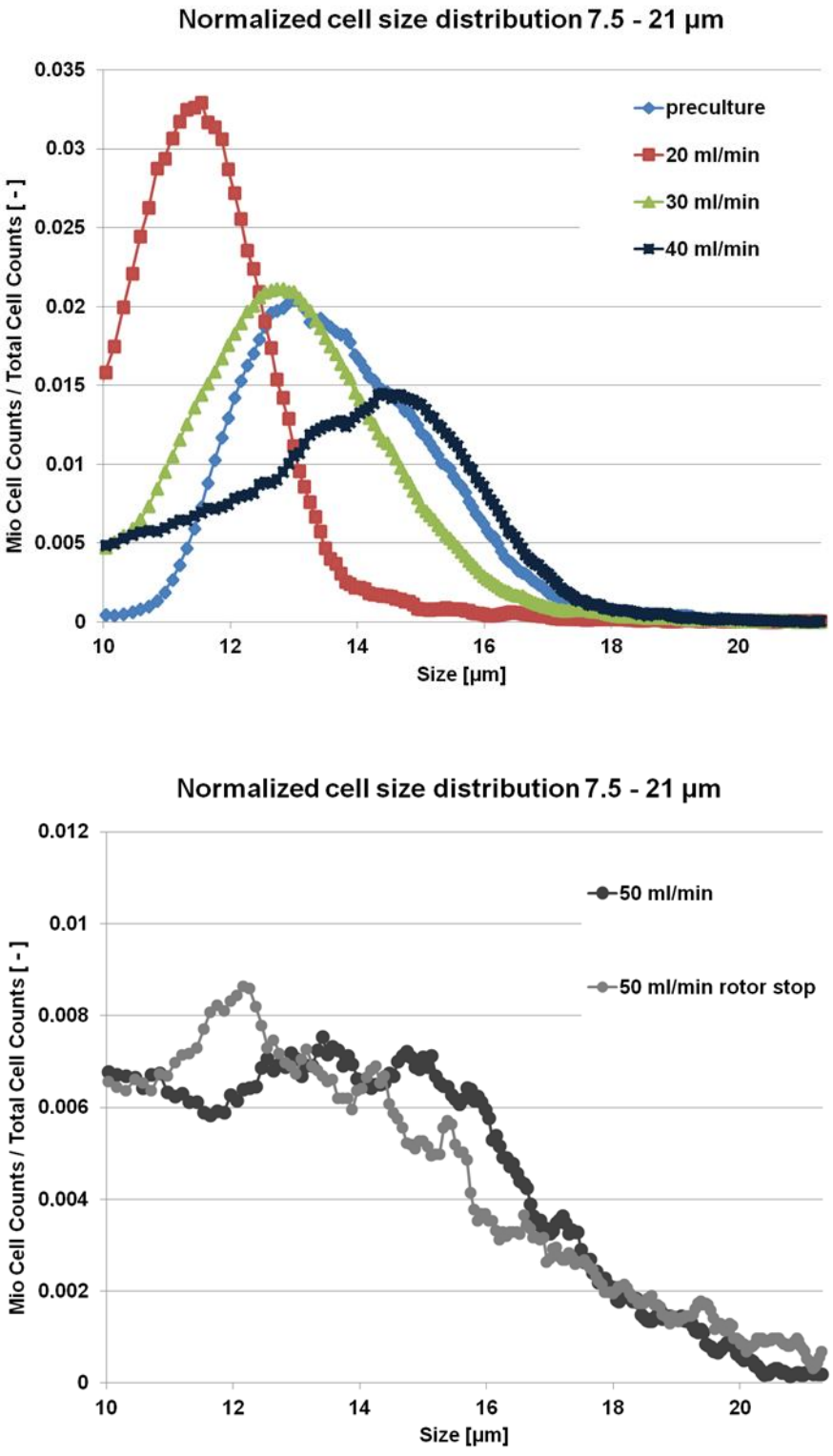

Figure 25: FUCCI elutriation fractions
Upper Section: Well distinguishable size distributions; lower Section: Non-specific size distributions. Preculture was separated into three fractions of distinct cell sizes.

In contrast to this, the fractions 50 ml/min and "rotor stop" contain cells of all cell cycle phases, comparable to the preculture (Figure 25, lower Section). This is also evident from the characteristic cell sizes of approximately 13 µm (Table 5: Characteristic cell sizes [µm] after elutriation).

This is a common effect (see 2nd and 3rd Chapter), caused by doublets or larger aggregates of cells. They behave like larger particles in the elutriation chamber but contain cells of different cell cycle phases. Hence, they are elutriated at higher flow rates but are non-specific for any cell cycle phase.

In summary, the elutriation procedure was successful, yielding three fractions (20, 30 and 40 [ml/min]) of CHO-K1 FUCCI CN cells with different cell sizes (11.86, 12.99 and 14.39 [µm]) and therefore cell cycle phases.

These fractions were used in parallel for all staining protocols described in 5.3.1. The cell cycle data, obtained by permeabilisation with EtOH and DAPI staining, was directly linked to the unstained FUCCI fluorescence, since both sets of data originate from the same elutriation fraction. This enables the use of both accurate methods, while maintaining comparability. For reference, the less accurate Hoechst33342 method for living cells was applied in parallel (see Section 5.3.1).

5.3.2.2 Gating and staining: DAPI

This protocol is based on permeabilisation of cells prior to staining (see Section 2.2.8.2) to allow the DAPI dye to enter the cells. Consequently, the cells die off and display the corresponding properties in the forward vs. sideward scatter plot (see Figure 26). Therefore, the gating strategy was changed, compared to Figure 22.

Instead of the "Living cells FSC vs. SSC", the "Dead cells FSC vs. SSC" gate was used for subsequent analysis.

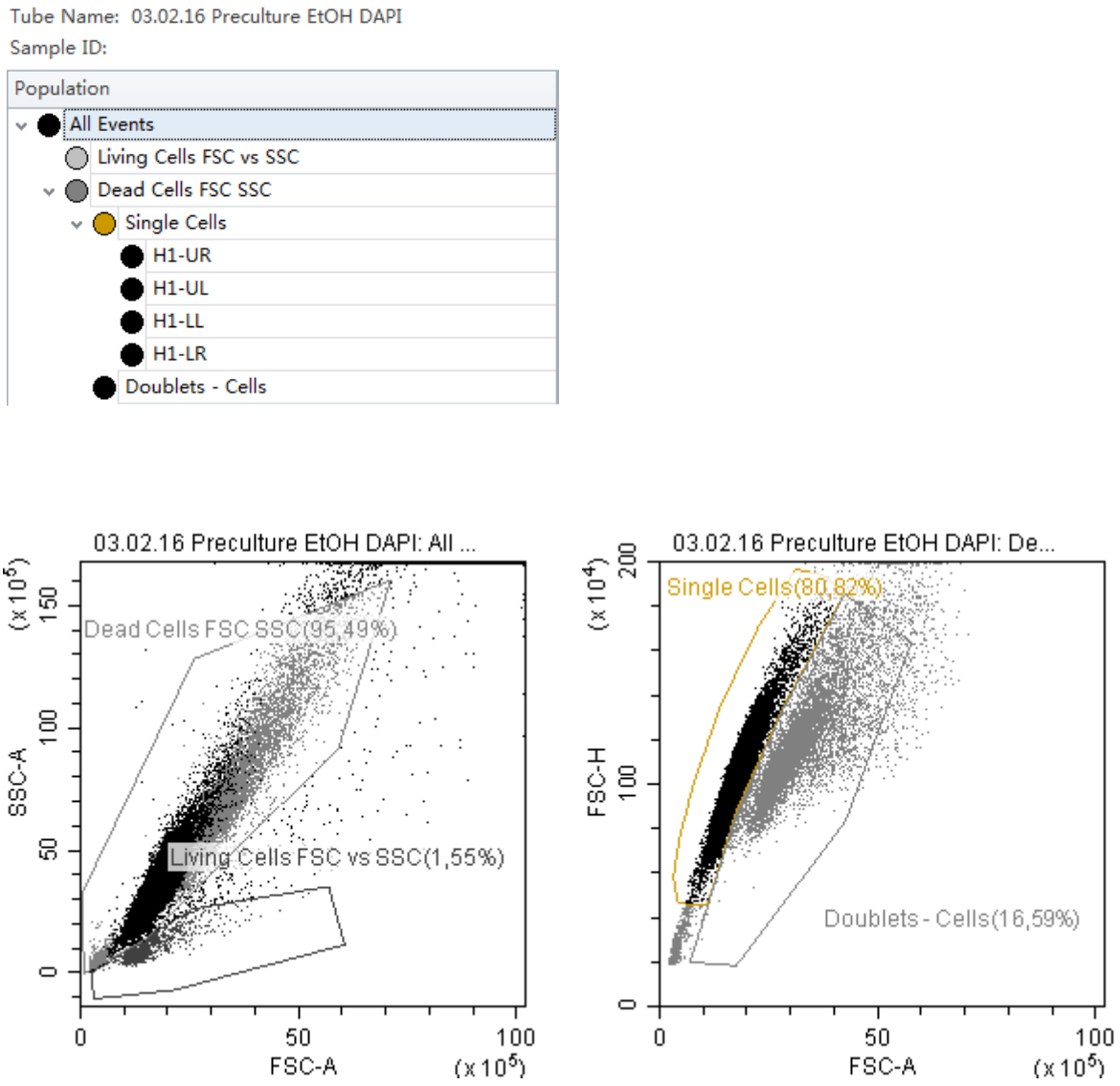

Figure 26: Gating permeabilised cells
Upper graph: Gating hirachy for permeabilised cells; Left graph: Gating for dead cells, right graph gating for single cells

The results reflect the same relationship between cell cycle (based on DNA analysis) and FUCCI fluorescence, observed in Section 5.3.1.2:

Figure 27, lower Section characterizes the fraction as almost entirely composed of cells in the G1 phase. This is accompanied by FUCCI fluorescence in the lower left (LL) and right (LR) region.

Likewise, the increased amounts of cells in the S and G2/M phase are accompanied by higher percentages in the upper left (UL) region (see Figure 28).

In line with the cell size data (Figure 25 and Table 5: Characteristic cell sizes [µm] after elutriation) the remaining fractions are less specific for single cell sizes, which is also in line with the DNA and FUCCI fluorescence pattern (Figure 29).

Once more it can be concluded that FUCCI fluorescence represents the same information, obtainable from DNA analysis. Hence, both methods are suitable indicators of the cell cycle state.

In this Section it could be shown that the strong relationship between FUCCI fluorescence and DNA data can not only be found in cultures growing under standard conditions but also in samples of strongly differing cell cycle distributions.

How this strong relationship can be expressed in terms of correlation is discussed in Section 5.3.3).

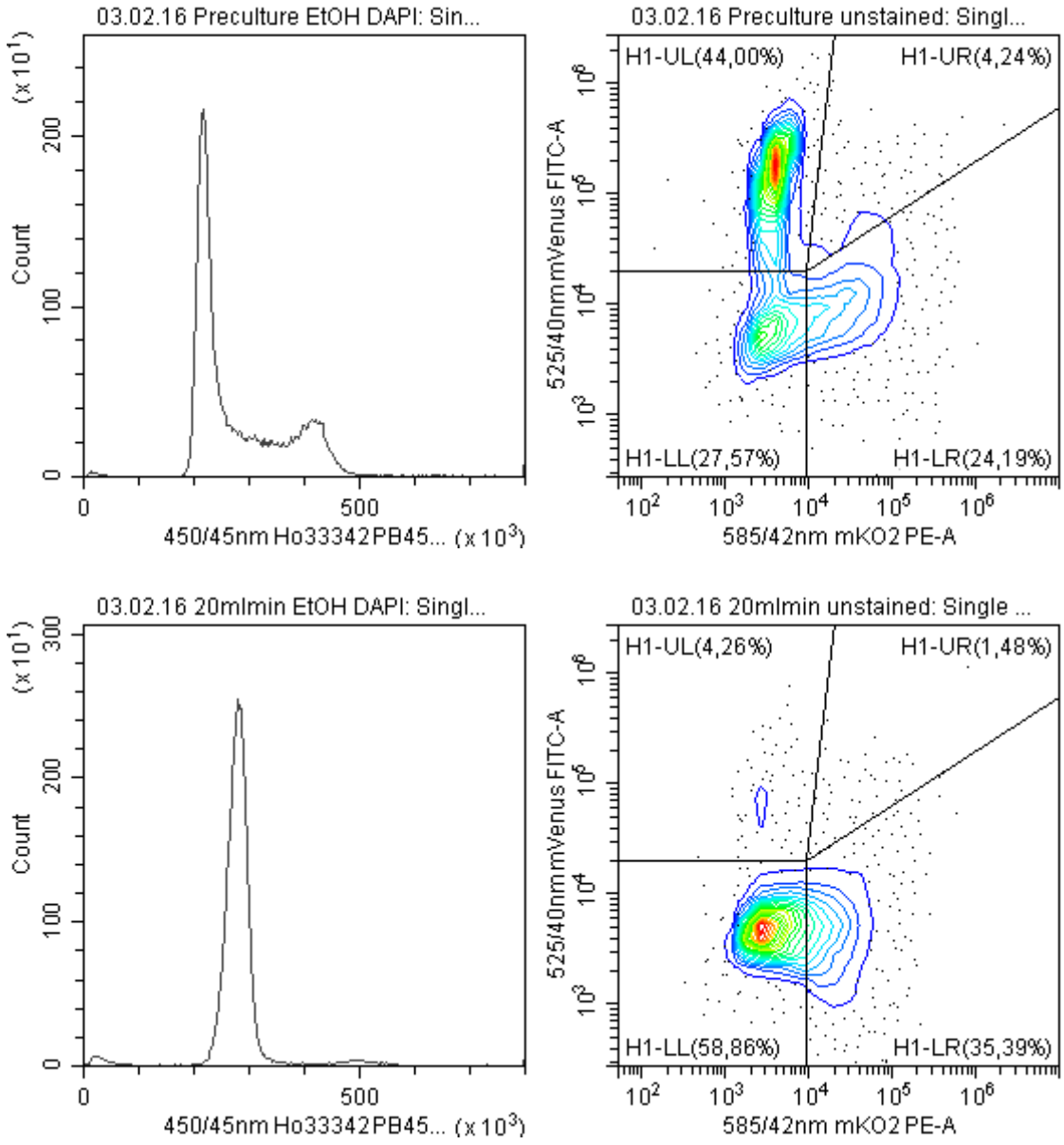

Figure 27: DNA histogram (DAPI) and FUCCI fluorescence: Preculture and fraction 20 ml/min

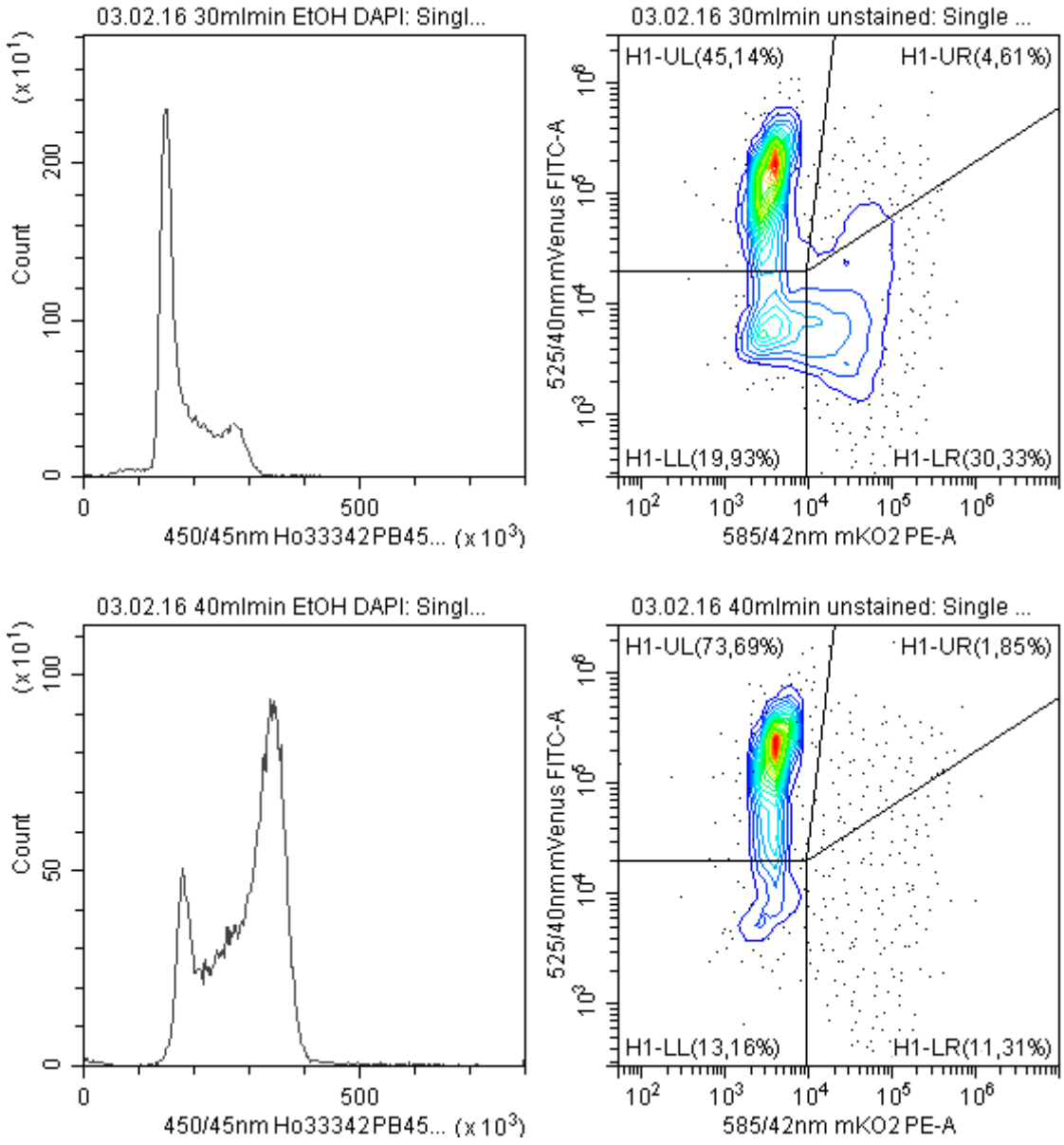

Figure 28: DNA histogram (DAPI) and FUCCI fluorescence: Fractions 30 and 40 ml/min

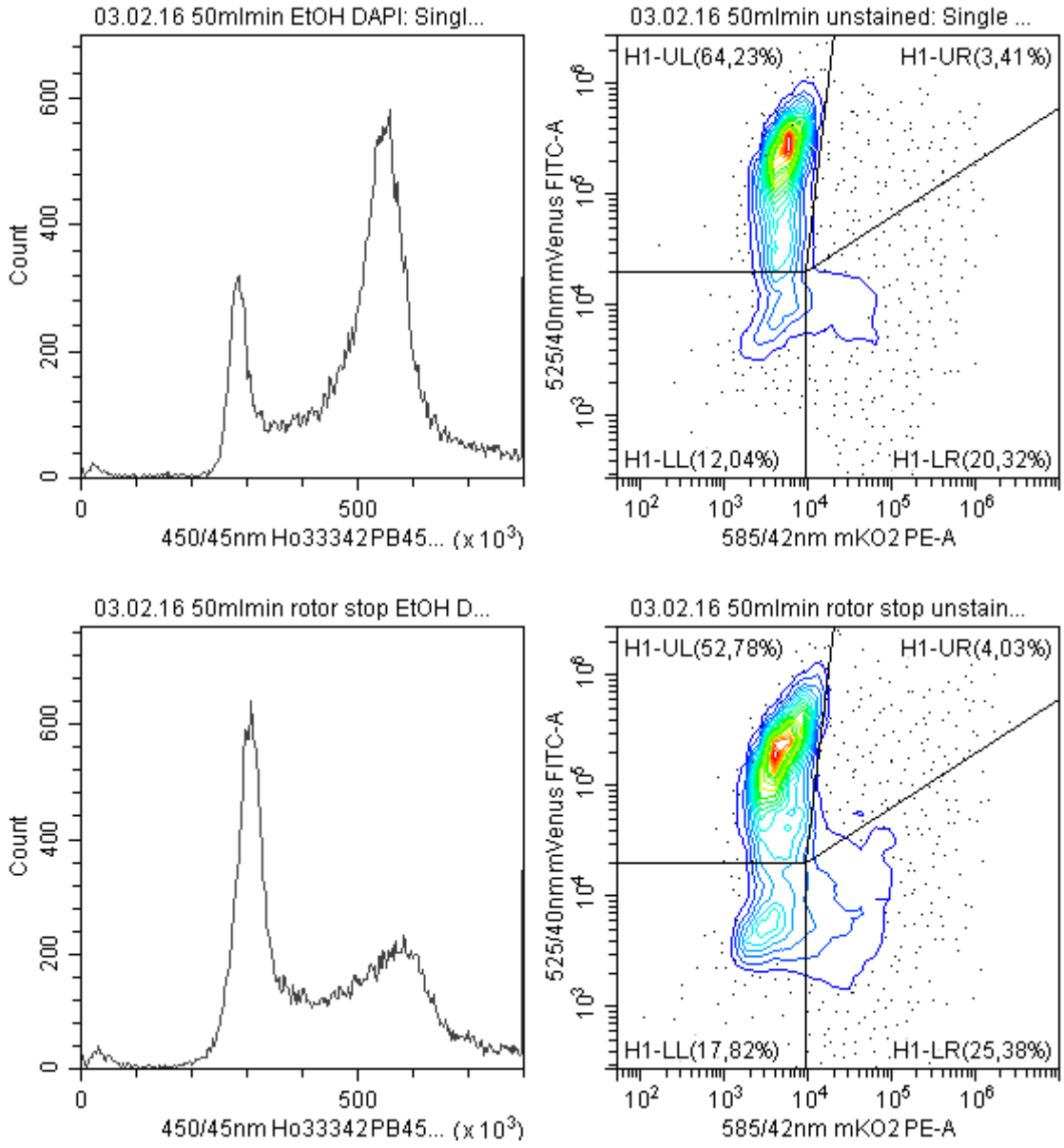

Figure 29: DNA histogram (DAPI) and FUCCI fluorescence: Fractions 50 ml/min and rotor stop

5.3.2.3 Vital cell staining with Hoechst33342

The same relationship explained in the previous Section was also tested, utilizing living cells and the cell dye Hoechst33342, as explained. The results support the conclusions drawn earlier. However, in line with the effects explained above (see Section 5.3.1.2) DNA peaks and FUCCI fluorescence patterns are less well defined.

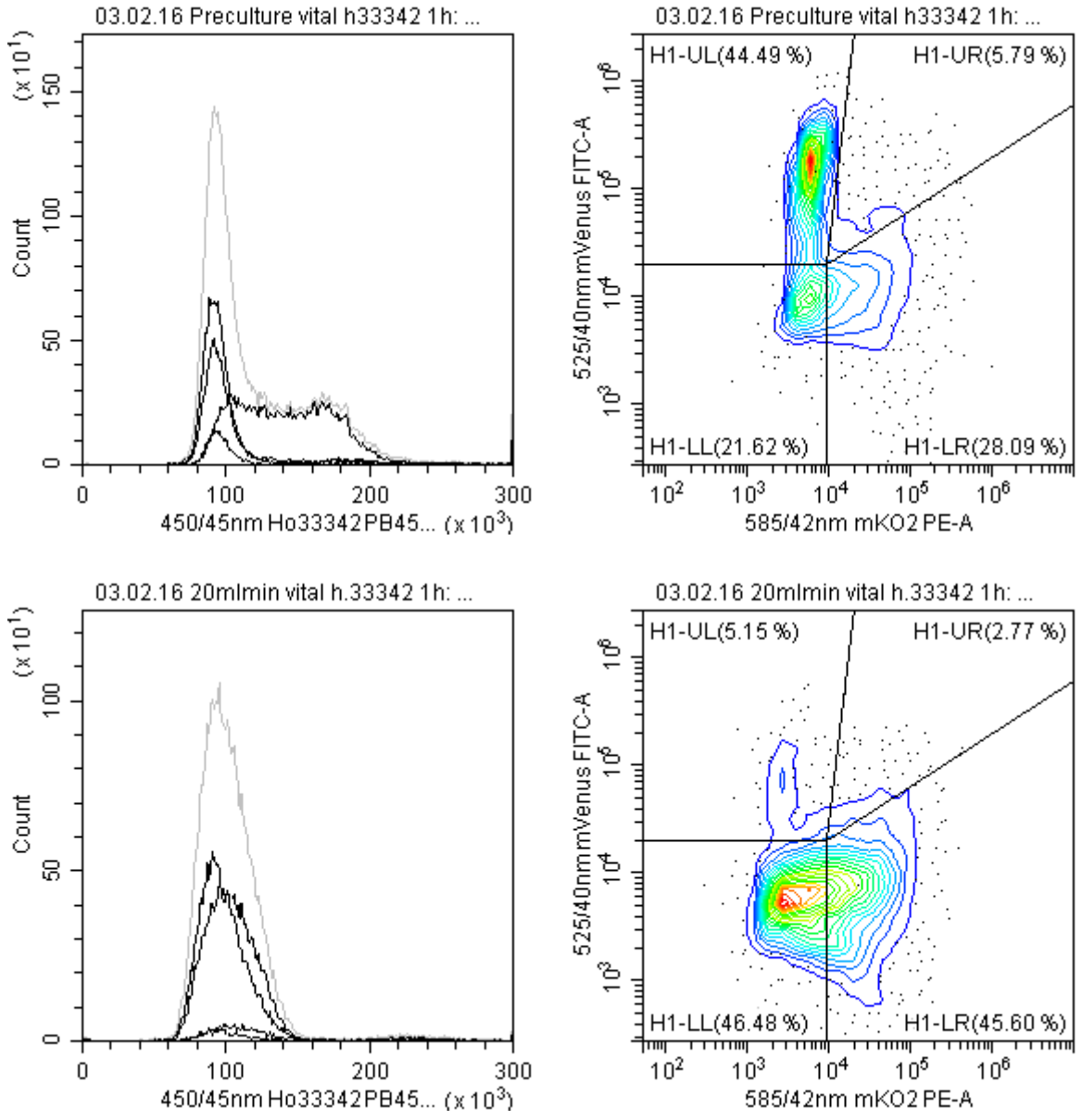

Figure 30: DNA histogram (Hoechst33342) and FUCCI fluorescence: Preculture and fraction 20 ml/min

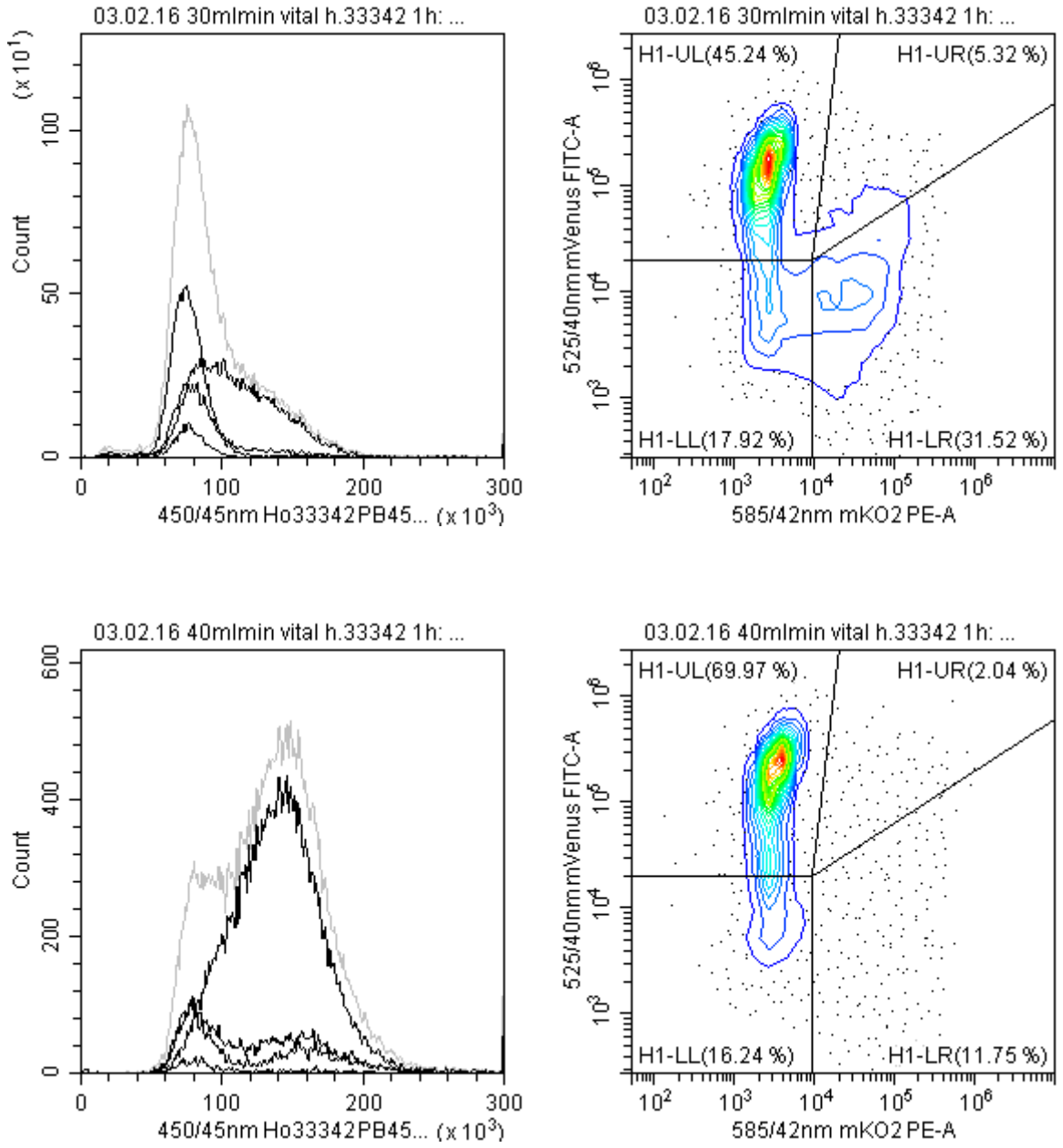

Figure 31: DNA histogram (Hoechst33342) and FUCCI fluorescence: Fractions 30 and 40 ml/min

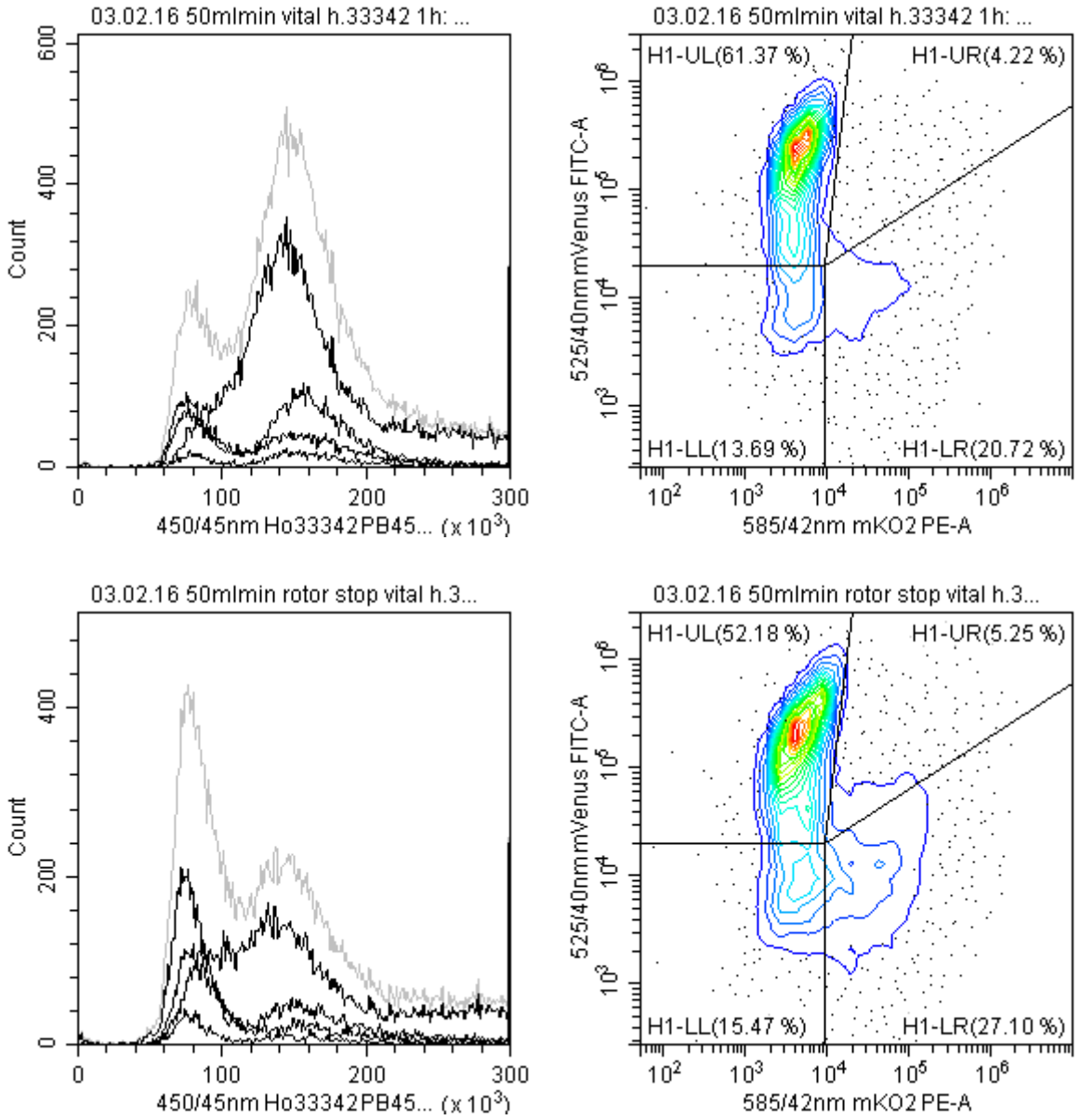

Figure 32: DNA histogram (Hoechst33342) and FUCCI fluorescence: Fractions 50 ml/min and rotor stop

5.3.3 Quantitative correlation of the fluorescence ratio i_{red}^{n} and the cell cycle distribution G1 [%]

Based on the qualitative results stated above (see Section 5.3.2.3), the approach using unstained, living cells for FUCCI fluorescence quantification (see Section 5.2.3.1), in combination with EtOH permeabilised, DAPI stained cells (see Section 5.2.3.3) was chosen for further quantitative analysis.

In order to avoid subjectivity, a standardised approach (see Section 5.2.5 for i_{red}^{n} and Section 5.2.6 for G1 [%]) was used for all samples.

The gating strategy is visible in Figure 33. It is a simple threshold and number-based method. Meaning, cells are either positive (fluorescence > threshold) or negative (fluorescence < threshold) for mKO2 and/or mVenus, the ratio i_{red}^{n} calculated from the numbers of cells. Differences in signal intensities are not considered.

In Figure 34 the data of two elutriation experiments as well as a bioreactor experiment are plotted. The bioreactor data discussed later (see Section 6.3.3), here the elutriation experiments are of particular interest.

RGP analysis (also called LINEST, using the "least squares" method) supports a strong linear correlation of the cell cycle distributions (G1 [%]), with i_{red}^{n}. Pearson correlation coefficients are 0.961 and 0.954, respectively; slopes 0.808±0.116 and 0.726±0.072. Considering the calculated standard deviations, both slopes are undistinguishable.

This is in line with the expectations for this simple threshold based model: the cells alter their fluorescence in accordance with the cell cycle.

For extremely high G1 fractions (>0.8), the linear correlation is less pronounced. This is likely to be caused by the uncertainty of classical, DNA staining based cell cycle determination method. Due to the fact that the second (G2) peak does not appear, quantification of G1 versus all other cells, is very inaccurate.

Nonetheless, differences in cell cycle distributions of cultures can be determined based on the fluorescence, despite the fact that each individual cell undergoes short phases of double positive or double negative fluorescence (see Figure 3).

It can be concluded that i_{red}^{n} is a suitable read out of the cell cycle state without the need of additional staining or sample preparation.

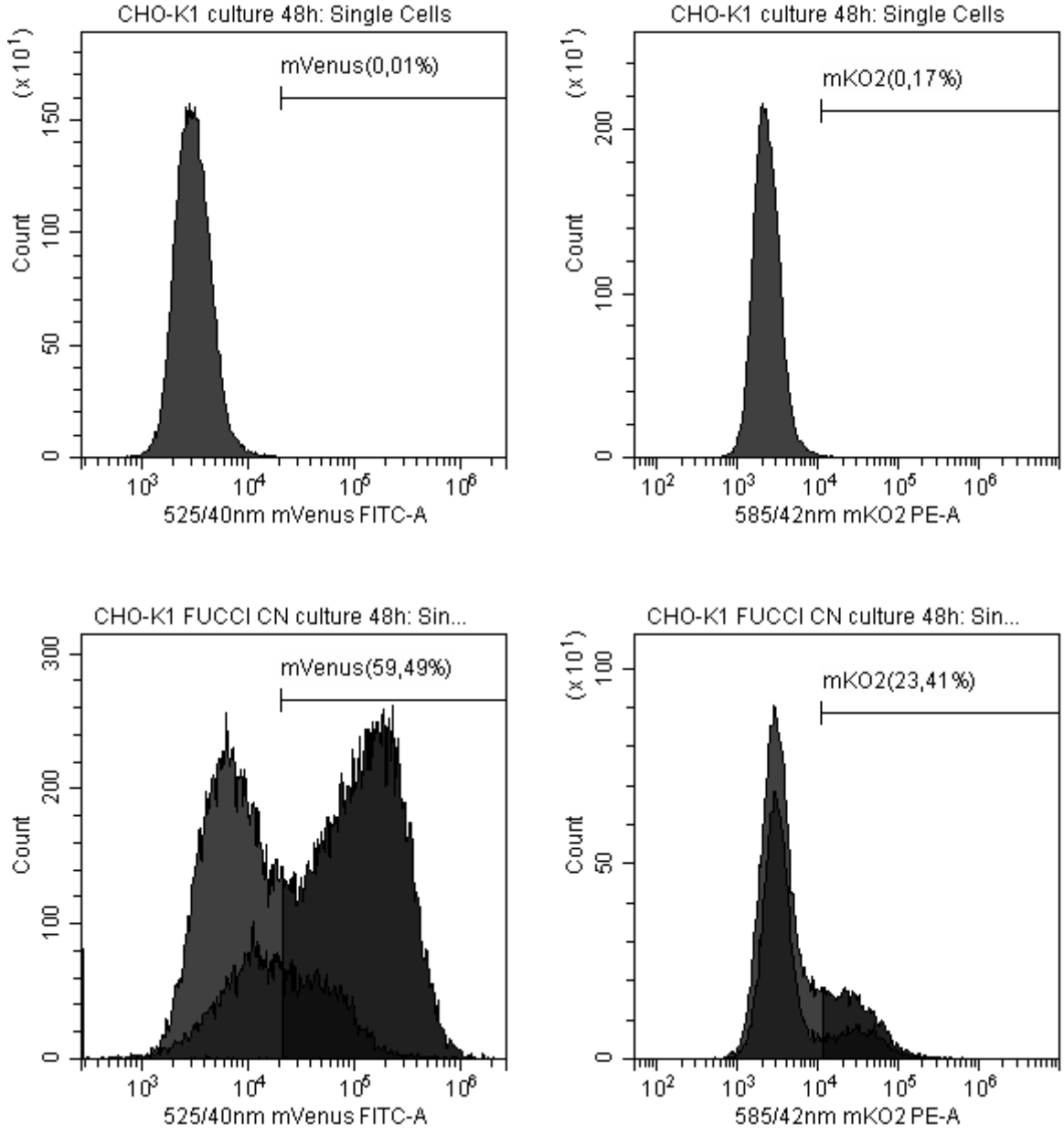

Figure 33: Positive and negative controls for fluorescence quantification thresholds
Left Section: mVenus; right: mKO2; upper Section: Negative controls, lower: positive controls - Determined thresholds distinguish between fluorescence and background

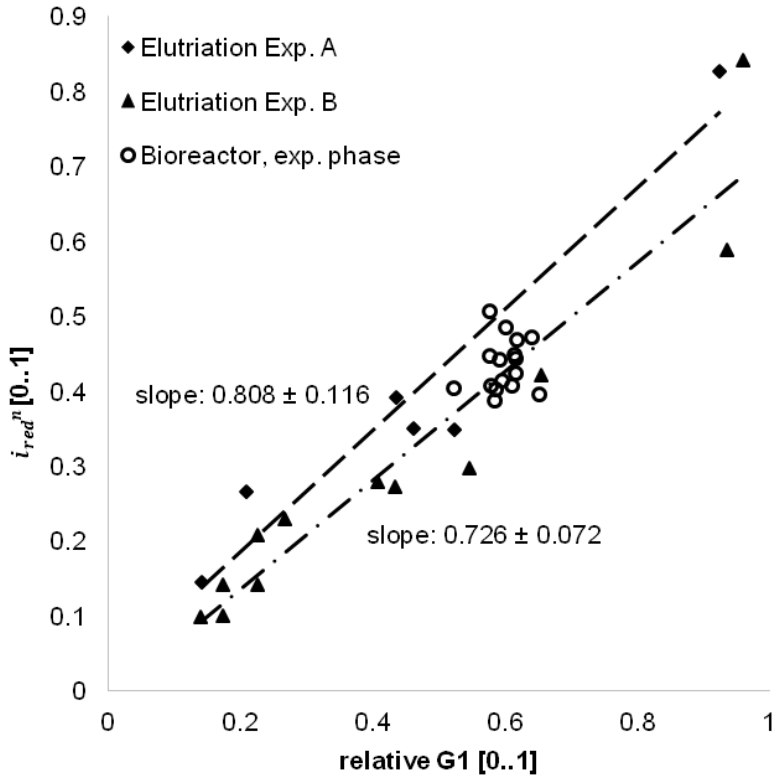

Figure 34: Correlation of i_{red}^{n} and G1 [%]
The data points of both elutriation experiments exhibit a linear correlation with the relative G1 fraction. Both slopes (Elutriation Exp. A and B) are indistinguishable, considering measurement accuracy. The corresponding distribution in the non-synchronized bioreactor experiment during its non-growth-limited phases (average G1 at (59.8 ± 3.0) %; average i_{red}^{n} (43.6 ± 3.5) %) is in line with the elutriation data. Data and graph were published previously [98].

5.4 Conclusion

In this Chapter it was shown that the *FUCCI* fluorescence is a suitable representation for the cell cycle state during cultivation of the newly developed CHO-K1 cell line derivatives.

In simple gaiting-based investigations, the qualitative relationship of the cell cycle (based on DNA content) and fluorescence was shown using different staining protocols (viable cells: Hoechst33342, permeabilised cells: DAPI). These findings were further validated by using samples of strongly differing cell cycle distributions, generated by counter flow elutriation. Said strong relationship was found to be consistent and quantitative analysis revealed that the number and threshold-based parameter i_{red}^{n} correlates with the cell cycle state (expressed as G1 [%]).

6. Interdependencies between FUCCI fluorescence and the specific growth rate (μ)

In the 5th Chapter it was demonstrated that the threshold and number based fluorescence ratio i_{red}^{n}, based on *CytoFlex* flow cytometer measurements, correlates with the cell cycle state (G1 [%]) in cultures of the novel cell line derivative *CHO-K1 FUCCI CN*, provided that all other conditions remain constant.

Since the cell cycle distribution is inevitably related to the specific growth rate (μ) of mammalian cell cultures, this information is most valuable for bioprocess monitoring and control. However, elaborate detection hardware capable of detecting the fluorescence of single cells is needed to calculate i_{red}^{n}.

Nonetheless, in bioreactor setups and possibly industrial application, it is desirable to obtain said information about the cell cycle distribution with simpler, more robust (e.g. autoclaving compatible) and cost-effective hardware, like fluorescence probes. In contrast to single cells, such probes detect the total fluorescence of cultures.

Hence, this Chapter[5] focuses on the relationship between cell cycle, total FUCCI fluorescence and specific growth rate.

[5]Some content of this Chapter was published previously [98]. Various experiments were performed with the involvement of bachelor student Yaeseong Hong and are part of his thesis [101].

6.1 Technical and theoretical background

In order to discuss the functional relationship between cell cycle, FUCCI fluorescence protein expression and specific growth rate (μ), several fundamental links need to be considered in detail.

During the G1 phase, *CHO-K1 FUCCI CN* cells exhibit red, throughout the S and G2+M phase green fluorescence (see Section 4.1.1). Proliferating cells pass from one phase to the next and hence, change their colour continuously.

Cells which enter the quiescent G0 phase [100] exhibit the same red fluorescence as cells in G1 [60, 61]. Therefore, it is useful in regard to observations based on *FUCCI* fluorescence, to limit and approximate the categories to S+G2+M = green and G1+G0 = red fluorescence, thereby neglecting the short double positive (yellow) and double negative (colourless) phases (see Figure 3).

Cells enter the putative G0 phase or remain longer in G1 phase when their growth is inhibited and continue normal progression if the inhibition is removed [100]. Accordingly, it is hypothesised that the percentage of cells in the G1+G0 phase and therefore red fluorescence should increase if the growth of *FUCCI* cell cultures is inhibited. Consequently, cultures during uninhibited growth have the lowest percentage of cells in the G1+G0 phase and the lowest red fluorescence. However, the percentage of cells in G1 can never be zero, since proliferating cells pass through the G1 phase once for each cell cycle.

Based on this, the general hypothesised relationship between total fluorescence, fluorescent protein concentration and density of cells in a certain cell cycle phase, is explained in the following.

For the sake of simplicity, these considerations are made under the assumptions of fluorescence measurements in the dynamic range with no interference from the inner filter effect (absorbance due to high concentrations of fluorophores, see below).

$$I_{red}^{total} \leftrightarrow c_{mKO2} \sim n_{\mathrm{G0+G1}}$$ **Equation 13**

I_{red}^{total}: Total red fluorescence

c_{mKO2}: Concentration of the mKO2 fluorescence protein

$n_{\mathrm{G0+G1}}$: Density of cells in the G0+G1 cell cycle phase

$$I_{green}^{total} \leftrightarrow c_{mVenus} \sim n_{S+G2+M}$$ **Equation 14**

I_{green}^{total}: Total green fluorescence

c_{mVenus}: Concentration of the mVenus fluorescence protein

$n_{\mathrm{S+G2+M}}$: Density of cells in the S+G2+M cell cycle phases

Hence, the total red fluorescence depends on the concentration of mKO2 and therefore the density of cells in G0+G1 (Eq. 13). The same applies to green fluorescence and mVenus (Eq. 14).

Accordingly, it could be possible to calculate the density of cells in a specific cell cycle phase directly from fluorescent measurements if the correlation is sufficiently linear and accurate proportionality factors ($K_{red\ CM}$, $K_{green\ CM}$, $K_{red\ CN}$ and $K_{green\ CN}$) are defined (Eqs. 15 - 18). Note that these factors would differ between *CHO-K1 FUCCI CM* and *CN*, due to the different sub-cellular localisation of mVenus-hGeminin(1/110) and mVenus-hGeminin(1/60) (see Section 4.1.1).

CHO-K1 FUCCI CM

$$n_{S+G_2+M} = \frac{I_{gree}^{total}}{K_{green\ CM}} \qquad \textbf{Equation 15}$$

$$n_{G0+G1} = \frac{I_{red}^{total}}{K_{red\ CM}} \qquad \textbf{Equation 16}$$

CHO-K1 FUCCI CN

$$n_{S+G_2+M} = \frac{I_{green}^{total}}{K_{green\ CN}} \qquad \textbf{Equation 17}$$

$$n_{G0+G1} = \frac{I_{red}^{total}}{K_{red\ CN}} \qquad \textbf{Equation 18}$$

Under real measurement conditions, however, such proportionality factors are difficult to define with sufficient accuracy and reproducibility as they are composed of several factors including possible variations. First of all, fluorescence quantification: the results may vary with the type and sensitivity of the detection method. Furthermore, all measurements have to be conducted within the dynamic range. If concentrations are too high, the excitation wavelengths are absorbed before reaching all fluorescent proteins. Likewise, the emitted wave lengths can be reabsorbed before reaching the detector.

This is problematic, especially if on-line fluorescence measurements shall be conducted using fluorescence probes. The application of this system is aimed at process control for a variety of applications, including, but not limited to, high cell density cultivation. Variations of cell densities over two orders of magnitude or more would make the determination of proportionality factors difficult.

Furthermore, the different localisations of the fluorescent proteins have to be considered. mKO2-hCdt1(30/120) can only be found in the nucleus. In case of *CHO-K1 FUCCI CN* the combination of cytosolic mVenus-hGeminin(1/60) with nuclear mKO2-hCdt1(30/120) may lead to a systematic underestimation of red fluorescence at higher cell densities.

These reasons do not generally exclude the option to identify such proportionality factors for a defined set of conditions. However, generalisations of these should be undertaken with caution.

For the purpose of robust analysis and potential process control it is instead more straightforward to compute the ratio of the total fluorescence (i_{red}^{total}; Eq. 19). In contrast to i_{red}^{n} it can be determined based on any method, capable of detecting total fluorescence, e.g. fluorescence probes. In this study a plate reader (see Section 6.2.3) as well as flow cytometry (6.2.4) were used.

$$i_{red}^{total} = \frac{I_{red}^{total}}{I_{red}^{total} + I_{green}^{total}} \qquad \textbf{Equation 19}$$

The parameter i_{red}^{total} is defined as ratio of red and total fluorescence. As discussed at the beginning of this Section, inhibition of growth should lead to an increased red fluorescence ratio (i_{red}^{total}) due to the assumed accumulation of cells in G0+G1 phase. Conversely, uninhibited growth should correlate with low i_{red}^{total} values.

Equation 16 and Equation 18 can be expressed in a generalised manner:

$$I_{red}^{total} = n_{G1} \cdot K_{red} \qquad \textbf{Equation 20}$$

Consequently, following from Equation 20, it can be hypothesised that the lowest possible i_{red}^{total} value during exponential growth is defined by the concentration of cells

in the G1 and S+G2+M phase during uninhibited growth as well as the corresponding proportionality factors. This value is referred to as basal i_{red}^{total} value ($i_{red\ basal}^{total}$, $i_{red\ basal}^{PR}$ or $i_{red\ basal}^{nmean}$, respectively; Eq. 21).

$$i_{red\ basal}^{total} = i_{red}^{total}(\mu_{max}) = \frac{n_{G1} \cdot K_{red}}{n_{G1} \cdot K_{red} + n_{S+G2+M} \cdot K_{green}} \qquad \textbf{Equation 21}$$

$i_{red}^{total}(\mu_{max})$: i_{red}^{total} value at maximum specific growth rate (μ_{max})

It is reasonable to expect minimal as well as maximal i_{red}^{total} values during the course of batch cultivations.

In the case of (partially) synchronised cultures, i_{red}^{total} is plausible to additionally oscillate in line with the G1 [%] (see Figure 9).

The $i_{red\ basal}^{total}$ values of *CHO-K1 FUCCI CN* can be anticipated to be lower compared to *CHO-K1 FUCCI CM*, due to the cytosolic localisation of *mVenus-hGeminin(1/60)*. It is probable to yield a stronger green fluorescence signal than *mVenus-hGeminin(1/110)*, which is limited to the nucleus.

Hypothetically, the general relationship between the specific growth rate (μ) and i_{red} should be as listed below (Table 6), independent from the cell line derivative (*CHO-K1 FUCCI CM* or *CHO-K1 FUCCI CN*) or the detection method (i_{red}^{n} or i_{red}^{total}).

Table 6: Hypothetical relationship of i_{red} vs. specific growth rate (μ)

$i_{red} > i_{red\ basal}$	$\mu < \mu_{max}$	Growth inhibited
$i_{red} = i_{red\ basal}$	$\mu = \mu_{max}$	Optimal growth
$i_{red} < i_{red\ basal}$	-	Only temporarily achievable through synchronisation

It is of significant interest for process control to investigate if this hypothesis is correct.

The specific growth rate of mammalian cells can conventionally be calculated based on measured cell densities at multiple points in time (Equation 3). Therefore, it can only be obtained in retrospect. Secondly, the oxygen uptake rate (OUR) can be monitored. However, it represents the total aerobic metabolism e.g. including recombinant protein expression in production processes - not exclusively the specific growth rate (µ).

Supposed that i_{red}^{total} proves to be a reliable indicator for the specific growth rate (µ), a fluorescence based online measurement could elegantly be applied to detect and potentially circumvent growth limitations in real time.

Furthermore, if said relationship could be robustly quantified for a defined system, it may even be possible to approximate the specific growth rate (μ) from a single measurement.

6.2 Materials and methods

Unless indicated otherwise, materials and methods are as described in the 5th Chapter.

6.2.1 Shaking flask based growth experiments

Cell culture was performed as described in Section 5.2.1. At the indicated points in time, samples were taken under sterile conditions and cells were quantified using a particle counter (Section 2.2.6) and *Neubauer* chamber (Section 2.2.5). The remaining cells were stored (Section 2.2.8.2) for later plate reader (Section 6.2.3) and glucose/lactate analysis (Section 6.2.7). The specific growth rate µ was calculated using a Gaussian filter (Section 6.2.5).

6.2.1.1 Shaking flasks: batch conditions

Experiments were conducted by inoculation of *CHO-K1 FUCCI CM* as well as *CHO-K1 FUCCI CN* cultures at cell densities 0.8 Mio/ml and continuous sampling for 100 h.

6.2.1.2 Shaking flasks: variation of L-glutamine concentration

The experiment was conducted in three subsequent steps. A preculture with an initial cell density of 1 Mio/ml, containing 4 mM L-glutamine was cultured for 21 h before split into two cultures with cell densities of 0.8 Mio/ml and different medium compositions. The culture termed "+Gln" contained fresh, fully supplemented medium including 4 mM L-glutamine. The "-Gln" culture was identical except for the fact that no L-glutamine was included. After a total culture time of 50 h, hence 29 h of L-glutamine depletion, the "-Gln" culture was split again. While half of the culture was maintained under L-glutamine depletion, the other half was supplemented with L-glutamine to yield a final concentration of 4 mM ("Gln addition"). No antibiotics were used at any time.

6.2.2 VSF 2000 bioreactor based growth experiments

A *VSF2000* bioreactor (BioEngineering, Wald, Switzerland) was used with an initial volume of 1.1 L. pH was actively controlled at 7.4, temperature at 37°C. pO2 was maintained at a minimum of 30% air oxygen saturation at all times - except for the induced period of induced oxygen limitation (<10% air oxygen saturation).

At the time of inoculation, the CHOMACS CD Medium (Miltenyi Biotec GmbH, Bergisch Gladbach, Germany) was supplemented with 1 mM glutamine. The initial cell density was 1 Mio/ml.

At the time of feed addition, the reactor volume had decreased to 1050 ml due to sampling. The feed consisted of 48 ml 10x concentrated medium including L-glutamine (Miltenyi Biotec GmbH, Bergisch Gladbach, Germany), raising the L-glutamine concentration by 1.45 mM. No antibiotics were used at any time.

6.2.3 Determination of i_{red}^{PR} using a plate reader - *Safire 2*

Of each sample 200 µl cells, stored in EtOH (see Section 2.2.8.2) were transferred to wells of black flat bottom 96 well plates (Type 655076; Greiner Bio-one, Kremsmünster, Austria). In parallel 200 µl of 70% EtOH were used as blank. Plate loading, and transport were conducted in cooled boxes, measurement was executed as brief as possible to minimise evaporation.

For total fluorescence measurements a *Safire 2* plate reader (Tecan, Männedorf, Switzerland) was used. Based on the fluorescence properties of mVenus and mKO2 (see Table 4: FUCCI fluorescent protein properties), the manufacturer's instructions and optimisation experiments, the following settings were used to avoid crosstalk:

- mVenus: Ex. 510 nm, Bandwidth 10 nm; Em. 533 nm, Bandwidth 10 nm
- mKO2: Ex. 546 nm, Bandwidth 10 nm; Em. 571 nm, Bandwidth 10 nm
- Integration time: 40 µs; Lag time: 0 µs
- Number of reads: 20
- Mode: High sensitivity
- manual Z axis: 6000 µm

The *gain* value was determined for each measurement using the *optimal gain* function in a first measurement, yielding separate values for mKO2 and mVenus. Subsequently, the lower *gain* value was set manually for both measurements to yield comparable total intensities. Measurements were conducted in technical triplicates.

The i_{red} value was calculated as follows:

$$i_{red}^{PR} = \frac{mKO2^{I} - mKO2^{\overline{I\,background}}}{mKO2^{I} - mKO2^{\overline{I\,background}} + mVenus^{I} - mVenus^{\overline{I\,background}}}$$

Equation 22

6.2.4 Quantification of FUCCI fluorescence distribution of viable cells: i_{red}^{n} and i_{red}^{nmean} using a flow cytometer - *CytoFlex*

Quantification of i_{red}^{n} was performed as described in Section 5.2.5. Additionally, i_{red}^{nmean} was calculated (Eq. 23).

Statistics settings were configured to include the *Mean* values of the *mVenus* gate in the *525/40 nm mVenus FITC-A* channel and the *Mean* values of the *mKO2* gate in the *585/42 mKO2 PE-A* cannel. Statistics were exported to the *.csv* file format and analysed using Microsoft Excel (Microsoft, Redmond, CA, USA).

For each sample, the number of cells in the *mKO2* gate was multiplied with the *Mean* value of the same gate to yield a value for the total fluorescence of mKO2. The same principle was applied for mVenus. Ultimately, the i_{red}^{nmean} value was calculated as follows:

$$i_{red}^{nmean} = \frac{mKO2^{n} \times mKO2^{mean}}{mKO2^{n} \times mKO2^{mean} + mVenus^{n} \times mVenus^{mean}}$$

Equation 23

6.2.5 Calculation of the specific growth rate (μ)

The specific growth rate (μ) can be calculated using Equation 3. However, the errors of both methods, particle counter (Section 2.2.6) as well as *Neubauer* chamber (Section 2.2.5) lead to high variations of *μ*, due to strong error propagation.

Therefore, a low-pass filter tool by Dr. Jandt [28] was used to apply Gaussian convolution and smooth cell density values before *μ* was calculated. This approach has been chosen, since Gaussian low-path filters don't produce high-frequency oscillations. However, filter artefacts can occur at the beginning and end of measurement series as a result of low numbers of data points [28].

Smoothed cell density values were generated for fixed intervals (Δt = 1 h), the period of time over which smoothing was conducted [h] was chosen to allow variations in the

range of 1/2 generation time (Equation 4), hence about 7 - 8 h, but suppress noise and measurement errors. It is indicated for each data set.

6.2.6 Significance analysis

The significance analysis was conducted by Dr. Jandt as described in a joint publication, which has been recently submitted [98].

It was applied to determine, without *a priori* knowledge or calibration, if a measured parameter (i_{red}^{nmean}, i_{red}^{PR}, $\mu(t)$, G1 [%]) deviates from the previous measurements and hence, potentially indicates a discrepancy to the "normal" cultivation behaviour.

6.2.7 D-glucose, L-lactate, L-glutamine and L-glutamate analysis

For the shaking flask experiments D-glucose and L-lactate concentrations were quantified from supernatants (see Section 2.2.8.2) using an YSI-2900D bio analytical system (YSI Systems, Yellow Springs, OH, USA). Directly before measurement, samples were centrifuged for 5 min at 5000 g on a Bio Fresco Table top centrifuge (Thermo Fisher Scientific Inc., Waltham, MA, USA). 400 µl of supernatant were used for each measurement. Glucose and lactate were measured at the same time as well as glutamine and glutamate, concurrent with the analytical abilities of the device.

6.2.8 Amino acid analytics

Amino acids concentrations from the bioreactor experiment were quantified by the central lab for chemical analytics, Hamburg University of Technology. In brief, reversed-phase-chromatography with fluorometric detection after protein precipitation and pre-column derivatization with o-phthaldialdehyde (OPA) was used. The device is an arrangement of auto sampler, quaternary pump, degasser and a temperature controlled column compartment (Agilent, Santa Clara, CA, USA), a 250 x 4.6 mm

Ultrasphere column (Beckman Coulter, Brea, CA, USA), FP1520 detector (JASCO, Easton, MD, USA) and Chromeleon data system (ThermoFisher, Waltham, MA, USA). The solvent was generated from solvent A (0.05 M sodium acetate buffer, pH 6.5/methanol/tetrahydrofuran 84/15/1) and solvent B (0.05 M sodium acetate buffer, pH 6.0/methanol 20/80).

6.3 Results and discussion

The results of this Chapter are structured into three Sections. The first (see 6.3.1) discusses the relationship between specific growth rate (μ) and i_{red}, using a total fluorescence method (plate reader, hence i_{red}^{PR}) under batch conditions in shaking flasks.

The second (see Section 6.3.2) elaborates how i_{red}^{PR} was used to detect the occurrence and vanishing of nutrient limitations, here L-glutamine, also conducted in shaking flasks.

The third (see Section 6.3.3) is concerned with the validation of the former results using a 2 litre scale bioreactor.

6.3.1 Batch conditions - shaking flask scale

The specific growth rate in Figure 35 exhibits a classic growth curve pattern. In line with the hypothesis, i_{red}^{PR} qualitatively follows a strong inverted relationship with specific growth rate (μ).

While the specific growth rate increases (in Phases I,II), µ decreases. During the exponential phase (III) both values are stable: μ at its maximum value of approx. 0.035; i_{red}^{PR} at its minimum value around 20%. In the following phases (IV-VI) μ decreases, while i_{red}^{PR} increases. After 90 h, μ shows another slight increase without correlation to i_{red}^{PR}. This is influenced by the filter artefacts discussed in Section 6.2.5.

The same general pattern is present in Figure 36, however less accurate. The graph of specific growth rate (μ) contains a high level of variation, caused by insufficiently accurate cell density values and strong error propagation. These are to be expected with a *Neubauer* chamber based calculation of μ and can only partially be corrected using the Gaussian low path filter approach.

The error bars of the i_{red}^{PR} curves indicate the standard deviation of the technical triplicates of the measurements. Interestingly, there seems to be another source of variation to the i_{red}^{PR} values, not represented by these error bars. This source of variation is likely to be connected to the fact that only small volumes of sample are used for the fluorescence analysis. Also, higher sampling rates would further increase the accuracy of this method. Nevertheless, even with few data points it is already less error prone than the quantification of μ.

Despite the discussed sources of inaccuracy, calculation of the Pearson correlation coefficient yields comparable results. For *CHO-K1 FUCCI CM* they are in phases I and II: -0.956; during phases IV to VI: -0.893. For *CHO-K1 FUCCI CN* they are in I and II: -0.936, for IV to VI: -0.971. Hence, they indicate a negative relationship and partially linear correlation. However, the data is not accurate enough to support a linear correlation for full cultivations and/or between different cultivations.

In line with the hypothesis in regard to sub cellular localisation of the fluorescent proteins, the $i_{red\ basal}^{PR}$ values (the i_{red}^{PR} values at $\mu = \mu_{max}$) differ. In case of *CHO-K1 FUCCI CM*, the lowest detected i_{red}^{PR} value is 20.5%, for *CHO-K1 FUCCI CN* it is 15.6%. This was discussed in Section 6.1: in case of *CHO-K1 FUCCI CN* the green fluorescent protein *mVenus-hGeminin(1/60)* is located in the cytosol. This is in contrast to *mVenus-hGeminin(1/110)* of *CHO-K1 FUCCI CM* which is only found in the nucleus. Therefore, the total green fluorescence in *CHO-K1 FUCCI CN* is higher and hence, $i_{red\ basal}^{PR}$ in fact, is lower.

In Summary, it could be shown that the simple total fluorescence method (i_{red}^{PR}) generates qualitative information about the growth behaviour of FUCCI expressing cell lines. Using it, reliable trends of specific growth rate increases, and decreases can be detected.

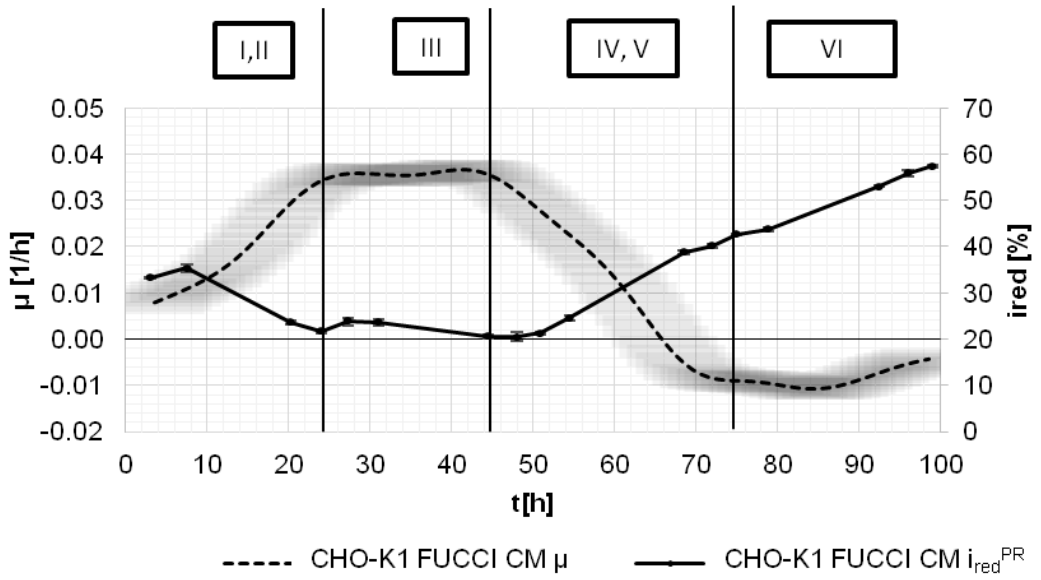

Figure 35: Batch CHO-K1 FUCCI CM - μ and i_{red}^{PR}
Specific growth rate μ [1/h] and i_{red}^{PR} plotted against the time. The specific growth rate μ exhibits the classical batch growth pattern: Starting with a lag (I) and acceleration phase (II), followed by exponential growth (III), deceleration (IV), stationary phase (V) and finally the death phase (VI). The horizontal error bars indicate the width of the Gaussian filter (σ=6 h). The i_{red}^{PR} values display a qualitatively inverted behaviour. The error bars indicate the standard deviation of the technical triplicates. Pearson correlation coefficients indicate a negative relationship but are not accurate enough to support negative correlation for all growth phases. For phases I and II: -0.956; for phases IV to VI: -0.893. Data and graph were published previously [98].

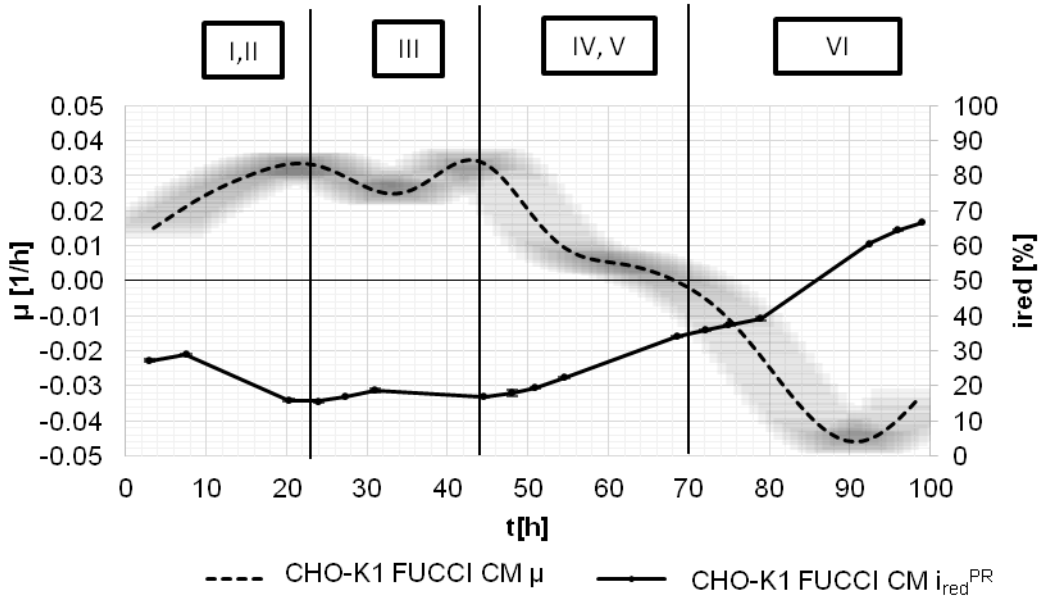

Figure 36: Batch CHO-K1 FUCCI CN - μ and i_{red}^{PR}
Specific growth rate μ and i_{red}^{PR} qualitatively follow the same pattern, described above for *CHO-K1 FUCCI CM*, further supporting the inverse relationship of μ and i_{red}^{PR}. Variations of μ illustrate the obstacle to yield noise free specific growth rate data. Pearson correlation coefficients are for phases I and II: -0.936, for IV to VI: -0.971. Data and graph were published previously [98].

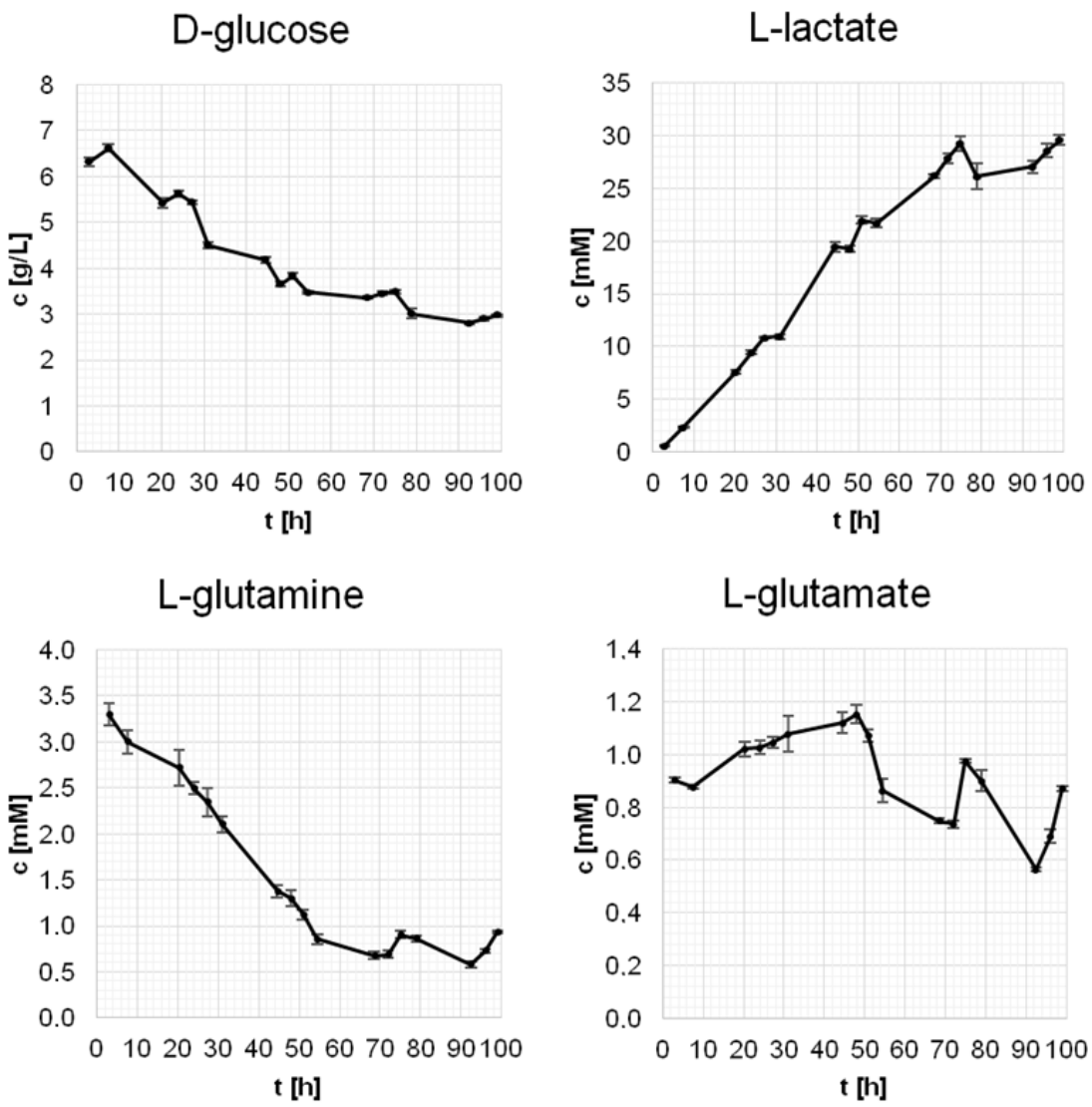

Figure 37: Batch CHO-K1 FUCCI CM - metabolites
Concentrations of D-glucose, L-lactate, L-glutamine and L-glutamate concentrations over the course of the fermentation of *CHO-K1 FUCCI CM*. The graphs are modifications of [101].

In order to elucidate the potential of i_{red}^{total} to indicate limitations in nutrients, the concentrations of glucose, lactate, glutamine and glutamate of the stated cultures were analysed

D-glucose and L-glutamine are important nutrients in the cell culture medium. As visible from both cultures both are continuously consumed throughout the culture. However, glucose is available in sufficient amounts until the end of the fermentation (approx. 3 g/L after 100 h) while L-glutamine is reduced to approx. 1 mM or less.

L-lactate is a by-product of the cells, especially if sufficient carbon sources are available and under stress. The glutamate concentration varies over the course of the culture but is neither systematically produced nor degraded.

The error bars indicate the standard deviation of the measurements using the *triplicates* function of the YSI-2900D device. As obvious from the plotted curves, the variations of the values exceed the plotted error bars. This can be assigned to the

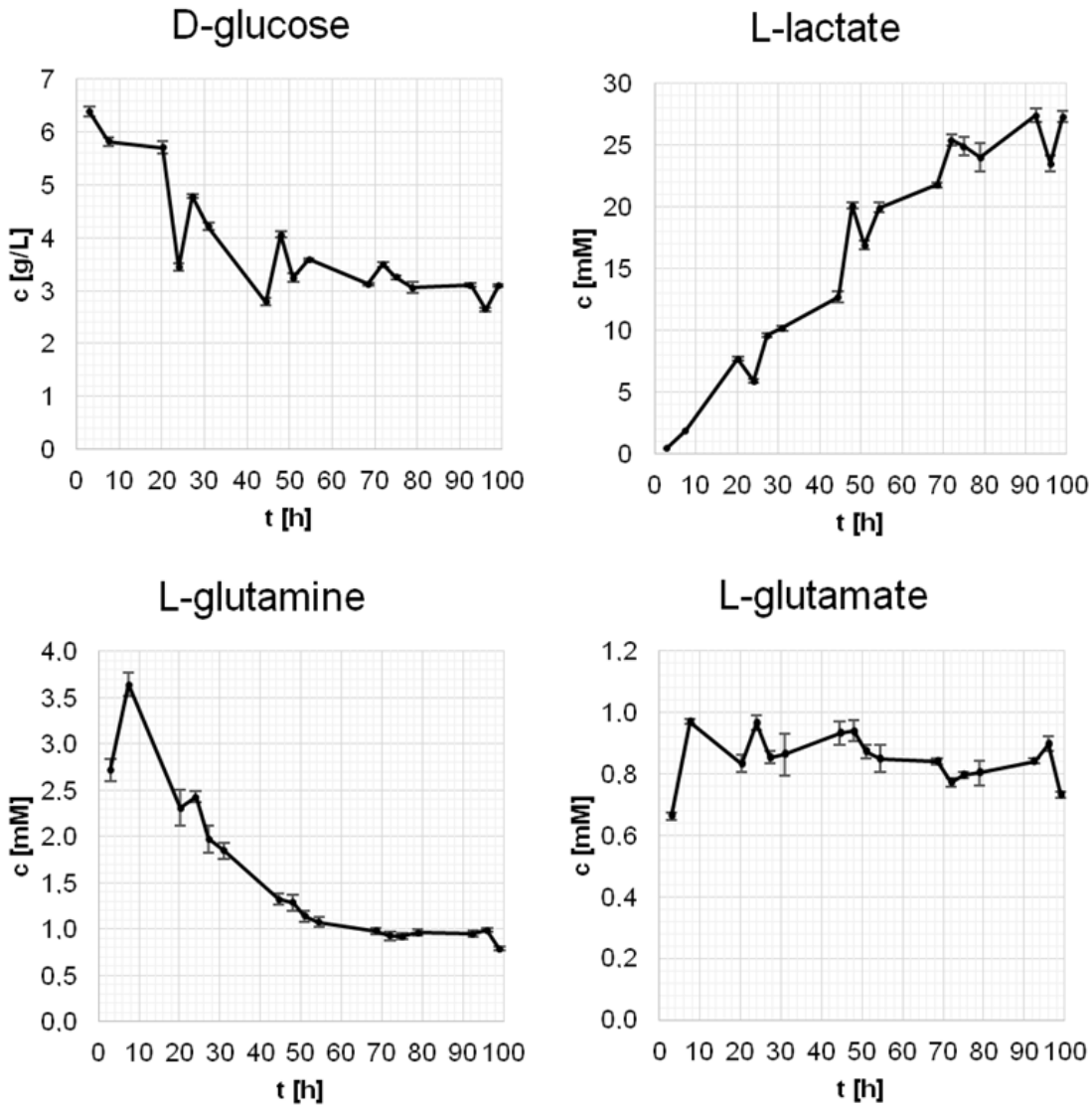

Figure 38: Batch CHO-K1 FUCCI CN - metabolites
Concentrations of D-glucose, L-lactate, L-glutamine and L-glutamate concentrations over the cause of the fermentation of *CHO-K1 FUCCI CN*. The graphs are modifications of [101].

comparable low accuracy of the device. The enzymatic detection method is prone to baseline shifts. Measured values can change over time. The *triplicates* function systematically underestimates these errors. Three values are measured consecutively from the same sample. Then, the next sample is analysed. For more accurate error estimation, the whole set of samples needs to be measured at once, applying no automated standard deviation calculation. This should be performed at least in triplicates. Subsequently, averages and standard deviations need to be calculated manually. The resulting standard deviations are plausible to be considerable higher.

From the data in this Section, in can be concluded that - in line with expectations - *CHO-K1 FUCCI CN* is the more suitable cell line derivative to monitor changes in i_{red}^{PR}, since it can yield a broader range of values. Furthermore L-glutamine is consumed quite rapidly and may act as limiting substrate.

Consequently, L-glutamine was chosen as a well suited model nutrient to study the effects of nutrient limitation on the cell line *CHO-K1 FUCCI CN.*

6.3.2 Variation of L-glutamine concentration - shaking flask scale

In the previous Section it was shown that i_{red}^{PR} displays a strong inverted relationship with the specific growth rate (μ) under batch culture conditions.

If some version of i_{red}^{total} (e.g. i_{red}^{PR}) should be used as a generalizable indicator for the growth state, the same relationship should be obtainable if external, rapid changes influence the culture conditions. This was experimentally tested by actively changing the L-glutamine concentration through medium exchange.

In Figure 39 it is visible that the cultures containing L-glutamine yielded the fastest increase of cell density. The preculture (black) and culture including L-glutamine (blue) display direct and constant growth until L-glutamine is removed (black) growth slows down after 80 h of cultivation (blue).

Much in contrast, the cell densities of the culture without L-glutamine increased slowly. This changed considerably after the addition of L-glutamine, raising the total concentration to 4 mM. The caused increased specific growth rate elevated the total cell concentration to a level similar to that of the culture continuously growing including L-glutamine. Therefore, it can be concluded that the growth behaviour was in fact L-glutamine limited, as intended.

In line with the hypothesis, the i_{red}^{PR} values of the preculture (black) and the culture including L-glutamine (blue) are comparably low and stable, until limitation sets in around 68 h of culture. In contrast, i_{red}^{PR} values increased considerably after L-glutamine depletion. Correspondingly, the i_{red}^{PR} value decreased sharply after addition of L-glutamine. It is noteworthy that the lowest detected i_{red}^{PR} value is around 12% and therefore lower than the $i_{red\ basal}^{PR}$ value of 15.6% reported in Section 6.3.1.

This could be due to the fact that the reported $i_{red\ basal}^{PR}$ value of 15.6% was obtained under less than optimal conditions. On the other hand, the culture may have been partially synchronised (as mentioned in Section 6.1). Since the L-glutamine limitation forced cells into the G0+G0 phase, reversal of the limitation allowed the cells to proceed to the S+G2+M phase at the same time.

Interestingly, the i_{red}^{PR} values of the culture without L-glutamine decreased after about 68 h of culture. This can be explained in the context of metabolic adaptation to the L-glutamine deprived conditions.

From Figure 40 the following conclusions can be drawn: first of all, in regard to the accuracy of analysis, the remarks from Section 6.3.1 apply.

From the D-glucose plot it is visible that D-glucose was consumed continuously. In the presence of L-glutamine total D-glucose consumption was higher. The same is true for the production of L-lactate. Concentrations increased over time in all cultures, with higher rates in presence of L-glutamine.

L-glutamine itself was consumed at a steady rate, where available. In case of the culture, which was first limited for L-glutamine and subsequently supplemented, L-glutamine consumption was more rapid.

The L-glutamate concentrations increase over time, despite high variation. The highest level of L-glutamate is detected in the culture after L-glutamine addition. This can be explained by the conversion of L-glutamine to L-glutamate in the presence of high L-glutamine concentrations [102].

In summary, it could be confirmed that growth of the cultures was L-glutamine dependent. As hypothesised, growth limitations due to L-glutamine depletion are associated with high i_{red}^{PR} values and vice versa. This was confirmed by re-feeding.

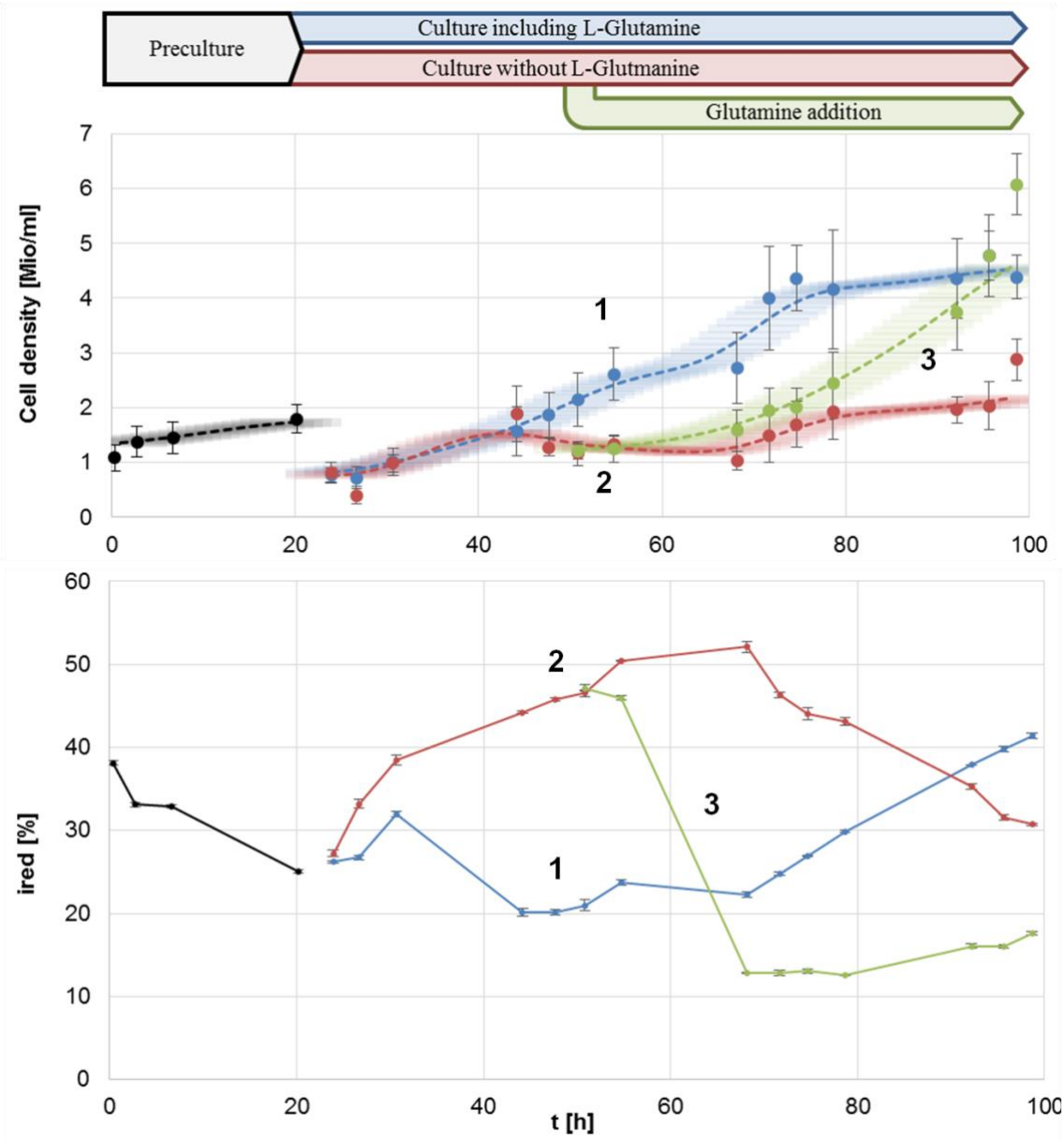

Figure 39: μ and i_{red}^{PR} in dependence on L-glutamine limitation
The upper graph illustrates that the increase in cell density (living cells, *Neubauer* chamber, error bars: standard deviation; horizontal dashed lines: Gaussian filter, width 5 h) is dependent on availability of L-glutamine (indicated in the pictogram above). The lower graph confirms L-glutamine limitation to be associated with high i_{red}^{PR} values. The error bars indicate the standard deviation of the technical replicates (all measurements conducted in triplicates). Data and graph were published previously [98].

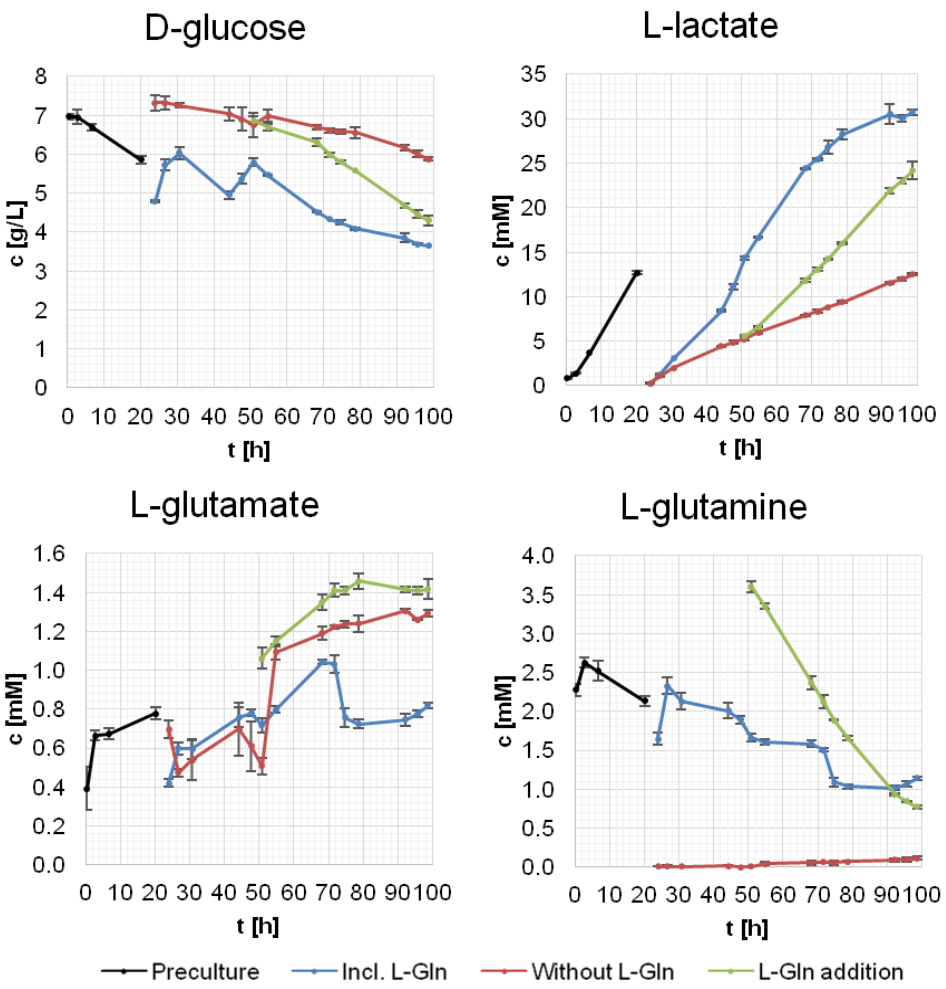

Figure 40: L-glutamine limitation - metabolites
Concentrations of D-glucose, L-lactate, L-glutamine and L-glutamate concentrations over the course of the fermentation of *CHO-K1 FUCCI CN* under different L-glutamine concentrations. The graphs are modifications of [101].

6.3.3 Variation of L-glutamine concentration - Bioreactor scale

In the previous Sections (see 6.3.1 and 6.3.2) it was demonstrated that the parameter i_{red}^{PR}, based on the total fluorescence, indicates the growth behaviour as well as limitations of the pivotal nutrient L-glutamine.

This Section focuses on the confirmation of these results at reactor scale using a *VSF2000* bioreactor. In order to elucidate the impact of different types of limitation, oxygen and glutamine depletion were applied in a consecutive manner. Furthermore, different methods to determine i_{red}^{total}, based on *CytoFlex* flow cytometry (i_{red}^{nmean}) and a *Safire 2* plate reader (i_{red}^{PR}) were used and compared.

In Figure 41 the following growth behaviour is apparent: total cell densities increased until 95 h of cultivation, after which they decreased. Accordingly, viabilities fell, following peak density.

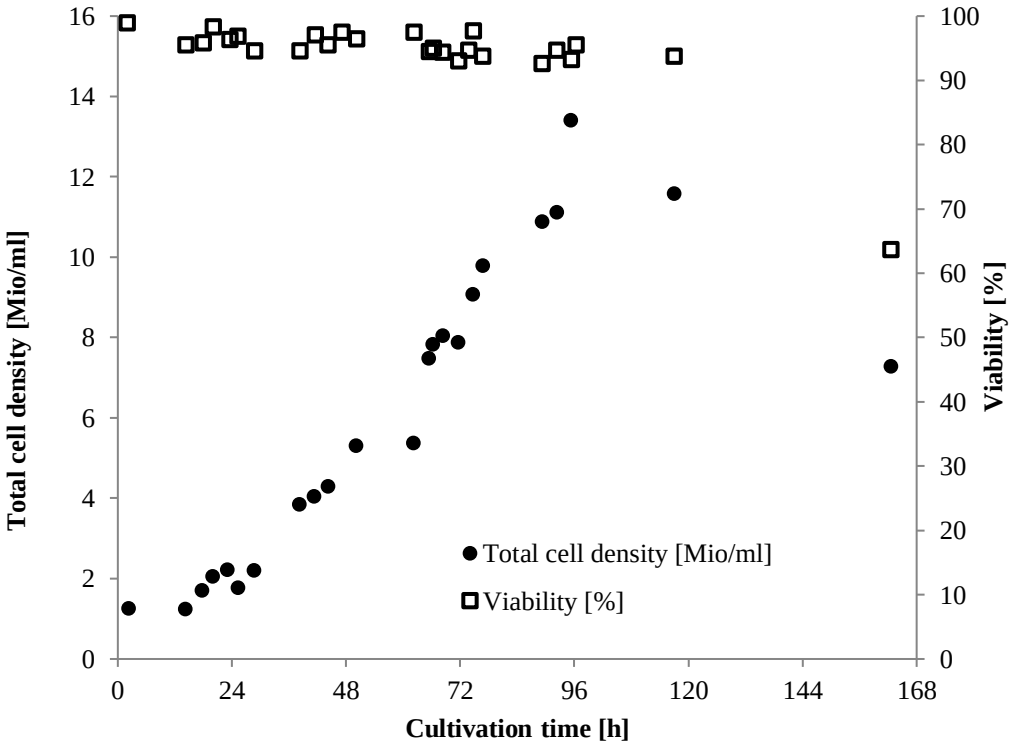

Figure 41: Total cell density [Mio/ml] and viability [%] - Bioreactor
Cell densities, based on Z2 particle counter measurements, increased continuously up to approx. 95 h of cultivation, afterwards they decreased. Accordingly, viabilities, measured using an *Improved Neubauer* chamber, fell considerably towards the end of the culture. Data and graph were published previously [98].

From Figure 42 and Figure 43 the following conclusions can be drawn. First of all, the cultivation can be divided into three approximated phases.

Phase 0 (0 h ≤ t < 24 h), the adaptation, respectively lag phase; Phase 1 (24 h ≤ t < 48 h) with uninhibited growth and no limitations ($\mu = \mu_{max}$) and Phase 2 (48 h ≤ t < 73 h) with partial limitation caused by glutamine depletion ($\mu < \mu_{max}$). Of this phase a further specification can be made: phase 2b (59 h ≤ t < 66 h) with intermediate oxygen depletion (DO < 10 %). Phase 3 (73 h ≤ t < 90 h) is characterised by re-feeding

of glutamine and other nutrients; Phase 4 (90 h ≤ t) by repeated depletion of several nutrients and sharp decline in viability.

From Figure 42, it is visible that all amino acid concentrations decrease during the cultivation at varying rates. Directly following the addition of the feed, all curves exhibited a promoted incline, followed by a steep decline. In Figure 43, the consumption rates per Mio. cells for each amino acid are represented. Directly after the start of the cultivation, glutamine consumption was at its maximum, but decreased in parallel to lowering concentrations. Meanwhile, glutamate as well as aspartic acid consumption rates increased until their availability diminished, too. Subsequent to the feeding, glutamine consumption rates went up, while those of glutamate and aspartic acid remained low.

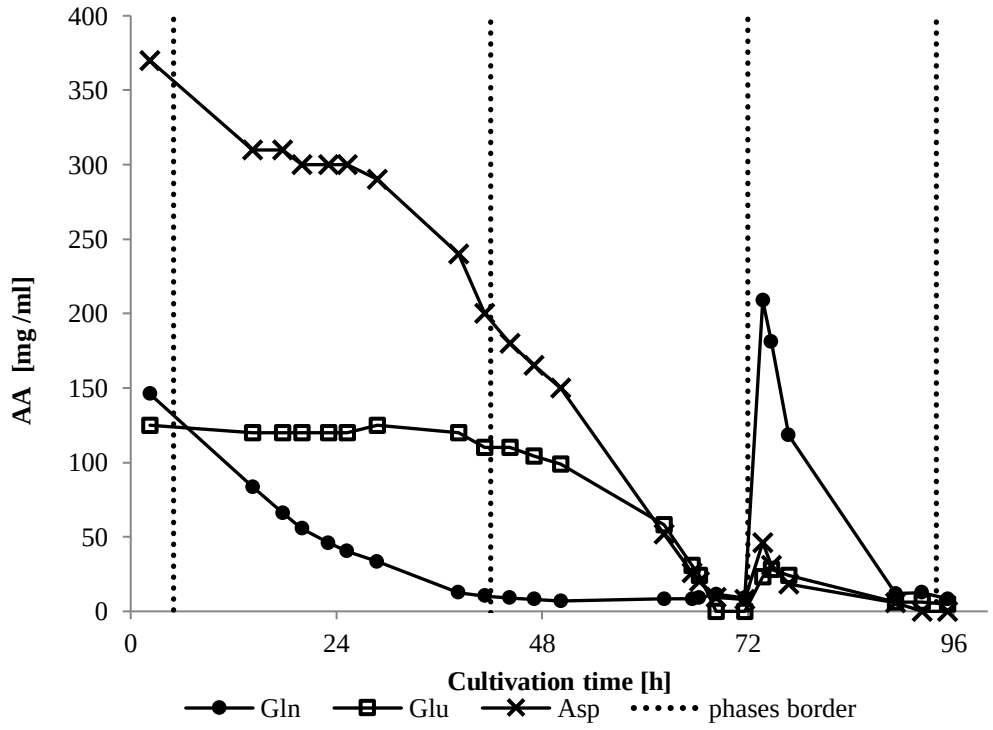

Figure 42: Amino acid concentration - Bioreactor
Amino acid concentrations [mg/l] decrease during cultivation and are increased through feeding. Data and graph were published previously [98].

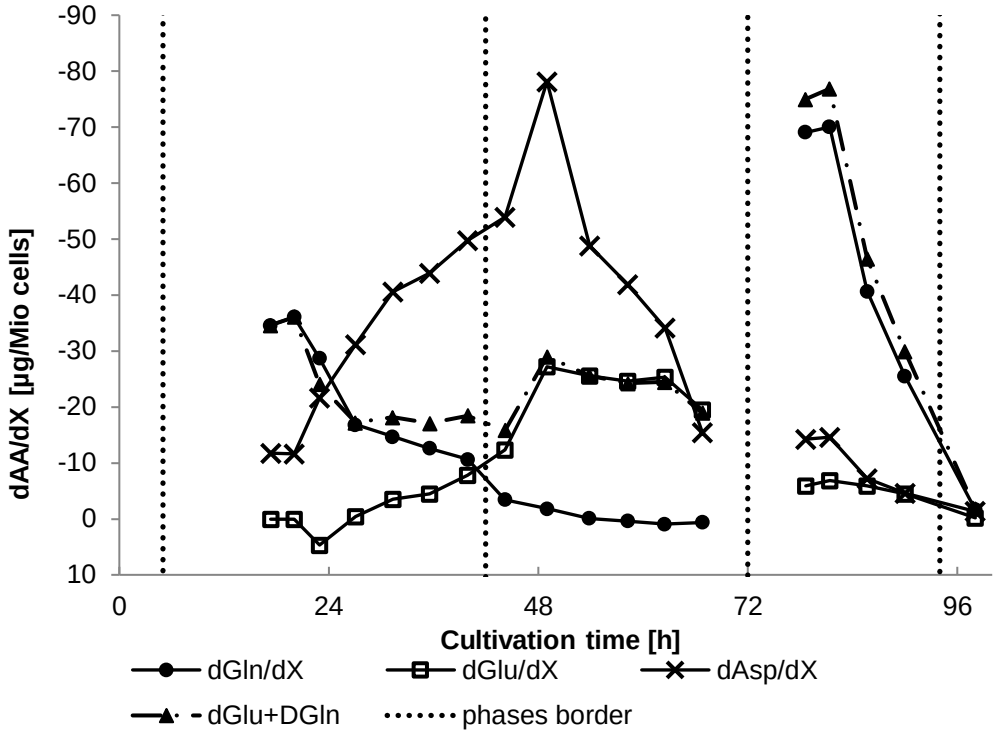

Figure 43: Amino acid consumption rates over time [h] - Bioreactor
Amino acid consumption rates vary considerably depending on available concentrations. Data and graph were published previously [98].

In Figure 44, the consumption rates are summarised in said culture phases. Accordingly, the metabolic shift of the cells is emphasised. In accordance with general knowledge and results from Section 6.3.2, these mammalian cultures favour glutamine catabolism but shift towards other amino acids if necessary. When glutamine becomes more available again, they respond with a shift back towards glutamine consumption.

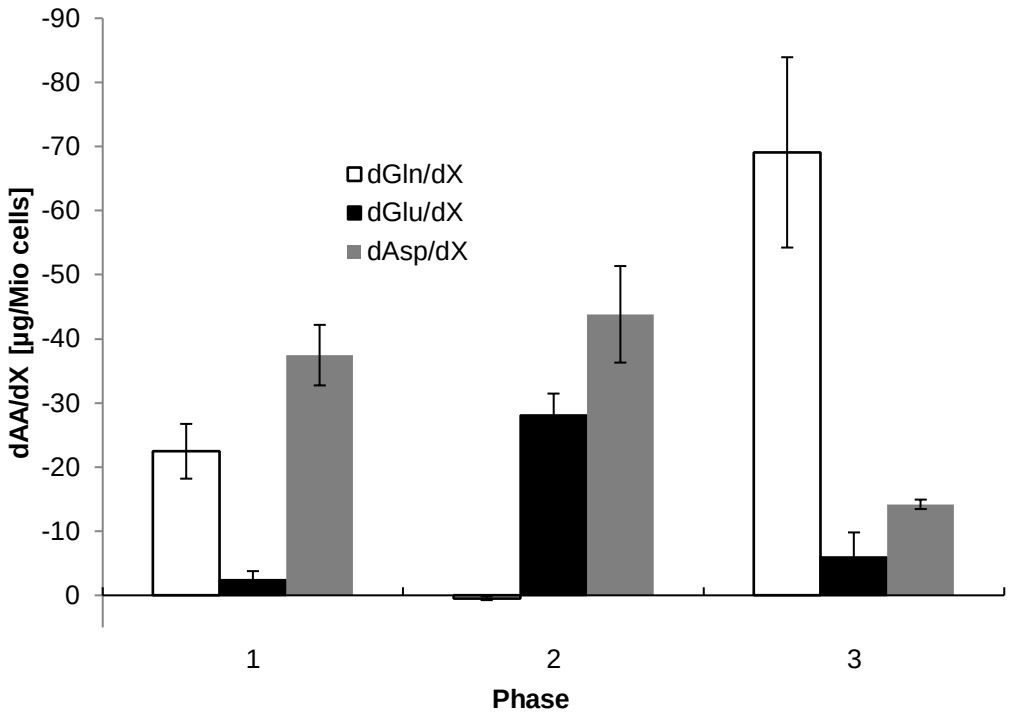

Figure 44: Amino acid consumption rates in phases - Bioreactor
Variation in amino acid consumption rates are more obvious when grouped into three distinct phases. Data and graph were published previously [98].

Based on these total cell densities (see Figure 41), specific growth rates were calculated (see Figure 45). Due to high variations they were subjected to low-pass filtering and re-sampling (sigma 12h) before computation of µ(t) (Model by Dr. U. Jandt [28]). Based on this *a posteriori* filtered specific growth rate (Z2 Sigma 12 h) it can be concluded that the growth stopped around 105 h of cultivation. A partial growth limitation can be determined around 50 h and strong limitation around 96 h. Note that this analysis is only available in retrospect and hence not applicable for real-time detection.

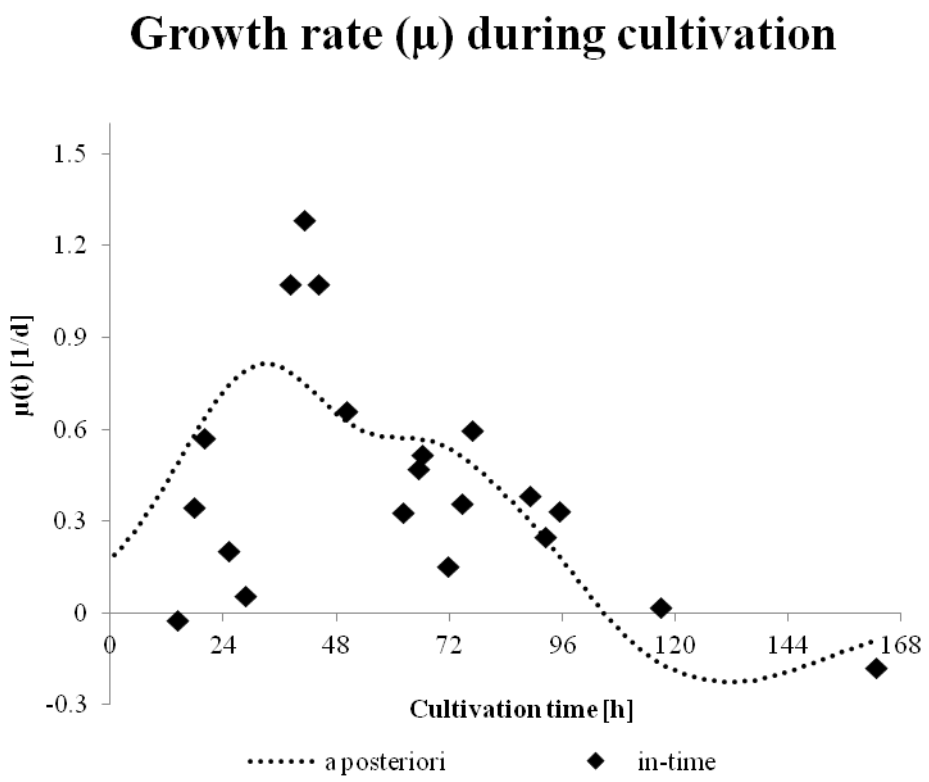

Figure 45: Specific growth rate during cultivation - Bioreactor
The specific growth rate was calculated based on particle counter data (Z2, Beckman Coulter), both in-time with a 4-point sliding average approach (rhombi), and *a posteriori* after low-pass filtering and re-sampling (σ=12h) before computation of μ(t) [28] (thin dotted line). Growth stopped around 105 h of cultivation. Data and graph were published previously [98].

In the following Sections, different representations of i_{red}^{total} are used for discussion. In Figure 46 these two parameters are plotted. Both are intended to mimic the total fluorescence measurements available with fluorescence probes. In fact, the data can be fitted to a linear equation ($y = m\,x + n$) with $m = 1.073 \pm 0.073$ and $n = 0.015 \pm 0.019$. The Pearson correlation coefficient is 0.961. However, the last data point, corresponding to a sample with a low viability, taken in the late dying phase (162.6 h) had to be excluded as an outlier.

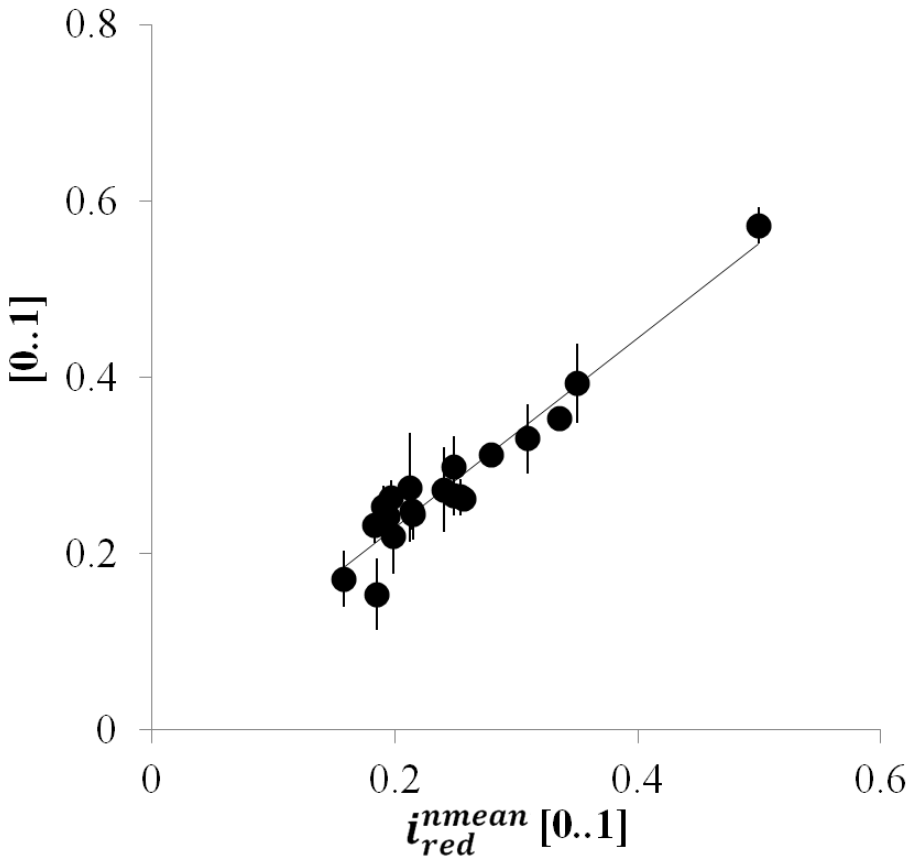

Figure 46: Correlation of i_{red}^{PR} and i_{red}^{nmean} - Elutriation fractions
Both values are calculated based on total fluorescence data, obtained using different analytical devices (Plate reader and CytoFlex flow cytometer) and sample preparation protocols (cells stored in EtOH vs. viable cells). Nevertheless, the data can be fitted to a linear equation (y=mx+n) with m=1.073±0.073 and n=0.015±0.019. PCC = 0.961. The last data point, corresponding to a sample from the late dying phase (162.6 h of cultivation) was excluded as outlier. Data and graph were published previously [98].

Taken together, it can be concluded that the type of fluorescence detection method is less important, and every method of sufficient specificity and sensitivity should be capable of monitoring the growth behaviour.

However, there is one aspect that should be considered: i_{red}^{PR} as well as i_{red}^{nmean} represent the total fluorescence, emitted by cells. Hence, they do not include the potential background fluorescence, detectable by fluorescence probes that can occur if cells leak fluorescent proteins into the cell culture medium. Such leaked protein concentrations could potentially build up over cultivation time, increasing the difference between the detection methods. However, at the current state, this effect is only

theoretical and would need to be tested when fluorescence probes are actually implemented.

In Figure 47 said parameters are plotted against the cultivation time. i_{red}^{PR} as well as i_{red}^{nmean} are very similar (as discussed above) and increase over time. Accordingly, they indicate reduced specific growth rates (μ), which again is in line with the growth data from Figure 41. Much in contrast to the G1 [%] data, which doesn't display any systematic pattern, although a certain amount of fluctuation occurs. This is accordance with the data plotted in Figure 34.

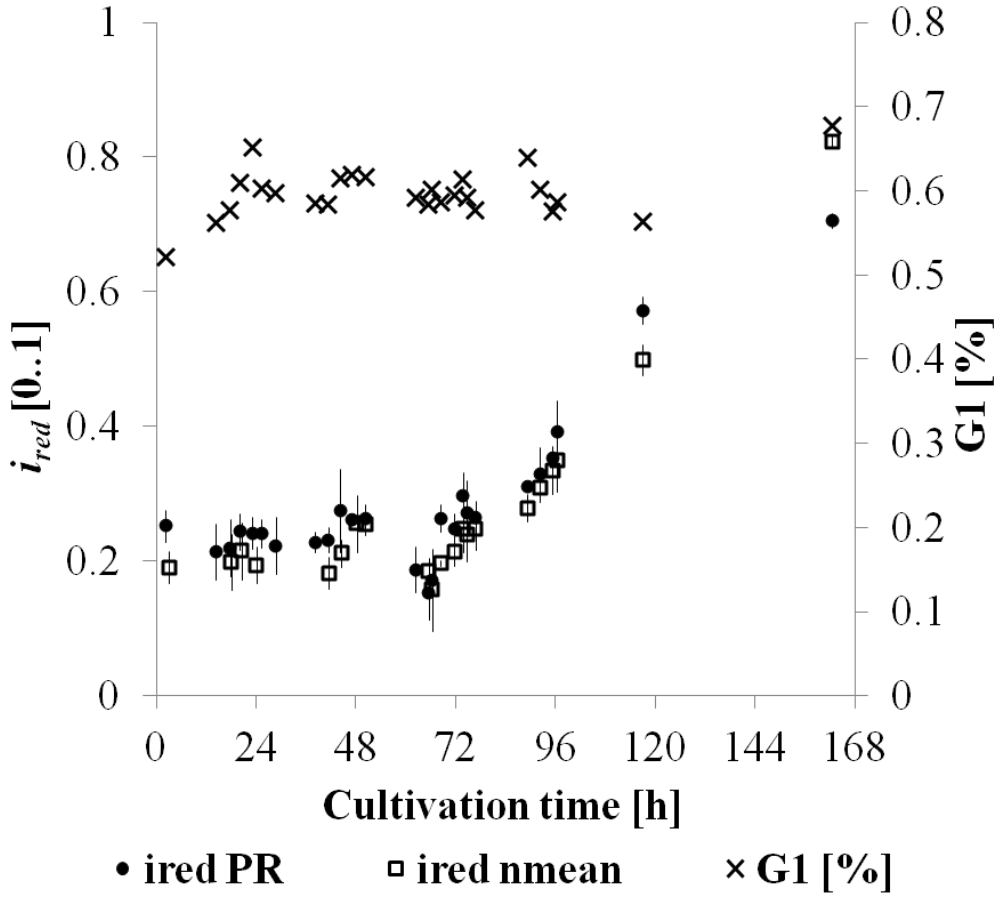

Figure 47: i_{red}^{PR}, i_{red}^{nmean} and G1 [%] during cultivation - Bioreactor
i_{red}^{PR} *and* i_{red}^{nmean} raise towards the end of the culture, displaying only minor differences from another. In contrast G1 [%] displays no systematic variation. Data and graph were published previously [98].

The G1 [%] data of the bioreactor run is in the typical range of values but inconclusive. This is even more evident after significance analysis by Dr. Jandt [98], the results are plotted in Figure 48.

The analysis yields low significance changes for i_{red}^{PR} ($p < 0.05$: first threshold, indicated as yellow line) after t = 47 - 50 h, indicating partial growth limitation due to glutamine depletion. Additionally, at t ~ 75 h which indicates prolonged and increasingly severe growth limitation. Highly significant changes ($p < 0.001$: second threshold, indicated as red line) are indicated after t ~ 89 h.

For i_{red}^{nmean} thresholds were exceeded after t ~ 77 h ($p < 0.05$: first threshold) and t ~ 95 h ($p < 0.001$: second threshold). Meanwhile, G1 did not yield any significant changes.

The dissolved oxygen as well as aeration were monitored in parallel to maintain the desired DO (data not shown). Additionally, changes in the oxygen uptake rate (OUR) were calculated from this data and subjected to significance analysis. The first trend change was calculated in retrospect and occurred around 85 h of cultivation.

While oxygen was partially limited, in the time between t ~ 59 h to t ~ 66 h of limitation, the i_{red} values displayed a very significant variation, this time below the normal level. Very high significance values for such a deviation ($p < 0.001$, n = 2) was detected for about 66 h of cultivation. It is still to be determined, if this signal can provide further information for the purpose of process monitoring and control, compared to the conventional DO probe signal.

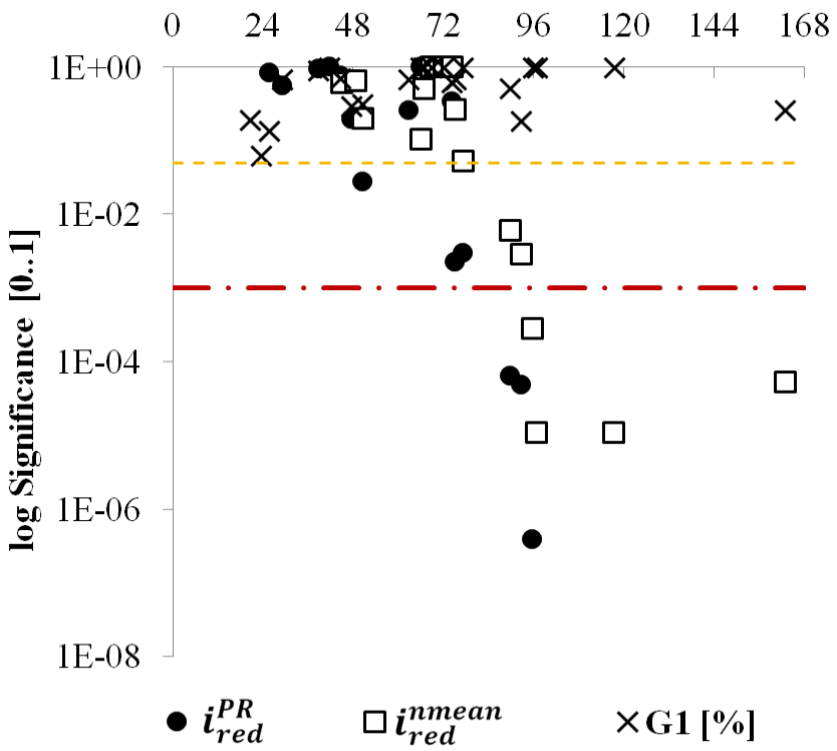

Figure 48: Significance analysis of i_{red}^{PR}, i_{red}^{nmean} and G1 [%] - Bioreactor
i_{red}^{PR} based analysis indicates significant changes at 89.25 h of cultivation, i_{red}^{nmean} based analysis at 95.3 h. G1 [%] analysis did not yield values above the significance level. Data and graph were published previously [98].

Based upon these results it can be inferred that determination of the parameters i_{red}^{nmean} as well as i_{red}^{n} in combination with a standardized significance analysis are able to detect inhibitions of growth many hours – here at least 19 h – earlier compared to conventional cell density based methods. Meanwhile partial growth limitations, adaptation phases and oxygen depletions can be observed with sound significance considering the limited number of samples employed.

A more in-depth reflection on the differences between i_{red}^{nmean} and i_{red}^{n} leads to the conclusion that different time points of significance detection are rather related to the amount of available data points, not the type of total fluorescence detection method. Therefore, sampling frequency is among the most important factors to detect significant changes as early and reliably as possible. The data presented here is considerably constrained by the manual sampling method and the required hands on time.

This emphasises the benefits of the fluorescence-based read-out and the i_{red} concept: When on-online or at-line probes are used, measurements of the total fluorescence ratio (i_{red}^{total}) can easily be repeated every few minutes or even seconds.

6.4 Conclusion

The detection of *FUCCI* fluorescence has been proven to indicate the growth behaviour of CHO suspension cell cultures reliably. Hence, it can be used to identify growth limitations noticeably earlier and more reliable than cell density or conventional cell cycle (DNA staining) based approaches.

These conclusions were validated in shaking flasks, under batch and L-glutamine limited growth conditions. Furthermore, a *fed batch* experiment in a *VSF 2000* bioreactor system was performed.

The *FUCCI* fluorescence detection is compatible with different detection methods. Furthermore, determination of the parameter i_{red}^{total}, based on the total fluorescence, (e.g. i_{red}^{PR}, i_{red}^{nmean} or using fluorescence probes) is by design less susceptible to error propagation, compared to fluorescence-per-cell-number based methods. It is self-normalized and hence independent from additional method of cell counting.

Furthermore, quantification of the fluorescence per volume may potentially be used to approximate the cell density. As indented by design, CHO-K1 FUCCI CN can display a broader range of values compared to CHO-K1 FUCCI CM (see Section 6.3.1).

The specific growth rate (μ), calculated based on derivatives of cell counts, are subject to considerable fluctuations due to limited accuracy of the available methods and high error propagation. Therefore, it was not possible to conduct a strong quantitative and generally valid analysis concerning the interdependency of the specific growth rate (μ) and i_{red}. Nevertheless, Pearson coefficients indicate a negative relationship with values between -0.971 and -0.893.

For future experiments, a more accurate, automated method for the determination of the cell density (e.g. a probe for on-line determination of the optical density or

impedance) would be beneficial. In combination with an on-line fluorescence probe, the full potential of the described concept could be used to elucidate the quantitative correlation between i_{red}^{total} and growth behaviour more accurately. Such fluorescence probes would benefit from specific filter sets in combination with automated significance analysis.

This could lead to a more precise method which allows to estimate the growth behaviour of cultures more rapidly and reliably. Ultimately, this may enable more accurately controlled industry scale production processes.

In general, the concept is compatible with any genetic fluorescent cell cycle indicator system in combination with a suitable fluorescence detection system. Nevertheless, the setup must be designed carefully. Combinations of fluorescence proteins with more spectral diversity can reduce requirements for detection specificity. On the other hand, fluorescent proteins should be chosen carefully with regard to signal intensities. These are dependent on the fluorescent proteins stokes shift, quantum yield and related parameters. When different light sources are used for excitation, intensities must be adjusted to yield comparable, fluctuation-free emissions.

Furthermore, the intended fluorescent protein expression levels (determined by integration site, number and promoter) need to be chosen wisely to balance signal intensity and the metabolic burden of fluorescent protein expression.

7. Summary and concluding remarks

This study focuses on examining the putative interdependencies between the cell cycle and the behaviour of mammalian suspension cell lines, as well as the corresponding implications for reliable process monitoring and control.

In the first part, an experimental setup was adapted in order to generate synchronised suspension cultures of the human producer cell line HEK293s under near-physiological conditions. Extensive optimisation efforts were required in order to achieve and maintain high viabilities and aggregation free growth.

Subsequently, these cultures were utilised for the first reported studies targeting cell cycle dependent transfection efficiencies using near-physiologically synchronised cultures. The results indicated that the strong effect of the timing of transfection with respect to the cell cycle phase, reported by other groups, could not be confirmed. Hence, the previously reported differences are more plausible to be associated with artefacts caused by the non-physiological, however commonly used, synchronisation methods.

In order to facilitate the cell cycle specific research and also to allow easy monitoring and potentially control of cell cultures based on the cell cycle state, two new derivatives of the widely used CHO-K1 production cell line were established. They indicate their cell cycle and growth state in an on-line feasible manner through fluorescence. For this purpose, the genetic FUCCI (Fluorescence Ubiquitination Cell Cycle Indicator) constructs were utilised, yielding *CHO-K1 FUCCI CM* and *CN*.

Based on FUCCI fluorescence, a set of novel parameters was defined to represent the fluorescence distributions of cultures. Quantitative analysis revealed that the number based parameter i_{red}^{n} correlates well with the cell cycle state (expressed as percentage of cells in the G1 cell cycle phase).

Additionally, it was demonstrated that the parameter i_{red}^{total}, based on the total fluorescence, indicates trend changes in the growth behaviour as well as ongoing limitations of cultures in shaking flask cultures and a bioreactor alike. These indications have been detected with significant values many hours earlier than traditional

parameters (specific growth rate based on cell counts, oxygen uptake rate). Moreover, different analytic methods (fluorescence plate reader and flow cytometer) were shown to yield consistent results.

It can be concluded that the previously and frequently used experimental approaches of non-physiological synchronisation methods cannot be considered valid tools to research of cell cycle dependent metabolism.

In contrast, the FUCCI fluorescence is inherently connected to the molecular mechanisms that regulate the cell cycle. After generation of the new FUCCI-based cell lines derivatives, both cell cycle state and specific growth rate (μ) can now be determined in real time, using an easily detectable parameter based bulk fluorescence (i_{red}^{total}).

This allows for rapid, robust, and cost effective process monitoring and control using fluorescence probes in bioreactor setups. Just like monitoring of the dissolved oxygen concentration to calculate the oxygen uptake rate (OUR), detection of i_{red}^{total} can be performed in real-time, with low financial effort, and by probes that can be subjected to standard autoclaving procedures.

Consequently, detection of i_{red}^{total} is not restricted to a single probe per bioreactor. Monitoring at different positions in the bioreactor can help to identify potential regions with non-optimal growth condition due to reactor heterogeneities.

Ultimately, i_{red}^{total} may hopefully be established as standard process parameter as it combines substantial benefits with ease of use and efficiency.

8. Acknowledgements

First of all, I would like to thank Prof. An-Ping Zeng for the opportunity to work in his Institute and under his supervision. Likewise, I would like to express my gratitude to Dr. Uwe Jandt for his support and constructive feedback, Dr. Oscar Platas Barradas for introducing me to the technology of counter flow elutriation, and in general all members of the Institute of Bioprocess and Biosystems Engineering for the good cooperation.

Additionally, I would like to thank PD Johannes Herkel, Dr. Antonella Carambia and Dr. Dorothee Schwinge (UKE Hamburg) for allowing me to access their elutriator equipment. As well as the group of Prof. Garabed Antranikian, especially Dr. Anna Krüger, for the use of their *Safire 2* plate reader. Furthermore, all members of the Flow Cytometry Core Facility, Universitätsklinikum Eppendorf, in particular Susanne Roscher and Melanie Lachmann.

I would particularly like to express my gratitude to all researchers, I had the privilege to publish with.

Also, I would like to acknowledge funding by the Deutsche Forschungsgemeinschaft (DFG) (research projects “TransExpress”, grantnumber: ZE542/3-3 and “Neue Ansätze zur populationsbasierten kinetischen Untersuchung und Modellierung von Hochzelldichte-Zellkulturen”, grant number: ZE 542/9-1), as well as partial funding by German Federal Ministry of Education and Research (BMBF, grant 031A128).

The reporter plasmid pcDNA3.3_d2eGFP was a kind gift from Derrick Rossi (Addgene plasmid # 26821).

The FUCCI plasmids were generous gifts from the Group of Dr. A. Miyawaki (Laboratory for Cell Function Dynamics, RIKEN Brain Science Institute, Saitama, Japan).

Furthermore, I would like to thank my students, who completed their theses under my supervision during this project. In order of appearance:

Alan Eduardo Castillo Salvador, Diploma thesis: “Physiological and Kinetic Analysis of Mammalian Production Cell Lines as Synchronised High-Density Cultures”

and

Yaeseong Hong, Bachelor thesis: “Systematische Evaluation von Zellkulturen im Hinblick auf Zellzyklus-Verteilung und Wachstumsrate”.

Last but not least I would like to express my gratitude to my family and friends for their continuous support. First and foremost, Eleanor, Johanna, Barbara, Rita and Weldon.

9. References

[1] Sidoli, F.R., Mantalaris, A., Asprey, S.P., Modelling of mammalian cells and cell culture processes. *Cytotechnology* 2004, *44*, 27–46.

[2] Wurm, F.M., Production of recombinant protein therapeutics in cultivated mammalian cells. *Nat. Biotechnol.* 2004, *22*, 1393–1398.

[3] Butler, M., Animal cell cultures: recent achievements and perspectives in the production of biopharmaceuticals. *Appl. Microbiol. Biotechnol.* 2005, *68*, 283–291.

[4] Hacker, D.L., De Jesus, M., Wurm, F.M., 25 years of recombinant proteins from reactor-grown cells — Where do we go from here? *Biotechnol. Adv.* 2009, *27*, 1023–1027.

[5] Bandyopadhyay, A.A., Khetan, A., Malmberg, L.-H., Zhou, W., et al., Advancement in bioprocess technology: parallels between microbial natural products and cell culture biologics. *J. Ind. Microbiol. Biotechnol.* 2017, *44*, 785–797.

[6] Lewis, N.E., Liu, X., Li, Y., Nagarajan, H., et al., Genomic landscapes of Chinese hamster ovary cell lines as revealed by the Cricetulus griseus draft genome. *Nat. Biotechnol.* 2013, *31*, 759–765.

[7] Jayapal, K., Wlaschin, K., Hu, W.-S., Yap, M., Recombinant Protein Therapeutics from CHO Cells - 20 Years and Counting. *CHO Consort. SBE Spec. Ed.* 2007, 40–47.

[8] Steger, K., Brady, J., Duskin, M., Donato, K., Literature Review : CHO versus HEK Cell Glycosylation. *MaxCyte.com* 2016, 1–6.

[9] Tjio, J.H., Puck, T.T., Genetics of somatic mammalian cells. II. Chromosomal constitution of cells in tissue culture. *J. Exp. Med.* 1958, *108*, 259–268.

[10] Puck, T.T., Cieciura, S.J., Robinson, A., Genetics of somatic mammalian cells. III. Long-term cultivation of euploid cells from human and animal subjects. *J. Exp. Med.* 1958, *108*, 945–956.

[11] Urlaub, G., Chasin, L.A., Isolation of Chinese hamster cell mutants deficient in

dihydrofolate reductase activity. *Proc. Natl. Acad. Sci. U. S. A.* 1980, *77*, 4216–4220.

[12] Urlaub, G., Käs, E., Carothers, A.M., Chasin, L.A., Deletion of the diploid dihydrofolate reductase locus from cultured mammalian cells. *Cell* 1983, *33*, 405–412.

[13] Wurm, F.M., Hacker, D., First CHO genome. *Nat. Biotechnol.* 2011, *29*, 718–720.

[14] Graham, F.L., Smiley, J., Russell, W.C., Nairn, R., Characteristics of a Human Cell Line Transformed by DNA from Human Adenovirus Type 5. *J. Gen. Virol.* 1977, *36*, 59–72.

[15] Garnier, A., Cote, J., Nadeau, I., Kamen, A., et al., Scale-up of the adenovirus expression system for the production of recombinant protein in human 293S cells. *Cytotechnology* 1994, *15*, 145–155.

[16] Cote, J., Garnier, A., Massie, B., Kamen, A., Serum-free production of recombinant proteins and adenoviral vectors by 293SF-3F6 cells. *Biotechnol. Bioeng.* 1998, *59*, 567–575.

[17] Research, C. for D.E. and, About the Center for Drug Evaluation and Research - OPS Process Analytical Technology - (PAT) Initiative. n.d.

[18] Biechele, P., Busse, C., Solle, D., Scheper, T., et al., Sensor systems for bioprocess monitoring. *Eng. Life Sci.* 2015, *15*, 469–488.

[19] del Val, I.J., Kontoravdi, C., Nagy, J.M., Towards the implementation of quality by design to the production of therapeutic monoclonal antibodies with desired glycosylation patterns. *Biotechnol. Prog.* 2010, *26*, 1505–1527.

[20] Pörtner, R., Jandt, U., Zeng, A.-P., Cell Culture Technology, in: *Industrial Biotechnology*, Wiley-VCH Verlag GmbH & Co. KGaA, Weinheim, Germany 2016, pp. 129–158.

[21] Noack, S., Wiechert, W., Wiechert, W., Noack, S., et al., Quantitative metabolomics: a phantom? *Trends Biotechnol.* 2014, *32*, 238–44.

[22] Rubakhin, S.S., Lanni, E.J., Sweedler, J. V, Progress toward single cell metabolomics. *Curr. Opin. Biotechnol.* 2013, *24*, 95–104.

[23] Vasdekis, A.E., Stephanopoulos, G., Review of methods to probe single cell metabolism and bioenergetics. *Metab. Eng.* 2015, *27*, 115–35.

[24] Zhang, J., Jensen, M.K., Keasling, J.D., Development of biosensors and their application in metabolic engineering. *Curr. Opin. Chem. Biol.* 2015, *28*, 1–8.

[25] Lara, A.R., Galindo, E., Ramírez, O.T., Palomares, L.A., Living with heterogeneities in bioreactors: understanding the effects of environmental gradients on cells. *Mol. Biotechnol.* 2006, *34*, 355–81.

[26] Saqcena, M., Menon, D., Patel, D., Mukhopadhyay, S., et al., Amino Acids and mTOR Mediate Distinct Metabolic Checkpoints in Mammalian G1 Cell Cycle. *PLoS One* 2013, *8*, e74157.

[27] Kaplon, J., van Dam, L., Peeper, D., Two-way communication between the metabolic and cell cycle machineries: the molecular basis. *Cell Cycle* 2015, *14*, 2022–2032.

[28] Jandt, U., Platas Barradas, O., Pörtner, R., Zeng, A.-P., Synchronized mammalian cell culture: Part II-population ensemble modeling and analysis for development of reproducible processes. *Biotechnol. Prog.* 2015, *31*, 175–185.

[29] Jandt, U., Platas Barradas, O., Pörtner, R., Zeng, A.-P., Mammalian cell culture synchronization under physiological conditions and population dynamic simulation. *Appl. Microbiol. Biotechnol.* 2014, *98*, 4311–4319.

[30] Brunner, S., Sauer, T., Carotta, S., Cotten, M., et al., Cell cycle dependence of gene transfer by lipoplex, polyplex and recombinant adenovirus. *Gene Ther* 2000, *7*, 401–407.

[31] Männistö, M., Reinisalo, M., Ruponen, M., Honkakoski, P., et al., Polyplex-mediated gene transfer and cell cycle: effect of carrier on cellular uptake and intracellular kinetics, and significance of glycosaminoglycans. *J. Gene Med.* 2007, *9*, 479–487.

[32] Männistö, M., Rönkkö, S., Mättö, M., Honkakoski, P., et al., The role of cell cycle on polyplex-mediated gene transfer into a retinal pigment epithelial cell line. *J. Gene Med.* 2005, *7*, 466–476.

[33] Karp, G., Beginnen, K., Molekulare Zellbiologie: Mit 36 Tabellen, 1., Au,

Springer, Berlin 2005.

[34] Graw, J., Zelle, Zellteilungen und Modellorganismen, in: Graw, J. (Ed.), *Genetik*, Springer-Verlag Berlin Heidelberg, Berlin, Heidelberg 2010, pp. 155–215.

[35] Cooper, S., Rethinking synchronization of mammalian cells for cell cycle analysis. *Cell. Mol. Life Sci.* 2003, *60*, 1099–1106.

[36] Schmitz, S., Der Experimentator: Zellkultur, 2nd ed., Spektrum Akad. Verl., Heidelberg 2009.

[37] Hu, W.-S., Zhou, W., Cell Culture Bioprocess Engineering, Cell Process Book, 2012.

[38] Liu, Y.-H., Bi, J.-X., Zeng, A.-P., Yuan, J.-Q., A population balance model describing the cell cycle dynamics of myeloma cell cultivation. *Biotechnol. Prog.* 2007, *23*, 1198–209.

[39] Sitton, G., Srienc, F., Mammalian cell culture scale-up and fed-batch control using automated flow cytometry. *J. Biotechnol.* 2008, *135*, 174–80.

[40] Kuystermans, D., Mohd, A., Al-Rubeai, M., Automated flow cytometry for monitoring CHO cell cultures. *Methods* 2012, *56*, 358–365.

[41] Kuystermans, D., Avesh, M., Al-Rubeai, M., Online flow cytometry for monitoring apoptosis in mammalian cell cultures as an application for process analytical technology. *Cytotechnology* 2016, *68*, 399–408.

[42] Cooper, S., Gonzales Hernandez, M., Experimental reconsideration of the utility of serum starvation as a method for synchronizing mammalian cells. *Cell Biol. Int.* 2009, *33*, 71–77.

[43] Cooper, S., Mammalian cells are not synchronized in G1-phase by starvation or inhibition: considerations of the fundamental concept of G1-phase synchronization. *Cell Prolif.* 1998, *31*, 9–16.

[44] Xeros, N., Deoxyriboside Control and Synchronization of Mitosis. *Nature* 1962, *194*, 682–683.

[45] Ma, H.T., Poon, R.Y.C., Synchronization of HeLa Cells, in: *Methods in Molecular Biology (Clifton, N.J.)*, 2011, pp. 151–161.

[46] Cooper, S., Chen, K.Z., Ravi, S., Thymidine block does not synchronize L1210 mouse leukaemic cells: implications for cell cycle control, cell cycle analysis and whole-culture synchronization. *Cell Prolif.* 2007, *41*, 156–167.

[47] Spellman, P., Reply: whole-culture synchronization? Effective tools for cell cycle studies. *Trends Biotechnol.* 2004, *22*, 270–273.

[48] Rola-Pleszczynski, M., Churchill, W.H., Purification of human monocytes by continuous gradient sedimentation in ficoll. *J. Immunol. Methods* 1978, *20*, 255–262.

[49] Rieseberg, M., Kasper, C., Reardon, K.F., Scheper, T., Flow cytometry in biotechnology. *Appl. Microbiol. Biotechnol.* 2001, *56*, 350–360.

[50] Lee, W.C., Bhagat, A.A.S., Huang, S., Van Vliet, K.J., et al., High-throughput cell cycle synchronization using inertial forces in spiral microchannels. *Lab Chip* 2011, *11*, 1359–67.

[51] Migita, S., Hanagata, N., Tsuya, D., Yamazaki, T., et al., Transfection efficiency for size-separated cells synchronized in cell cycle by microfluidic device. *Biomed. Microdevices* 2011, *13*, 725–9.

[52] Lebleu, V.S., Thornton, M., Gonda, S.R., Helmstetter, C.E., Technology for cell cycle research with unstressed steady-state cultures. *Cytotechnology* 2006, *51*, 149–157.

[53] Thornton, M., Eward, K.L., Helmstetter, C.E., Production of minimally disturbed synchronous cultures of hematopoietic cells. *Biotechniques* 2002, *32*, 1098–100, 1102, 1105.

[54] Banfalvi, G., Cell cycle synchronization of animal cells and nuclei by centrifugal elutriation. *Nat. Protoc.* 2008, *3*, 663–673.

[55] Beckman Coulter, JE-5.0 Elutriation System. 2012, 80.

[56] Barford, J.P., A mathematical model for cell separation technique of centrifugal elutriation. *Biotechnol. Bioeng.* 1986, *28*, 570–577.

[57] Kauffman, M.G., Noga, S.J., Kelly, T.J., Donnenberg, A.D., Isolation of cell cycle fractions by counterflow centrifugal elutriation. *Anal. Biochem.* 1990, *191*, 41–46.

[58] Barradas, O.P., Jandt, U., Becker, M., Bahnemann, J., et al., Synchronized mammalian cell culture: Part I-A physical strategy for synchronized cultivation under physiological conditions. *Biotechnol. Prog.* 2015, *31*, 165–174.

[59] Castillo Salvador, A.-E., Fuge, G., Jandt, U., Zeng, A.-P., Growth kinetics and validation of near-physiologically synchronized HEK293S Cultures. *Eng. Life Sci.* 2015, *15*, 509–518.

[60] Sakaue-Sawano, A., Ohtawa, K., Hama, H., Kawano, M., et al., Tracing the silhouette of individual cells in S/G2/M phases with fluorescence. *Chem. Biol.* 2008, *15*, 1243–1248.

[61] Sakaue-Sawano, A., Kurokawa, H., Morimura, T., Hanyu, A., et al., Visualizing spatiotemporal dynamics of multicellular cell-cycle progression. *Cell* 2008, *132*, 487–498.

[62] Goldstein, G., Scheid, M., Hammerling, U., Schlesinger, D.H., et al., Isolation of a polypeptide that has lymphocyte-differentiating properties and is probably represented universally in living cells. *Proc. Natl. Acad. Sci. U. S. A.* 1975, *72*, 11–15.

[63] Teixeira, L.K., Reed, S.I., Ubiquitin ligases and cell cycle control. *Annu. Rev. Biochem.* 2013, *82*, 387–414.

[64] Hershko, A., Ciechanover, A., The ubiquitin system. *Annu. Rev. Biochem.* 1998, *67*, 425–479.

[65] Nishitani, H., Lygerou, Z., Nishimoto, T., Proteolysis of DNA replication licensing factor Cdt1 in S-phase is performed independently of geminin through its N-terminal region. *J. Biol. Chem.* 2004, *279*, 30807–16.

[66] Nishitani, H., Lygerou, Z., Nishimoto, T., Nurse, P., The Cdt1 protein is required to license DNA for replication in fission yeast. *Nature* 2000, *404*, 625–628.

[67] Benmaamar, R., Pagano, M., Involvement of the SCF complex in the control of Cdh1 degradation in S-phase. *Cell Cycle* 2005, *4*, 1230–1232.

[68] Wei, W., Ayad, N.G., Wan, Y., Zhang, G.-J., et al., Degradation of the SCF component Skp2 in cell-cycle phase G1 by the anaphase-promoting complex. *Nature* 2004, *428*, 194–198.

[69] Nishimura, K., Oki, T., Kitaura, J., Kuninaka, S., et al., APC(CDH1) targets MgcRacGAP for destruction in the late M phase. *PLoS One* 2013, *8*, e63001.

[70] Kremers, G.-J., Gilbert, S.G., Cranfill, P.J., Davidson, M.W., et al., Fluorescent proteins at a glance. *J. Cell Sci.* 2011, *124*, 157–160.

[71] Nagai, T., Ibata, K., Park, E.S., Kubota, M., et al., A variant of yellow fluorescent protein with fast and efficient maturation for cell-biological applications. *Nat. Biotechnol.* 2002, *20*, 87–90.

[72] Website Miyawaki et al. n.d.

[73] Tomura, M., Sakaue-Sawano, A., Mori, Y., Takase-Utsugi, M., et al., Contrasting quiescent G0 phase with mitotic cell cycling in the mouse immune system. *PLoS One* 2013, *8*, e73801.

[74] Sakaue-Sawano, A., Hoshida, T., Yo, M., Takahashi, R., et al., Visualizing developmentally programmed endoreplication in mammals using ubiquitin oscillators. *Development* 2013, *140*, 4624–4632.

[75] Fukuhara, S., Zhang, J., Yuge, S., Ando, K., et al., Visualizing the cell-cycle progression of endothelial cells in zebrafish. *Dev. Biol.* 2014, *393*, 10–23.

[76] Nakajima, Y.-I., Kuranaga, E., Sugimura, K., Miyawaki, A., et al., Nonautonomous apoptosis is triggered by local cell cycle progression during epithelial replacement in Drosophila. *Mol. Cell. Biol.* 2011, *31*, 2499–2512.

[77] Horie, T., Shinki, R., Ogura, Y., Kusakabe, T.G., et al., Ependymal cells of chordate larvae are stem-like cells that form the adult nervous system. *Nature* 2011, *469*, 525–528.

[78] Hama, H., Kurokawa, H., Kawano, H., Ando, R., et al., Scale: a chemical approach for fluorescence imaging and reconstruction of transparent mouse brain. *Nat. Neurosci.* 2011, *14*, 1481–1488.

[79] Sakaue-Sawano, A., Kobayashi, T., Ohtawa, K., Miyawaki, A., Drug-induced cell cycle modulation leading to cell-cycle arrest, nuclear mis-segregation, or endoreplication. *BMC Cell Biol.* 2011, *12*, 1–12.

[80] Dan, S., Okamura, M., Mukai, Y., Yoshimi, H., et al., ZSTK474, a specific phosphatidylinositol 3-kinase inhibitor, induces G1 arrest of the cell cycle in vivo.

Eur. J. Cancer 2012, *48*, 936–943.

[81] Cold Spring Harbor Protocols, Phosphate-buffered saline (PBS). *Cold Spring Harb. Protoc.* 2010, 8247.

[82] Schmid, I., Sakamoto, K.M., Analysis of DNA content and green fluorescent protein expression. *Curr. Protoc. Cytom.* 2001, *Chapter 7*, Unit 7.16.

[83] Chu, Y.W., Wang, R., Schmid, I., Sakamoto, K.M., Analysis with flow cytometry of green fluorescent protein expression in leukemic cells. *Cytometry* 1999, *36*, 333–339.

[84] Terho, P., Flowing Software. 2015.

[85] ThermoFisher, HEK 293 Cell Culture Media. 2015.

[86] Warren, L., Manos, P.D., Ahfeldt, T., Loh, Y.-H., et al., Highly efficient reprogramming to pluripotency and directed differentiation of human cells using synthetic modified mRNA. *Cell Stem Cell* 2010, *7*, 618–630.

[87] Lifetechnologies, Lipofectamine 2000. 2013, 1–2.

[88] Rosser, M.P., Xia, W., Hartsell, S., McCaman, M., et al., Transient transfection of CHO-K1-S using serum-free medium in suspension: a rapid mammalian protein expression system. *Protein Expr. Purif.* 2005, *40*, 237–243.

[89] Fuge, G., Zeng, A.-P., Jandt, U., Weak cell cycle dependency but strong distortive effects of transfection with Lipofectamine 2000 in near-physiologically synchronized cell culture. *Eng. Life Sci.* 2017, *17*, 348–356.

[90] Jandt, U., Shao, S., Wirth, M., Zeng, A.-P., Spatiotemporal modeling and analysis of transient gene delivery. *Biotechnol. Bioeng.* 2011, *108*, 2205–2217.

[91] Lifetechnologies, Lipofectamine 2000. 2002, 1–2.

[92] Glick, B.R., Metabolic load and heterologous gene expression. *Biotechnol. Adv.* 1995, *13*, 247–261.

[93] Hutter, K.-J., Flow cytometry - a new tool for direct control of fermentation processes. *J. Inst. Brew.* 2002, *108*, 48–51.

[94] Kuystermans, D., Mohd, A., Al-Rubeai, M., Automated flow cytometry for monitoring CHO cell cultures. *Methods* 2012, *56*, 358–365.

[95] Addgene, Lentiviral Guide. 2015.

[96] Weber, K., Bartsch, U., Stocking, C., Fehse, B., A multicolor panel of novel lentiviral “gene ontology” (LeGO) vectors for functional gene analysis. *Mol. Ther.* 2008, *16*, 698–706.

[97] Weber, K., Lentiviral Gene Ontology Vectors. 2007.

[98] Fuge, G., Hong, Y., Riecken, K., Zeng, A.-P., et al., CHO cells engineered for fluorescence read out of cell cycle and growth rate in real time. *Biotechnol. Prog.* 2017.

[99] Harvard Systems Biology Flow Facility, Cell Cycle Analysis with DAPI. 2009.

[100] Hermey, G., Der Experimentator: Neurowissenschaften, Spektrum Akademischer Verlag, Heidelberg 2011.

[101] Hong, Y., Bachelor Thesis: Systematische Evaluation von Zellkulturen im Hinblick auf Zellzyklus-Verteilung und Wachstumsrate, Hamburg University of Technology, 2015.

[102] Wahrheit, J., Nicolae, A., Heinzle, E., Dynamics of growth and metabolism controlled by glutamine availability in Chinese hamster ovary cells. *Appl. Microbiol. Biotechnol.* 2014, *98*, 1771–1783.

[103] Platas Barradas, O., Dissertation: Process and cultivation strategies for the human industrial cell line AGE1.HN, 1. Aufl., Hamburg University of Technology 2014.

[104] Eduardo Castillo Salvador, A., Diploma Thesis: Physiological and Kinetic Analysis of Mammalian Production Cell Lines as Synchronized High Density Cultures, Hamburg University of Technology, 2014.